The Processing of Titanium Hydride Powders into Uniform Hollow Spheres

A Thesis
Presented to
The Academic Faculty

by

Kevin Michael Hurysz

In Partial Fulfillment
of the Requirements for the Degree
Master of Science in Materials Science and Engineering

19991001 056

Georgia Institute of Technology
August 1998

DISTRIBUTION STATEMENT A
Approved for Public Release
Distribution Unlimited

DTIC QUALITY INSPECTED 4

The Processing of Titanium Hydride Powders into Uniform Hollow Spheres

Approved:

Joe K. Cochran

Joe K. Cochran, Jr., Chairman

T. H. Sanders Jr.

T. H. Sanders, Jr.

K. Jim Lee

Date Approved 8/19/1998

ACKNOWLEDGEMENTS

Thank you to everyone at Georgia Tech who has provided discussion, criticism, suggestions, and coffee toward the advancement of this work. To my advisor, Dr. Joe K. Cochran, Jr. for his guidance and encouragement, Dr. T. H. Sanders, Jr. for all things metal, Dr. K. Jim Lee for his technical expertise, Tim Banks for keeping the labs from degenerating into chaos, and the academic support staff of the MSE department. To students who have graduated and moved on, Canan Uslu who worked previously on this project, Adam Nagel for his work on stainless steel spheres, and Nate Baxter. And to the students that currently reside in our office, Justin Clark, Bill Nemeth, and Yancy Riddle.

Thanks to mom and dad, Sandra and Leonard Hurysz for their continued support.

This work was partially supported by Defense Advanced Research Projects Agency (DARPA) and the Office of Naval Research (ONR) through a United Technologies Research Center (UTRC) prime program under contract E18-X88.

TABLE OF CONTENTS

SUMMARY

Economically produced metallic foams having low density and high strength are potentially useful materials in a wide variety of applications. As a result, these materials show great promise as replacements for bearing and support structures, for impact and sound absorption, and where the advantages of both metallic character and low density are required. In many industries, especially aerospace and automotive, the need for weight and cost reduction without a compromise in quality has become a dominant driver. The advantage to sphere formation using TiH_2 is that Al, V, and other master alloy powders can be added to the Ti, forming spheres with a variety of alloy compositions.

The objective of the current work is to investigate the surface properties of TiH_2 and the interaction of polymer dispersants and binders with this surface. The ultimate goal is to disperse TiH_2 in acetone, forming slurries exhibiting the viscosity, drying characteristics, and repeatability necessary to form highly uniform TiH_2 hollow spheres. Slurry suitability is dictated by the solids loading and degree of dispersion, the influence of polymer additives on rheology and the evaporation of acetone, and the minimization of impurities soluble in the metal lattice that serve to embrittle the Ti. Heat treating these spheres results in dehydrogenation, leaving shells of titanium metal that can be bonded into lightweight foams. It is not yet possible to achieve ductile titanium foams because of the inability to control the purity of the heat treated Ti metal during firing.

Of those tested, the only combination of polymers that resulted in favorable viscosity and evaporation rates when used in TiH_2 slurries were Z-6020 polysilane and 2008 PMMA. Visual inspection and digital analysis found spheres made from slurries dispersed with polysilane and PMMA to be significantly more uniform than any alternative. The batch with the highest measured uniformity was formed from a slurry with a solids loading of 44 vol.% TiH_2 treated with 1.0 wt.% Z-6020 polysilane and dispersed with 3.0 wt.% 2008 PMMA.

LIST OF TABLES

LIST OF FIGURES

CHAPTER I

INTRODUCTION

Economically produced metallic foams having low density and high strength are potentially useful materials in a wide variety of applications. As a result, these materials show great promise as replacements for bearing and support structures, for impact and sound absorption, and where the advantages of both metallic character and low density are required. In many industries, especially aerospace and automotive, the need for weight and cost reduction without a compromise in quality has become a dominant driver.

Foams for stiffening, energy absorption, and foam core construction are increasing in use but their applications are limited by thermal and mechanical considerations. By fabricating hollow, highly uniform ceramic and metal spheres and bonding these spheres at points of contact, high strength to weight ratio materials can be constructed. These materials can be readily fashioned into complex shapes and to close dimensional tolerances.

There are two broad classifications of light weight materials currently in production. These are foil stamped honeycombs and gas foamed metals. The potential exists for point contact bonded hollow spheres to replace these materials for weight savings and compressive support.

Foil stamping is a process by which metal sheets are corrugated by rolling. These sheets are then stacked and bonded, resulting in a hexagonal cross-section when viewed along the sheet direction. Properties parallel and perpendicular to the c-axis are anisotropic. Strength parallel to the c-axis is very high whereas perpendicular strength can be a factor of ten or more less. These materials also behave anisotropically perpendicular to the c-axis because of the doubling of sheet at contact regions. Cost is also a major consideration limiting more widespread use of honeycomb material.

In foamed metals, gas is introduced into the molten metal via high shear mixing or chemical decomposition. Like honeycombs, these materials are currently in commercial production. *Alporas*, an Al-5Ca foam from Shinko Wire and *Alulight*, an Al-Si hypoeutectic alloy are two examples. The low viscosity and high surface tension of liquid metals result in a wide distribution of pore sizes and foams that will have inconsistent mechanical behavior.

The superior bulk properties of metals enhance the properties of foams constructed from metal systems. The next generation of ultra light weight materials will require increasingly mass efficient architectures and the uniformity presently not attainable in foaming processes. However, uniform, monosized, point contact bonded hollow spheres made into foams exhibiting closed cell character can provide the isotropy, specific strength, and stiffness that alternative light weight materials cannot.

The foundation of the hollow sphere technology used in this research was studied by Lord Rayleigh in the late nineteenth century (1). He described the stable state of a cylindrical fluid column as a series of droplets. The application of an axially symmetric, sinusoidal wave with wavelength greater than the circumference of the column causes instability in the column. A jet of liquid forced from a nozzle will thus separate into randomly sized droplets with a behavior governed by the wavelength range that most rapidly causes instability. The droplet diameter is related to the disturbance wavelength.

Later technologies relied on acoustic and electrical transducers to provide a single wavelength disturbance and cause uniform decomposition of the fluid. Expensive alternatives such as carbonizing polymer shells and vapor deposition of metal coatings were also investigated to form hollow spheres (2). Large amplitude oscillations can be generated by injecting gas through the inner orifice of a dual jet coaxial nozzle forming hollow spheres. Liquid flowing through the annulus formed between the inner and outer jets will temporarily form a hollow column. Within several sphere diameters, the oscillations amplify sufficiently to pinch the column into individual droplets. The frequency of the decomposition is highly stable and results in the amount of material in each sphere being nearly identical. Sphere size and spacing can become extremely uniform by using the inner jet flow of gas as a perturbation on the liquid jet. The effect of this instability is far more powerful than the Rayleigh instability associated with fluid columns (3).

In the 1980's, smooth, dimensionally precise, high tensile strength metallic spheres were desired for use as inertial confinement fusion targets. These were formed directly from the melt using a coaxial nozzle approach. Shells of a variety of metal compositions including tin, aluminum, and gold alloy, were made with diameters ranging from 460 to 3000 μm (4). An effort at Georgia Tech involved forming aluminum spheres using a similar technique (5).

The technology currently under investigation employs powder metallurgy and a coaxial nozzle approach to form polymer bonded powder shells from a dispersed slurry. The dispersions used are similar to those used in tape casting. Several alloy systems have been studied including the dehydrogenation of TiH_2 and Ti-6Al-4V hydride to Ti metal and Ti-6Al-4V, respectively, and the reduction of Fe_2O_3 and Cr_2O_3 mixtures to 88Fe-12Cr steels.

The objective of this research was to maximize the quality and uniformity of Ti and Ti alloy hollow spheres. The TiH_2 powder in the slurry precursors was dispersed with a number of polymer systems, including PS3, PMMA, and polysilane and the viscosity of these slurries characterized. The evaporation of acetone from these slurries was studied to understand the hardening of the hollow spheres after their formation. Defects associated with sphere production were quantified and reduced by changing processing variables. Sphere wall thickness variations were also quantified and compared to formulate a batch composition limiting the presence of these and other defects. Lattice parameter measurements using x-ray analysis were conducted to arrive at impurity contents and explain the brittle behavior of heat treated Ti foams.

CHAPTER II

BACKGROUND

The coaxial nozzle process is a complex technology with a large number of independent variables. These variables must be carefully controlled to optimize the process and obtain uniform hollow spheres of high quality. This chapter will address the potential of titanium hollow sphere foams from a mechanical standpoint and consider the method of their fabrication. The required characteristics of slurry precursors, including methods of dispersion and evaporation of the slurry solvent will be discussed.

II.1 Materials Selection

Titanium is one of the most desirable materials from which to construct hollow sphere foams. A comparison of the properties of titanium alloys to a number of other common alloys can be found in Figure 2.1 (6). Clearly, titanium outperforms other high performance metallic systems over a substantial temperature range.

Titanium exists in two polymorphic states. The room temperature phase of titanium is the α–phase (α-Ti). It is a light weight, hexagonal closed packed (HCP) metal with a density of 4.54 g/cc and an elastic modulus of 116 GPa. At the β-transus temperature of 883 °C, α-Ti undergoes an allotropic transformation from HCP to a body centered cubic (BCC) crystal structure (7). Depending on the alloying elements added, this transformation allows the possibility of having α, β, and mixed α + β phase alloys by varying heat treatment schedules. The β-phase remains stable to the melting temperature, 1668 °C. Table 2.1 shows the chemical compositions and typical applications of unalloyed titanium metal (7). Good target values for impurity levels in several grades of titanium can be found in this table.

By using titanium hydride (TiH_2) as a starting material, it is possible to obtain pure α-Ti by heat treating in an inert atmosphere. A schematic of the TiH_2 unit cell showing the relative positions of Ti and H can be found in Figure 2.2 (8). A wide variety of titanium containing alloys can be formed through additions to TiH_2 in the initial batch. Hydrides lend themselves to slurry processing because they are brittle. They can therefore be milled to very fine particle sizes. Hydrides are relatively stable chemically and can be dispersed at high solids concentrations. Slurry processing is a room temperature operation, allowing complex shapes to be formed without high energy expenditures.

II.2 α-stabilization

Interstitials such as O, H, N, and C dissolve preferentially into the α-phase of titanium, expanding the field and increasing the β-transus temperature (9). This effect is known as α-stabilization and is represented generically in Figure 2.3 (7). In addition to interstitial elements, substitutional α-stabilizers such as aluminum can be employed. The phase diagram for the Ti-O system is shown in Figure 2.4 (10). Small changes in the amount of oxygen solute greatly influence the β-transus temperature.

In α-Ti, interstitials reside in octahedral sites due to size constraints. There is a single octahedral site for each titanium atom in the low temperature, HCP phase. Hydrogen is a notable exception and is found in tetrahedral positions. In β-Ti, there are three octahedral and three tetrahedral sites for each titanium atom. The location of oxygen atoms in this phase have not been clearly identified but are also likely octahedral sites (11). Table 2.2 outlines the interstital hole sizes in α- and β-Ti (12). Table 2.3 outlines some properties of the interstitials commonly found in titanium metal (12).

II.3 Ductility of Titanium

Although the low temperature phase of titanium has a hexagonal structure, it exhibits a high degree of ductility. This behavior is unusual for hexagonal metals and can be attributed to the subideal c_o / a_o lattice parameter ratio of pure α-Ti. The axial ratio of α-Ti is 1.587 ($a_o = 0.2950$ nm, $c_o = 0.4653$ nm) compared to the ideal of 1.633. A direct consequence of this deviation to deformation behavior is the activation of a larger number of slip systems. These include the $\{10\bar{1}0\}$ prism, $\{10\bar{1}1\}$ pyramidal, and $\{0001\}$ basal planes. When the interstitial impurity concentration exceeds 0.1 wt.%, slip is generally confined to $\{10\bar{1}1\}$. Twinning is also a more important contributor to the deformability of titanium than many other HCP metals, occurring predominantly on the $\{10\bar{1}2\}$, $\{11\bar{2}1\}$, and $\{11\bar{2}2\}$ pyramidal planes.

This ductility is difficult to retain following thermal processing because of the high temperature reactivity of titanium with atmospheric gases. The ductility of subideal axial ratio hexagonal metals is sensitive to a variety of interstitial alloying elements (13). Gases such as hydrogen, oxygen, and nitrogen, as well as CO, CO_2, water vapor, and ammonia contribute directly to embrittlement (14). Diatomic gas molecules dissociate to dissolve as monatomic solutes in metal. Reduction of gases at the metal surface and diffusion through the bulk can result in further contamination (15).

Reactions involving impurity gases are especially important in the titanium system. Following the formation of a surface layer, the high solubility of impurity atoms in the metal lattice results in rapid diffusion. The affinity of titanium for these impurity elements is sufficient to render the reactions irreversible, as evidenced by the large difference in bond energies between titanium and several other atoms of particular interest: (16, 17)

Ti - Ti	2.56 eV
Ti - N	2.22 eV
Ti - C	2.18 eV
Ti - O	2.13 eV

Changes in ductility can be explained by the dependence of the c_o / a_o lattice parameter ratio on interstitial content. As the c_o / a_o ratio increases, fewer slip planes are operational and there is a concomitant decrease in ductility. Although the presence of carbon, nitrogen, and oxygen interstitials cause an increase in both a_o and c_o as shown in Figure 2.5, the c-axis distortion is significantly more pronounced (17). X-ray diffraction can be used to determine lattice parameter and from this, an equivalent impurity content.

The solubility of oxygen in α-Ti is 15.5 wt.% (30 at.%) but severe embrittlement can be realized with oxygen contents as low as 0.6 wt.% (1.2 at.%) (18). Embrittlement at such low concentrations is indicative of an inhomogeneous distribution of solute in the lattice. Interstitial solubility at constant pressure increases with temperature according to LeChatlier's principle.

Elemental analysis of fired Ti metal spheres derived from TiH_2 found oxygen to be the predominant impurity at concentrations of 1.81 wt.% (19). As has been shown, this is significantly greater than the concentration required to embrittle α-Ti. Although titanium oxides are extremely stable, it is thermodynamically favorable for magnesium (Mg) metal to reduce the oxides to Ti metal. Difficulties exist however because Mg has a melting temperature of 649 °C and a boiling temperature of 1090 °C (20). As a result, heat treating of any hydrides containing Mg must be conducted at temperatures lower than the normal 1100 °C. Liquid phase sintering in the presence of Mg also becomes a possibility.

From the phase diagram in Figure 2.6, it can be seen that Mg is not soluble in Ti. The Mg must therefore have a small particle size and be well dispersed in the precursor slurry to effectively reduce any oxides present in Ti spheres.

II.4 Mechanics of Foams

There are two fundamental architectures used to describe foams. These are open cell and closed cell. Each results in characteristic thermal and mechanical behavior. In open cell foams, the porosity is continuous and material resides in pore interstices forming a strutted structure. The material in closed cell foams is located entirely in the cell walls. Schematic diagrams of the two types of foams can be found in Figure 2.7 (21).

Gibson and Ashby (21) modeled the elastic modulus of brittle foams as being proportional to the shear modulus according to the relation given in (1) where E^* and E_s

$$\frac{E^*}{E_s} \propto \frac{G^*}{G_s} \propto C_1\phi^2\left(\frac{\rho^*}{\rho_s}\right)^2 + C_2(1-\phi)\left(\frac{\rho^*}{\rho_s}\right) \tag{1}$$

are the elastic modulus of the foam and bulk solid, G^* and G_s are the shear modulus of the foam and bulk solid, and ρ^* and ρ_s are the density of the foam and solid, respectively. The volume fraction of foam material residing in the cell edges is given as ϕ. The volume fraction of the remaining material $(1-\phi)$ must therefore represent the material present in the cell faces. For a foam exhibiting solely open cell character, that is one with all material distributed throughout the cell walls, ϕ is unity, $(1-\phi) = 0$, and the elastic constant is found to be proportional to the square of the relative density as in (2). The value of the constant

$$E^* = E_s\left(\frac{\rho^*}{\rho_s}\right)^2 \tag{2}$$

C_2 is 0.5 for the Hashin-Shtrikman limit (22) and 0.35 for the Kelvin solid (23). As a result, the closed cell modulus may be as high as shown in (3).

$$E^* = \frac{1}{2}E_s\left(\frac{\rho^*}{\rho_s}\right) \tag{3}$$

Gibson and Ashby also modeled the strength behavior of foams. The equation given in (4) calculates the ultimate tensile strength of brittle foams and the yield strength

$$\frac{\sigma^*}{\sigma_s} = C_3\phi\left(\frac{\rho^*}{\rho_s}\right)^{\frac{3}{2}} + C_4(1-\phi)\left(\frac{\rho^*}{\rho_s}\right) \tag{4}$$

of plastic foams where σ^* and σ_s are the yield stress of the foam and bulk solid. The constant C_3 has been determined to be 0.30, C_4 is 0.35 (21, 24). The resulting expressions for the strength of open cell foams is given in (5), that of closed cell foams is given in (6).

$$\sigma^* = 0.30\sigma_s\left(\frac{\rho^*}{\rho_s}\right)^{\frac{3}{2}} \tag{5}$$

$$\sigma^* = 0.35\sigma_s\left(\frac{\rho^*}{\rho_s}\right) \tag{6}$$

The ultimate result of this modeling shows that closed cell foams are far more desirable than open cell foams from the standpoint of mechanical properties. At a relative density of 20%, the modulus of closed cell foams is 2.5 times greater and the strength 2.6

times greater than the equivalent open cell foam. At 5% relative density, these numbers improve to a modulus 10 times greater and a strength 5.2 times greater than the equivalent open cell foam. A comparison of the relationship between modulus, specific strength, and relative density for several materials can be found in Figures 2.8 (a) and (b), respectively. To generate these plots, reasonable average values for σ_s were chosen: 1575 MPa for stainless steel, 864 MPa for Ti-6Al-4V, and 385 MPa for aluminum.

II.5 Powder and Slurry Processing

Hollow sphere technology from powders was originally developed for the formation of ceramic structures (25, 26). It is now being applied to metals using brittle powders with average particle diameters between 1 and 10 μm. These powders are dispersed in acetone with polymer additives forming a low viscosity slurry.

The suitability of slurry for use in the coaxial nozzle process is dictated by the solids loading and degree of dispersion, the influence of polymer additives on the evaporation of acetone from the formed spheres, and the minimization of impurities soluble in the metal lattice that serve to embrittle the foam. Poorly dispersed slurries will not process smoothly and those containing excess acetone will have insufficient time to dry.

II.6 Slurry Stability

One of the most pressing obstacles to forming a powder dispersion is stability. Unstable dispersions will not behave uniformly because of rheological changes due to agglomeration and settling. They are thus unsuitable for the coaxial nozzle process. Particles in suspension must not be too large or gravity will cause settling. If the van der Waals attractive force between particles is large enough, agglomeration and subsequent gravity induced settling can also occur.

Slurries composed of insoluble particles in liquids are examples of lyophobic colloidal systems. Lyophobic systems are those in which the liquid and particles are substantially different and do not show an affinity for each other. These systems are inherently unstable and require a repulsive mechanism to effect dispersion.

There are two means by which a slurry can be stabilized. Electrostatic stabilization occurs when repulsive electrical charges overcome the van der Waals attractive force and prevent particle agglomeration and settling. Steric stabilization occurs when adsorbed or chemisorbed polymer molecules, or polymer molecules free in solution, provide the repulsive force. It is possible to stabilize a slurry through a combination of these methods, known as electrosteric stabilization.

For particles that are stabilized by electric charge, the charge on the particle surface is balanced by an equal and opposite countercharge in the solution. Diffusional forces or space charge limitations prevent these counterions from being adsorbed so they are distributed throughout the liquid surrounding the particle. This results in an electrical double layer as illustrated in Figure 2.9 (a) (27).

The electrical double layer consists of two regions, as can be seen in Figure 2.9 (b) (27). The Stern layer refers to the compact layer of adsorbed species at the particle surface and is typically only several angstroms in thickness. The behavior of the electric potential in the Stern layer is linear decreasing. The diffuse layer found beyond the Stern layer is known as the Gouy-Chapman layer. In this region, the potential decreases exponentially with distance from the particle.

Two particles in suspension will begin to interact when their electrical double layers overlap. The repulsive effect of the electrical double layer opposes the attractive van der Waals force. If the repulsive force is greater than the attractive force, dispersion will result. If the attractive force is greater, the system will flocculate.

Steric stabilization can result from either of two processes. In systems that are stabilized sterically, polymer molecules can adsorb directly onto the surface of powder particles. There must be sufficient coverage of the particles by the polymer or unoccupied sites on the surface can be used to bridge particles, increasing the likelihood of settling.

The extended chains of these polymers can interpenetrate upon close particle approach. Repulsion arises from a demixing effect caused by the thermodynamic requirement that extended polymer chains avoid like chains. The effect is repulsive only when the polymers introduced into the slurry are highly soluble. The local polymer concentration increases as the interpenetration becomes more severe and an osmotic pressure builds between particles. Solvent invades to reduce the concentration of the polymer, forcing the particles apart. It is also possible for the polymer chains to be compressed on close particle approach. This generates an elastic contribution to stabilization behavior.

Depletion stabilization, the second steric process, is less common and arises when polymer molecules free in solution facilitate dispersion. For two particles to closely approach, there must be an associated demixing of polymer between the particles. If the energy of demixing overcomes that of the van der Waals attractive force, it is possible to stabilize the dispersion in this manner.

II.7 Zeta Potential

When the particles in a suspension are charged, the application of an electric field will cause the particles to move with a velocity proportional to the field strength. This motion, called electrophoresis, can be used to determine the charge associated with the electrical double layer. The ζ-potential of particles in organic liquids can be calculated using the Hückel equation (7) where ν_E is the electrophoretic mobility, η is the viscosity of

$$\zeta = 3\, \nu_E\, \eta / 2\, \varepsilon_o \varepsilon \tag{7}$$

the medium, ε_o is the permitivity of vacuum (8.85×10^{-12} C^2/Nm^2) and ε is the dielectric constant of the medium.

The ζ-potential is not a measure of the potential at the particle surface. The particle moves with an adsorbed layer, creating a shear plane at the interface between the adsorbed layer and the liquid. As a result, the ζ-potential is measured at this shear layer, at some distance removed from the surface. For simplicity, it is usually said to be measured at the Stern layer. When studying the interactions of the electrical double layer, the ζ-potential is the appropriate variable to consider as long as the size of the Stern layer can be reasonably estimated. A schematic of the ζ-potential can be found in Figure 2.10 (27).

II.8 Polymer Adsorption

The amount of polymer adsorbed from solution onto a particle is related to the interactions between polymer, solvent, and particle surface. Polymers can be physically adsorbed when van der Waals or hydrogen bonding is involved. Physical adsorption is a reversible process. If the adsorption process involves a chemical reaction, the polymer is said to be chemisorbed. Chemisorption involves the covalent bonding of polymers to particle surfaces.

Hydrogen bonding provides a strong force for the adsorption of solute onto the surface of a particle. This adsorption is facilitated if one material contains hydrogen bond donor groups and the other contains acceptor groups. According to Lewis acid-base theory, basic sites on the particle surface will adsorb acidic sites of solutes. As a consequence, polymer dispersants for materials with basic surfaces must be acidic and vice versa. Interactions between the solvent and the particle surface can also influence adsorption behavior. Basic surfaces in acidic solvents will exhibit positive potentials and acidic surfaces in basic solvents will exhibit negative potentials.

A typical adsorption isotherm begins with a line of positive slope at low equilibrium concentrations of solute, labeled (1) in Figure 2.11 (28). This is a result of increasing adsorption of solute from the solvent, onto the particle surface. The slope will begin to rapidly decrease and form a knee at (2) as the particle becomes crowded with adsorbed material. Eventually it will become a plateau (3), the height of which indicates the monolayer capacity. It is also possible to have a stepped isotherm or one with no discernible plateau, indicating multilayer adsorption or other complex behavior.

II.9 Sphere Formation Parameters

Several parameters can be varied that have direct effect on the characteristics, properties, and quality of the spheres produced. The properties of the slurry most strongly influence sphere quality. Slurry properties are more specifically dependent on the surface chemistry of the powder being dispersed. It is the interaction between polymer dispersants, binders, and the powder at the interface between particle and solvent that dictate the properties of the slurry jet and by extension, the properties of the final hollow spheres. Slurry homogeneity and viscosity are a result of these surface interactions.

The evaporation rate of solvent from the slurry is also related to the polymers used for dispersing and binding. The slurry must "case harden" rapidly after forming to freeze a rigid shell that will not collapse upon contact with the collection apparatus. Particle size and the relationship between the total solids loading and particle surface area must also be considered. Particles that are too large will not remain in suspension and will rapidly settle. Large particles can compromise the mechanical properties of a fired sphere if their diameter is a significant fraction of the total wall thickness.

The flow rate of gas and liquid (slurry) through the coaxial nozzle will also affect sphere properties. At a constant liquid flow rate, there are lower and upper boundaries for the gas flow rate that allow for the formation of spheres. At the lower extreme, zero gas flow, the result is homogeneous liquid drops (29). Increasing the gas flow rate while retaining a constant liquid flow rate constant will increase the frequency of sphere formation and decrease the wall thickness accordingly (30). At some maximum gas flow rate, dependent on the properties of the slurry being blown, the spheres will burst. The diameter of unfired spheres can typically be changed between 1 and 6 mm through variation of processing parameters. Wall thickness, and thus foam relative density, can be tailored in this way.

II.10 The Coaxial Nozzle Process

The coaxial nozzle process provides a number of advantages over conventional foaming techniques. Slurry compositions can be easily varied allowing for numerous foam compositions. By controlling heat treatment schedules, microstructures can be tailored as desired.

The sphere formation apparatus consists of a pair of coaxial nozzles. The inner jet sustains a flow of an inert gas while the annulus formed between the inner and outer jets carries slurry. The slurry is a high solids content, low viscosity combination of solvent, polymer binders and dispersants, and powder. The slurry solvent must be inexpensive, able to dissolve a wide variety of organic materials, and have a vapor pressure sufficiently high to evaporate before contacting the collection apparatus. Acetone is used primarily because it satisfies each of these conditions, is safe to handle, and is environmentally friendly.

Upon exiting the nozzle, an unstable hollow column of slurry is formed. This column rapidly decomposes into hollow spheres due to hydrostatic forces and the effects of surface tension. The shell expansion rate is determined by a balance between the stresses caused by gas pressure inside the shell, the viscous stress due to liquid motion, and surface tension. The solvent evaporates in free flight resulting in hard, polymer bonded powder shells that can withstand impact with the collection apparatus. An updraft of heated air is used to improve drying characteristics and lessen the impact of the spheres on the conveyor belt. Fluid dynamic models of this process have been developed that consider gas and liquid flow rates, slurry viscosity, and surface tension (30). A series of photographs showing the sphere blowing cycle can be found in Figure 2.12 (29).

The frequency stability of the coaxial nozzle process is extremely high and results in spheres with narrow mass and diameter distributions. Wall defects and deviation from a uniform wall thickness can compromise the mechanical properties of individual spheres and become nucleation sites for failure of the foam. There are several common classes of sphere defects, many of which can be identified visually and non-destructively. In addition, defective spheres can be separated from a batch using a rolling technique (31). Sifting spheres through sieves of appropriate size can further reduce the presence of defects.

Table 2.1 Chemical compositions (maximum values) and typical applications of unalloyed titanium.

% Ti	Grade	ASTM No.	% C	% Fe	% N	% O	% H	Typical applications
99.5	1	B265	0.08	0.20	0.03	0.18	0.015	Airframes; chemical, desalination, and marine parts; plate-type heat exchangers; cold-spun or pressed parts; platinized anodes; high formbility.
99.2	2	B265	0.08	0.25	0.03	0.20	0.015	Airframes; aircraft engines; marine chemical parts; heat exchangers; condenser and evaporator tubing; formability.
99.1	3	B265	0.08	0.25	0.05	0.30	0.015	Chemical, marine, airframe, and aircraft engine parts which require formability strength, weldability, and corrosion resistance.
99.0	4	B265	0.08	0.50	0.05	0.40	0.015	Chemical, marine, airframe, and aircraft engine parts; surgical implants; high-speed fans; gas compressors; good formability and corrosion resistance, high strength.

† After "ASM Databook," published in *Met. Prog.*, mid-June, vol. 114, no. 1, 1978.

Table 2.2 Interstitial hole sizes in α- and β-Ti.

Phase	Octahedral Radius (Å)	Tetrahedral Radius (Å)
α-Ti	0.61	0.33
β-Ti		0.44

Table 2.3 Some properties of the interstitials commonly found in titanium metal.

Interstitial	Neutral Atomic Radius (Å)	Volume Expansion ($Å^3$ / at.%)	Maximum α Solubility (at.%)
Hydrogen	0.46	0.00	8
Oxygen	0.60	0.13	30
Nitrogen	0.71	0.18	19
Carbon	0.77	0.49	2

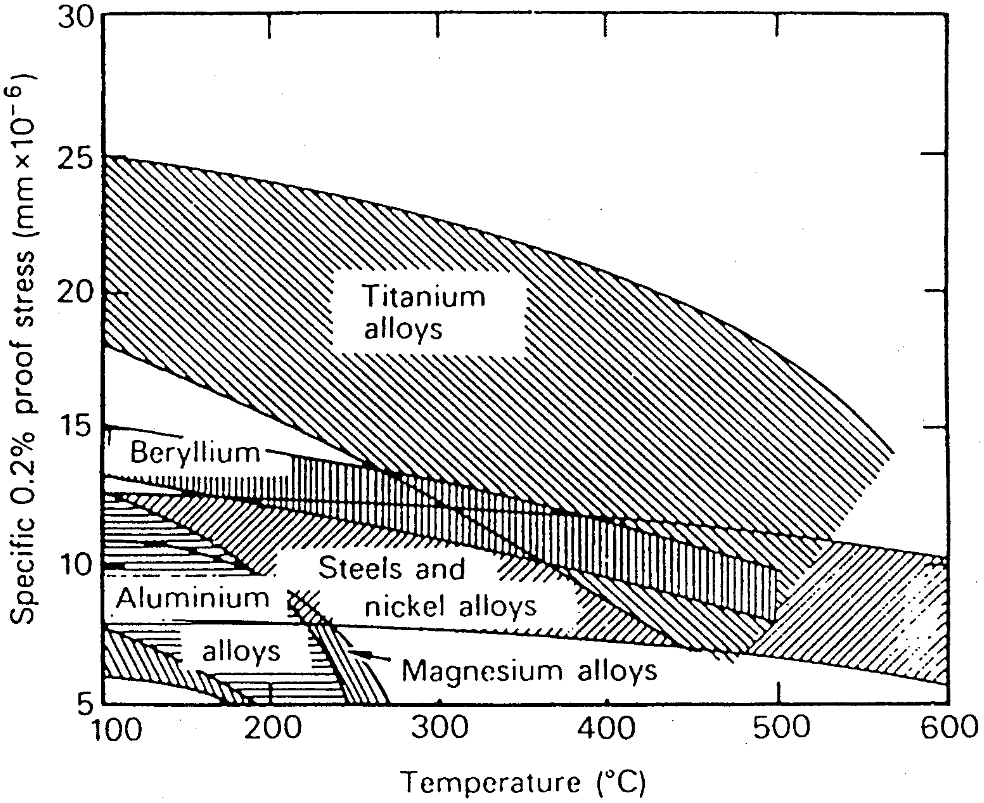

Figure 2.1 The properties of titanium alloys as compared to other common alloys.

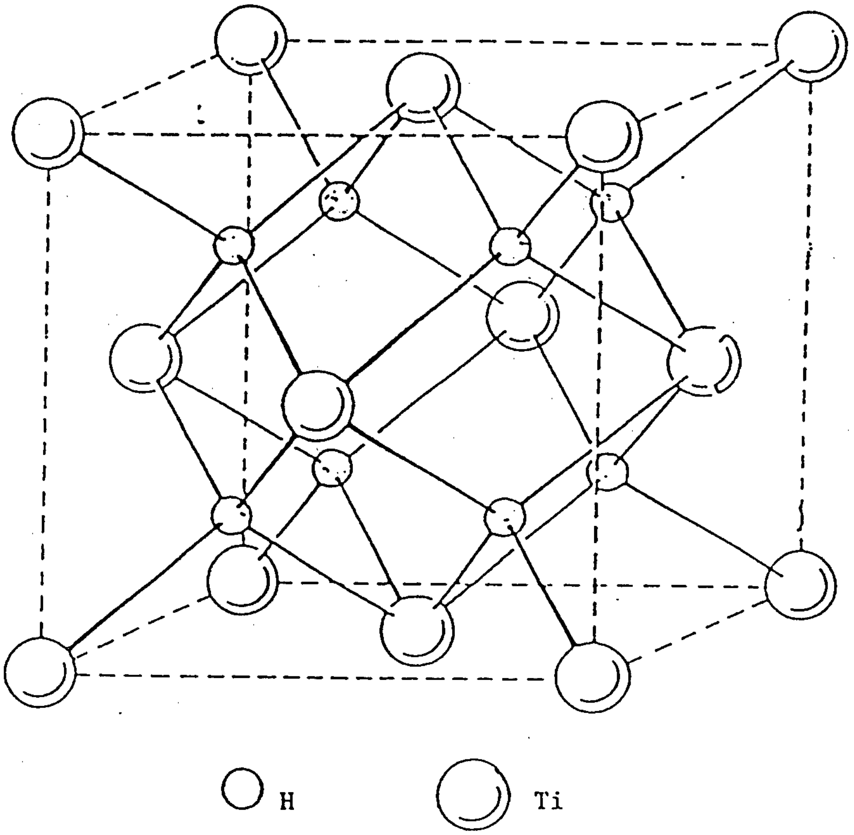

Figure 2.2 A schematic of the TiH_2 unit cell showing the relative positions of Ti and H.

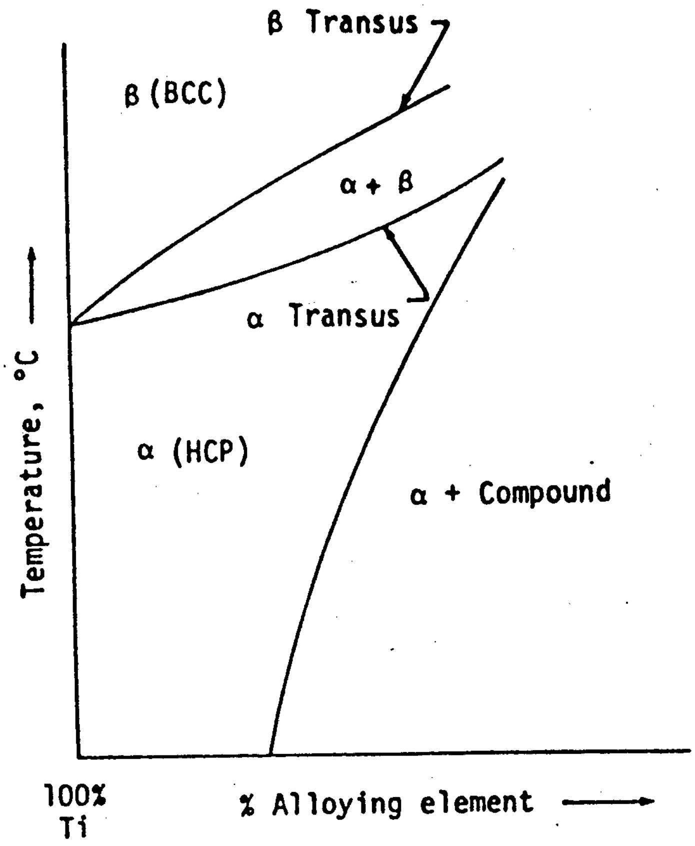

Figure 2.3 Schematic representation of α-stabilization in titanium.

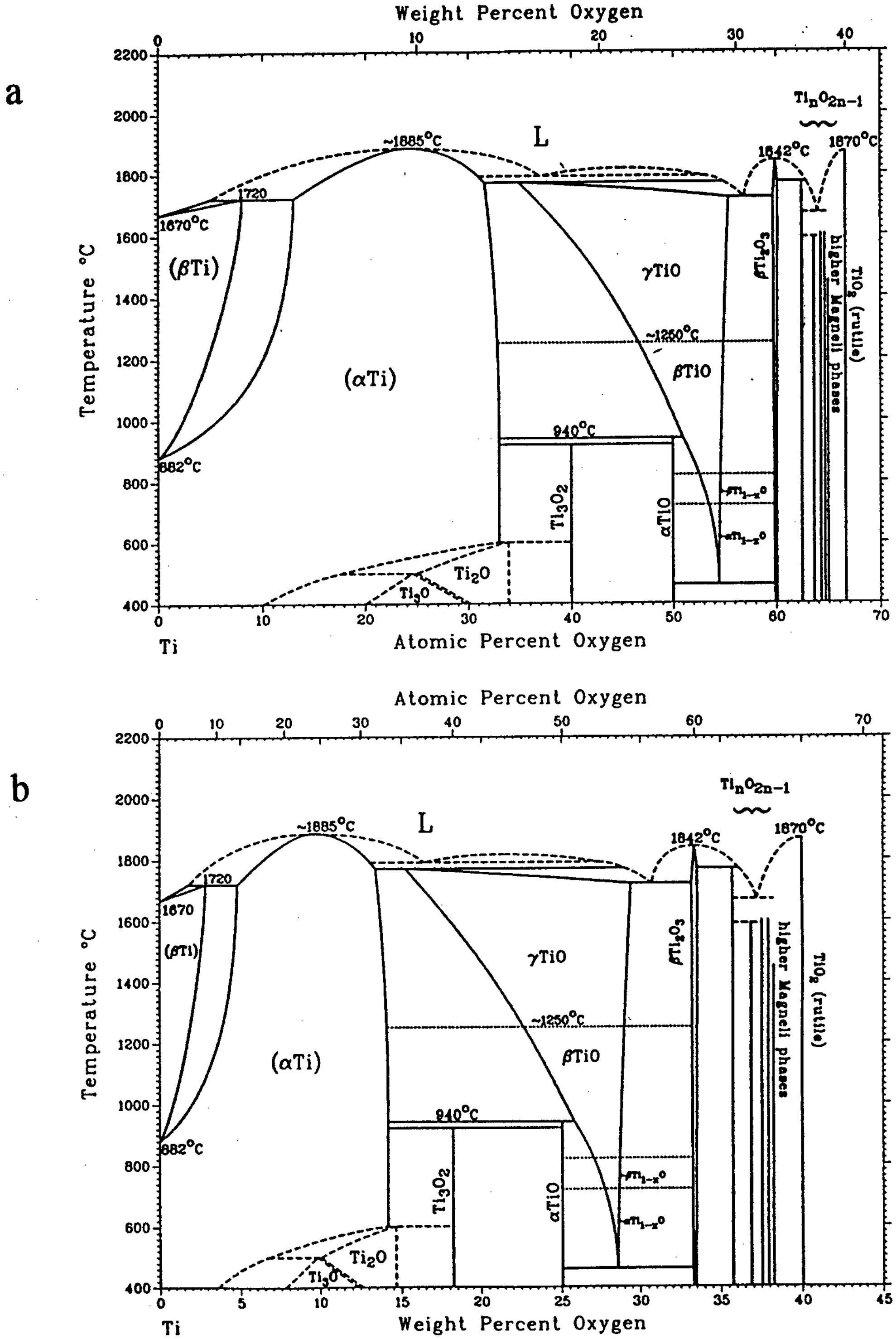

Figure 2.4 Phase diagrams for Ti-O (a) by at.% oxygen, (b) by wt.% oxygen.

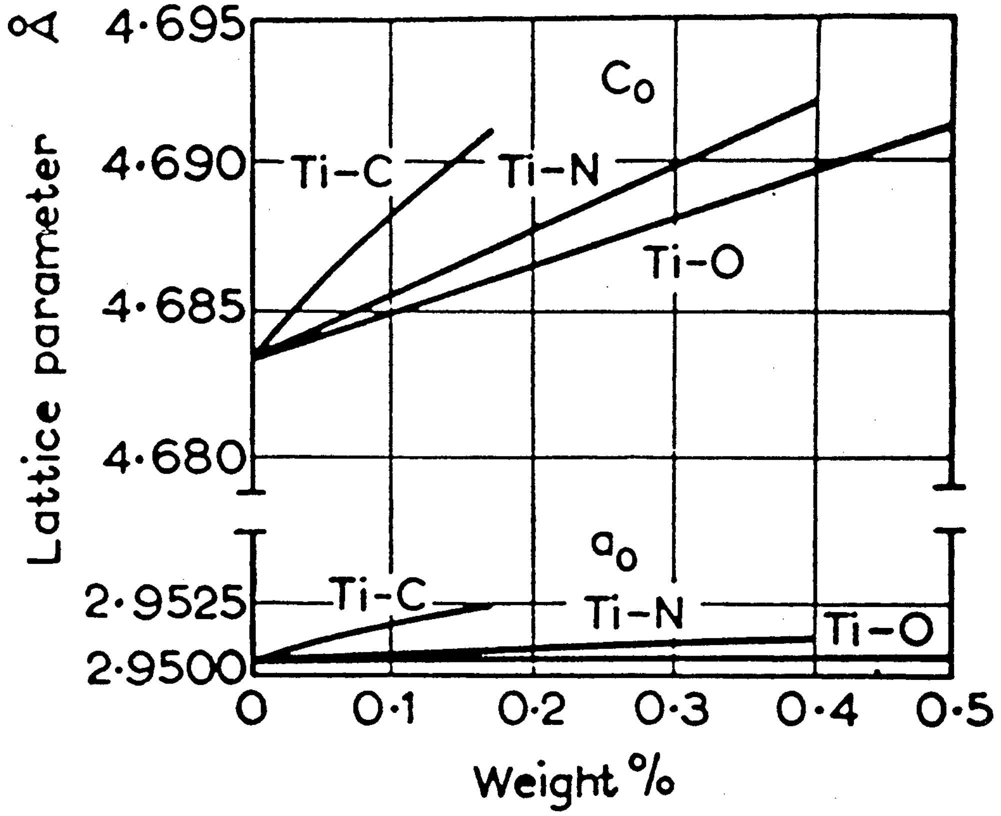

Figure 2.5 Changes in titanium lattice parameter associated with carbon, nitrogen, and oxygen.

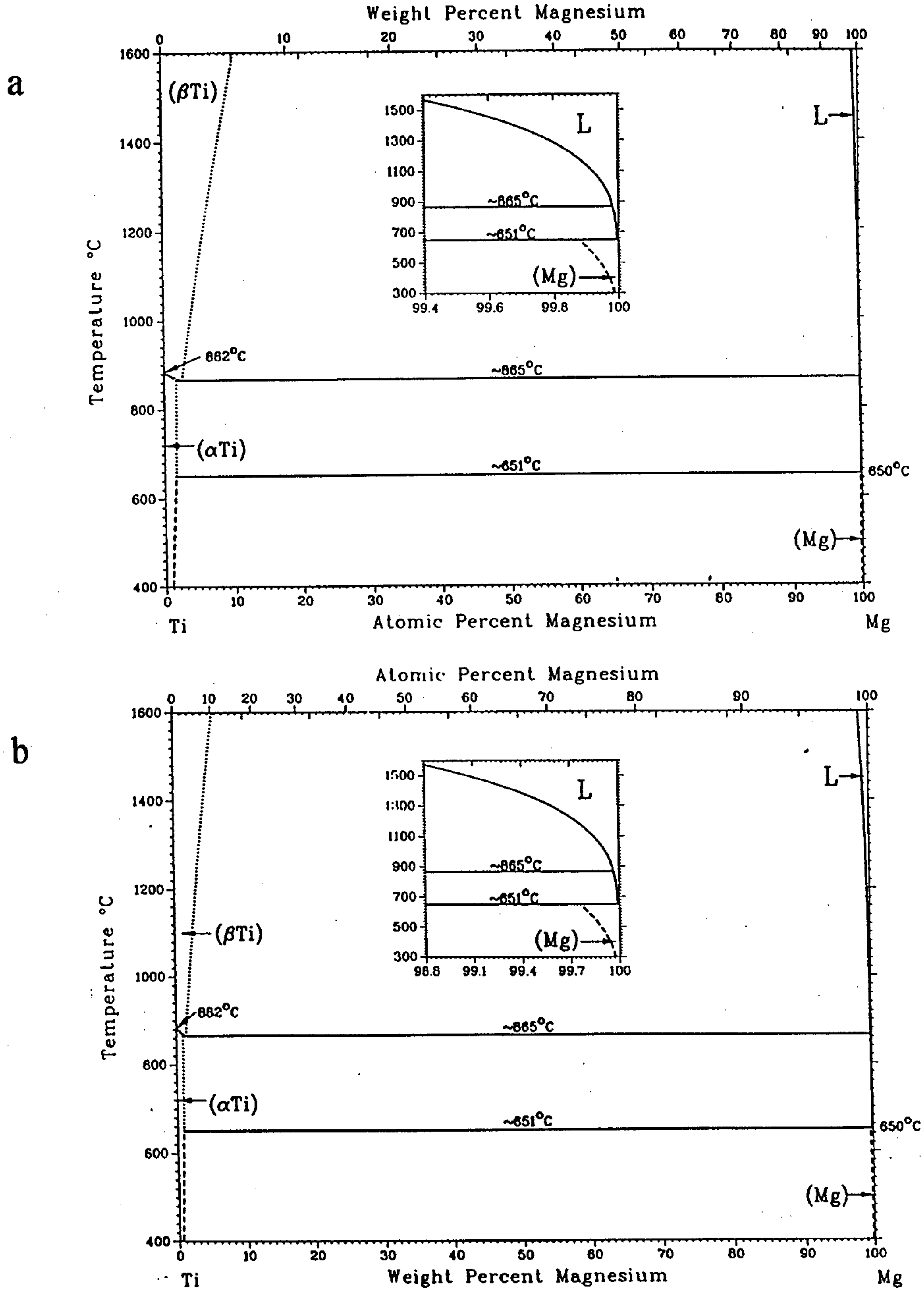

Figure 2.6 Phase diagrams for Ti-Mg (a) by at.% magnesium and (b) by wt.% magnesium.

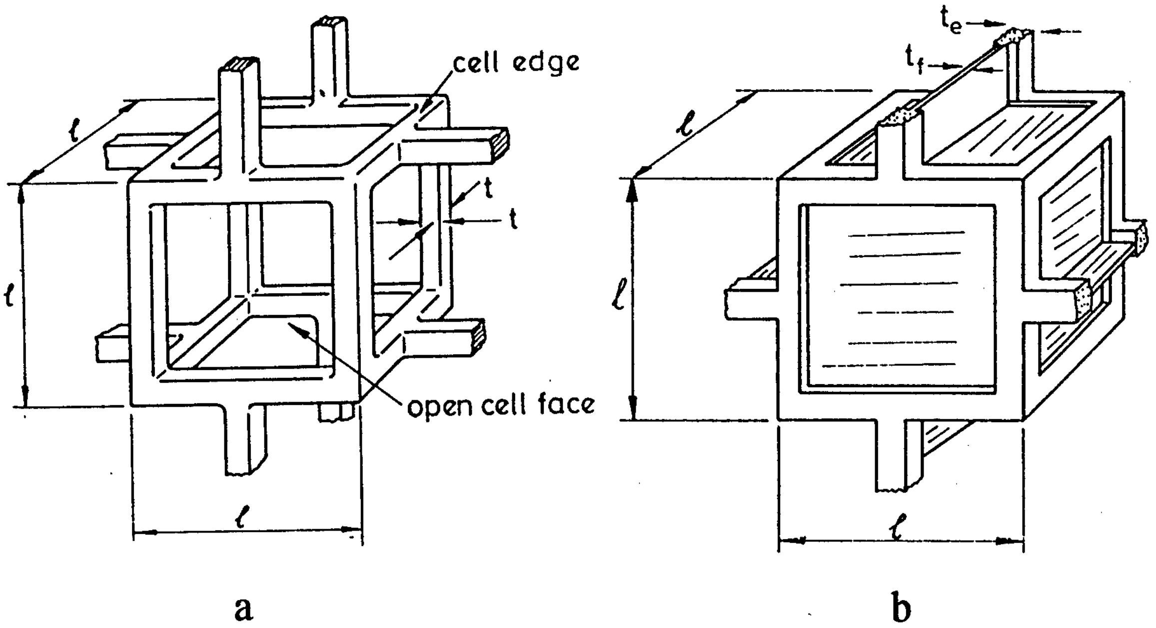

Figure 2.7 Schematics of (a) open and (b) closed cell foams.

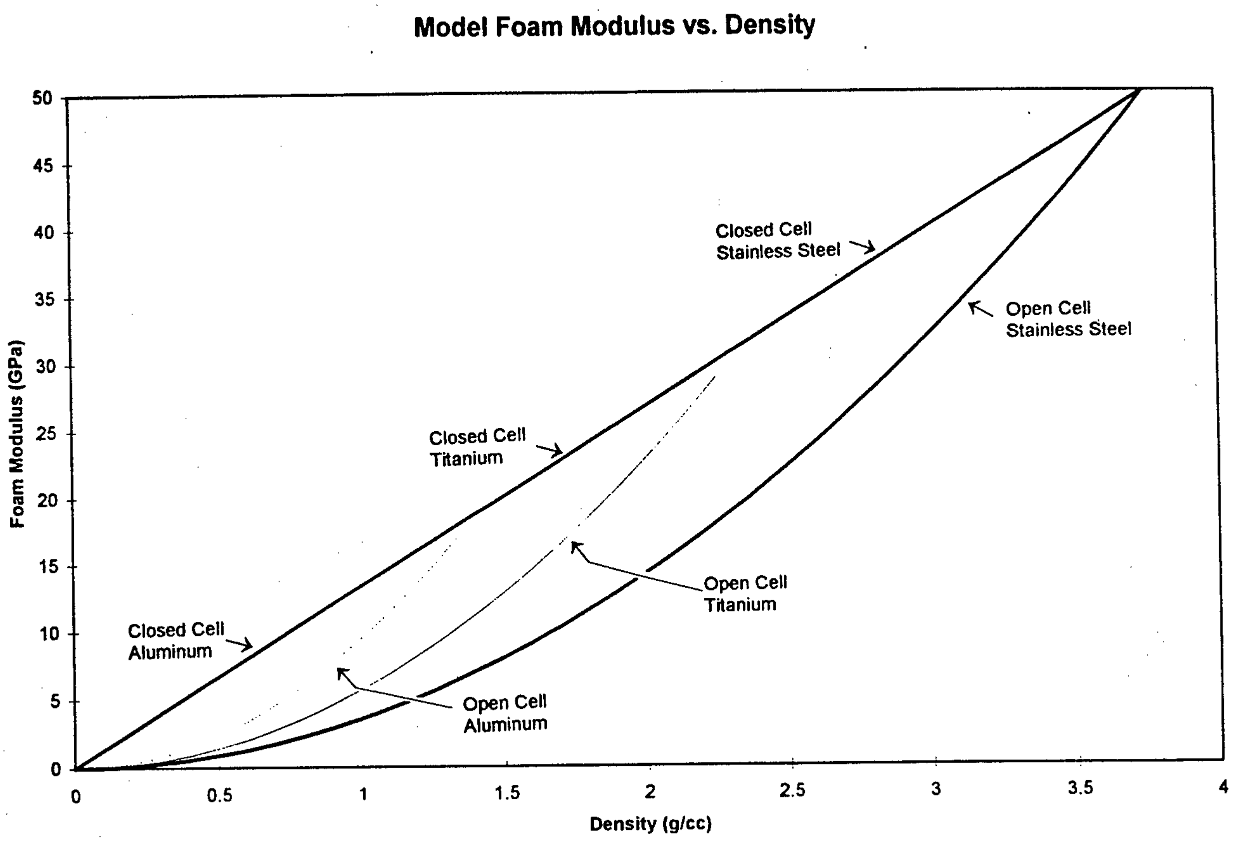

Figure 2.8 (a) The relationship between modulus and relative density of open and closed cell foams for stainless steel, titanium, and aluminum. After Gibson and Ashby.

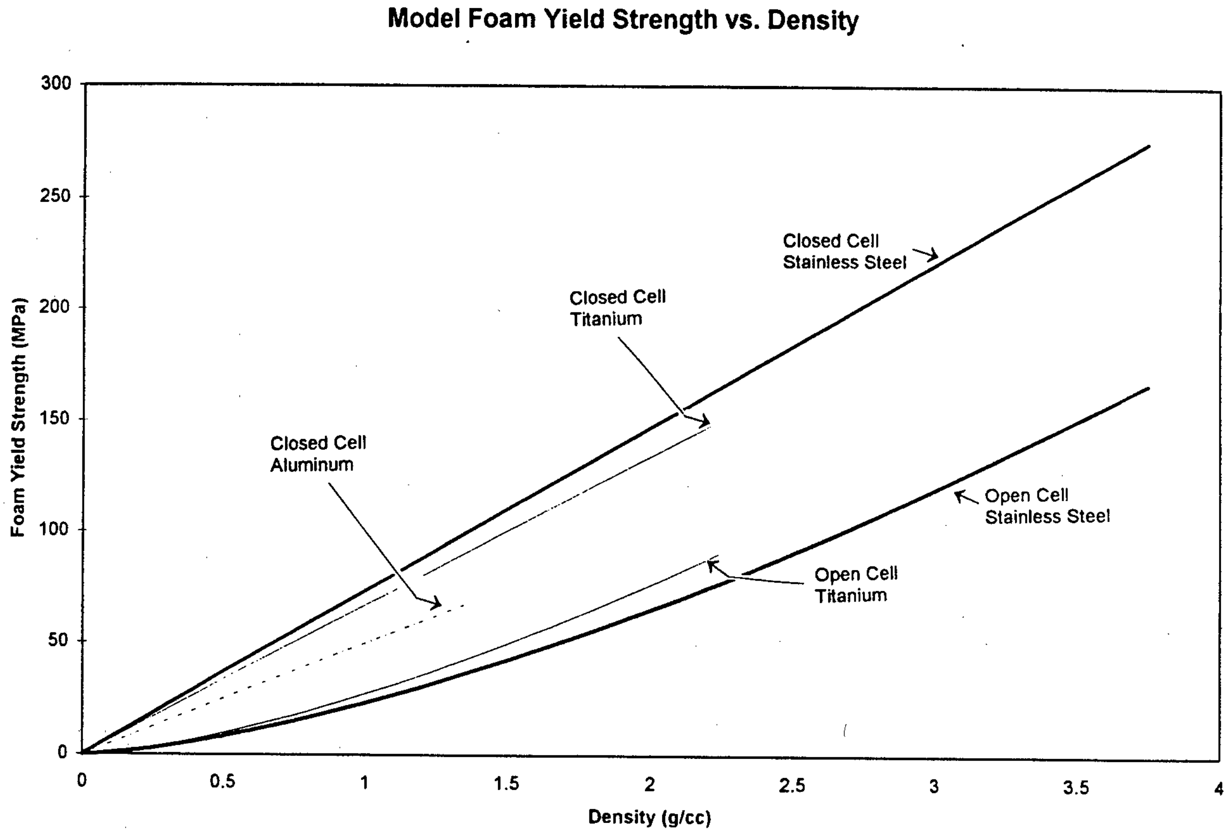

Figure 2.8 (b) The relationship between specific strength and relative density of open and closed cell foams for stainless steel, titanium, and aluminum. After Gibson and Ashby.

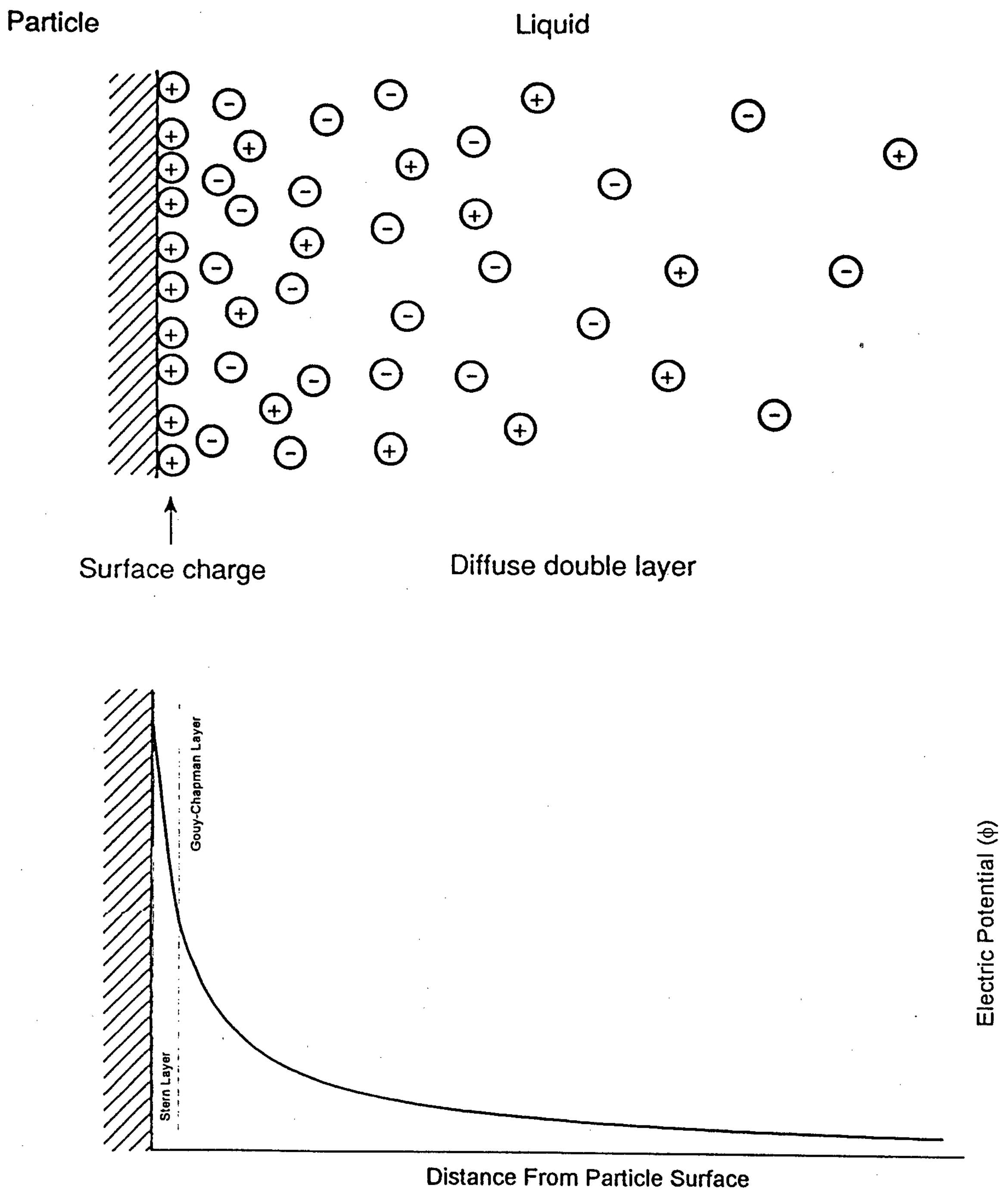

Figure 2.9 Schematics of (a) the electrical double layer and (b) the relationship between electrical potential and distance from the particle surface.

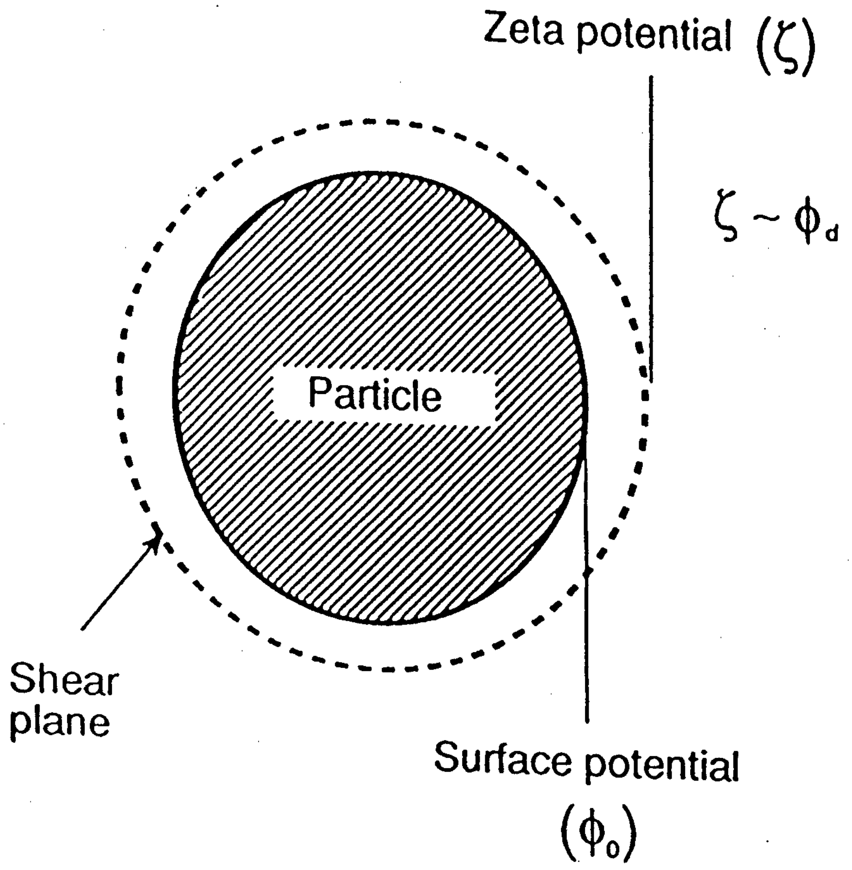

Figure 2.10 Schematic of ζ-potential.

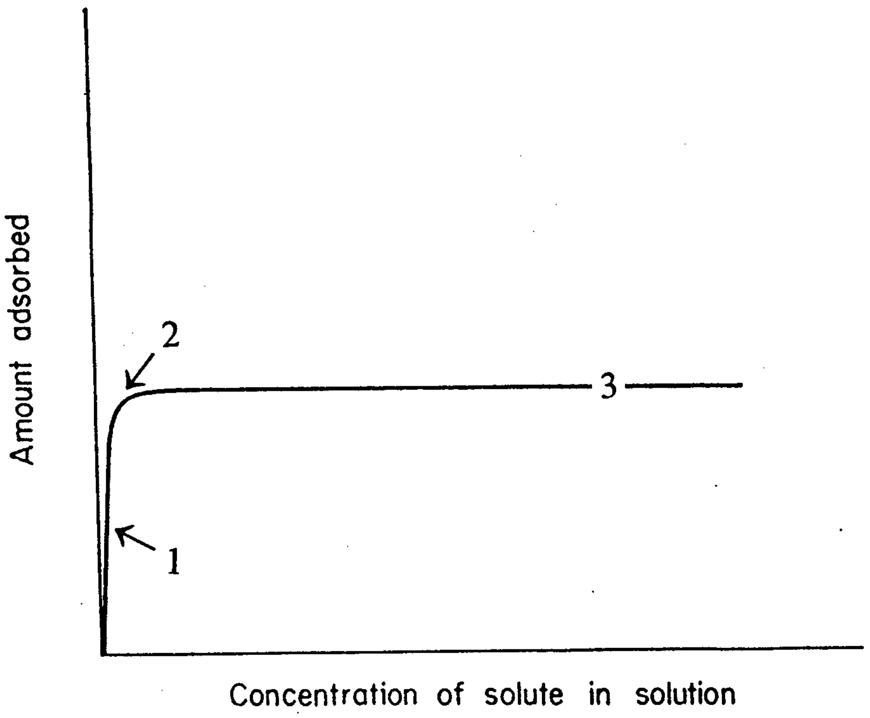

Figure 2.11 An adsorption isotherm for solids adsorbing solute from solution, showing a sharp knee and a clearly defined plateau.

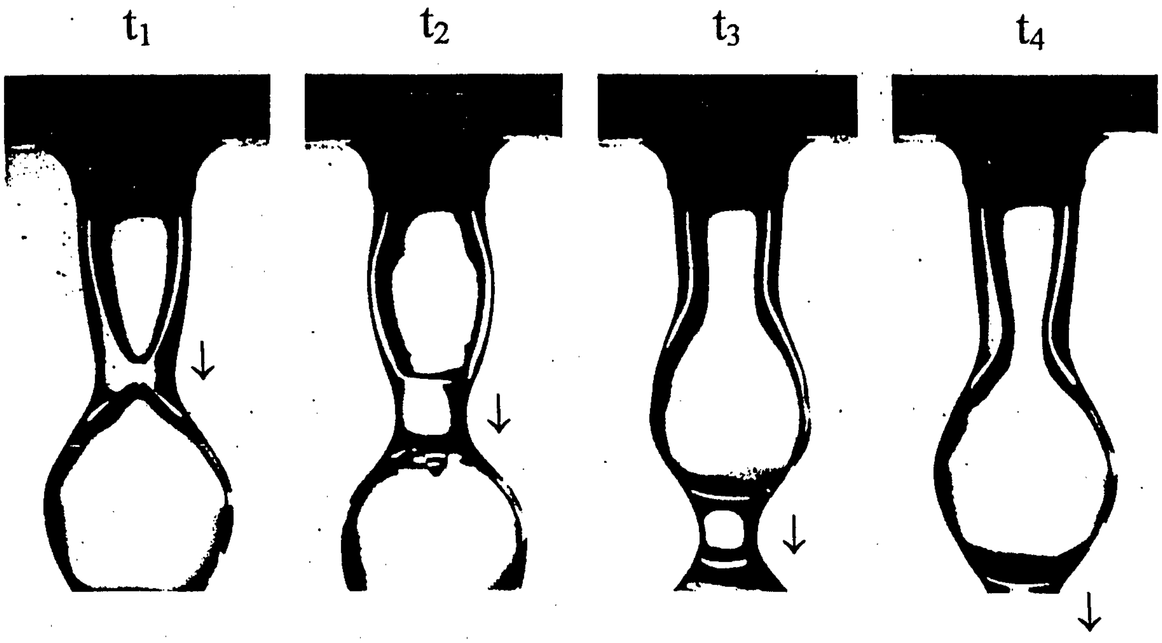

Figure 2.12 Hollow sphere blowing cycle.

CHAPTER III

EXPERIMENTAL PROCEDURE AND EQUIPMENT

Previous work involving the coaxial nozzle process suggests that the characteristics of titanium hydride and titanium alloy hydride powders are such that they can form slurries with the necessary rheological properties to blow hollow spheres. The advantage to sphere formation using TiH_2 is that Al, V, and additional master alloy powders can be added to the slurry in order to form spheres with a wide variety of alloy compositions. For example, 60Al-40V powder can be added to the appropriate amount of TiH_2 slurry to obtain Ti-6Al-4V alloy in fired spheres.

Titanium hydride powder is chemically stable at room temperature. It is safe to handle but should not be inhaled. If the hydride powder has sufficient surface area and has not been exposed to oxygen, a possible fire hazard may exist. The hydrogen present in TiH_2 is released at moderate temperatures and the remaining titanium begins to densify rapidly at and above 850 °C. Hydride powders can be purchased in bulk quantities, allowing the process to be easily scaled to an industrial production level.

III.1 Objective

The objective of the current work is to investigate the surface properties of TiH_2 and the interaction of polymer dispersants and binders with this surface. The ultimate goal is to disperse TiH_2 in acetone, forming slurries exhibiting the viscosity, drying characteristics, and repeatability necessary to form TiH_2 hollow spheres that become ductile titanium upon heat treating.

III.2 Materials

Hollow spheres are formed by premixing slurries of the desired sphere composition and forming spheres using the coaxial nozzle process. For optimum performance, powders must be in the 1 to 10 μm size range and be able to be dispersed in acetone.

Raw TiH_2 material as-received from Reading Alloys, Inc. contained particles as large as 1 mm and thus required a reduction in size before use in the coaxial nozzle process. The particles were ball milled in unreactive Bel-Art polymer containers backfilled with an ultra high purity (UHP, 99.999% pure) Ar atmosphere in a glove box. This inert atmosphere prevents the reaction of TiH_2 with undesirable contaminant gases such as oxygen and nitrogen during the milling process. Milling of each 250 g powder batch was achieved through action of 25 yttria-stabilized-zirconia (YSZ) milling balls, each ½ inch in diameter, for 64 hours. After 64 hours, size analysis confirmed that the powders ranged from 1 to 10 μm in diameter with an average particle size of 6 μm.

Several materials were evaluated as dispersants and binders for the preparation of TiH_2 slurries. Elvacite 2008 grade poly-methyl methacrylate (PMMA) was obtained from ICI Americas, Inc. (ICI). The molecular weight of this polymer, as described by the manufacturer, averages 25,000. PMMA is highly soluble in organic liquids such as acetone, and has polar functional groups following dissolution and ionization. Adsorption of PMMA onto powder surfaces from the solvent acts to sterically stabilize the slurry. Following the formation of hollow spheres, PMMA begins to evaporate leaving behind the PMMA. PMMA forms a tough, flexible film that yields sufficient strength to the green spheres that they may be collected and handled without damage. When the spheres are fired in an inert atmosphere, PMMA breaks down into the methyl methacrylate monomer and vaporizes between 200 and 430 °C, leaving no residue.

In some experiments, Dow Corning Z 6020 polysilane (ethylene diaminepropyl trimethoxysilane) was used to precoat the surface of the TiH_2 powder prior to the addition of acetone with the intent of forming better dispersions. This material has a density of 1.03 g/cm^3 and a molecular weight of 179.98 g/mol.

To work effectively, 5% polysilane was first dissolved in methanol and the solution mixed with the powder at a low shear rate. The methanol (CH_3OH) used was certified A.C.S. reagent grade with a residue of 0.2 ppm following evaporation. Methanol has a formula weight of 32.04 g/mol and a density of 0.79 g/cm^3 at room temperature. The methanol was allowed to evaporate completely and the resulting powder cake gently broken up using a mortar and pestle. For the remainder of this work, TiH_2 precursor powder prepared in this manner will be considered "polysilane treated TiH_2".

Ethyl cellulose (EC) and poly vinyl butyral (PVB) were also used in the attempts to disperse TiH_2. Hypermer PS3 from ICI was used in evaporation experiments to explain why PS3 exhibited appropriate characteristics for sphere formation and why the spheres made from these slurries would not dry properly. The effect of PS3 on the dispersion of TiH_2 was studied previous to this investigation. PS3 is a proprietary, polyester-polyamine copolymer with a density of 1.13 g/cm^3 at 25 °C. The melting temperature of PS3 is 48 °C and the vaporization temperature is 425 °C. The technical literature provided by ICI suggests the possible combustion products of PS3 as CO, CO_2, NO_X, and ammonia compounds.

Certified A.C.S. reagent grade acetone (CH_3COCH_3) from Fisher Scientific was used as the solvent for the polymer binders and dispersants, and as the carrier vehicle for the TiH_2 powder. Acetone is suitable for the process because it is inert with respect to the TiH_2 powder, polymer additives, and containers, and is highly volatile. The assay of the lots used showed water contents of 0.4% and a residue following evaporation of 200 ppm or 0.02%. Acetone has a formula weight of 58.08 g/mol and a density of 0.79 g/cm^3 at room temperature.

The attempt was made to getter the atmosphere of the furnace and reduce any oxides of titanium by using magnesium metal. The Mg used was obtained from Cerac, Inc. and had a particle size range of -200 +325 mesh (37 to 60 µm). The powder was certified as at least 99.6% pure.

III.3 Particle Size Analysis

To conduct particle size measurements, an aqueous suspension was prepared containing 1.0 vol.% powder. Agglomeration was prevented by adding several drops of Darvan 851, from R. T. Vanderbilt and by milling overnight with several mill balls.

A Leeds and Northrup Microtrac particle size analyzer, model 7997-20, was used to measure average particle size and particle size distributions of milled powders. The instrument was fitted with the small particle size (0.12 to 60 μm) option to measure powders in this size range. Three separate runs were averaged to obtain the final results.

III.4 Evaporation Rate

The evaporation rate of acetone from TiH_2 slurries stabilized with different dispersants was studied to evaluate the suitability of these dispersants for the coaxial nozzle process. Sample slurries of TiH_2 were prepared with a solids content of 35 vol.% and divided into 10 cm^3 sample volumes. The samples were dispersed with 3.0 wt.% 2008 grade PMMA, 3.0 wt.% PS3, a combination of 2.5 wt.% 2008 PMMA and 0.50 wt.% PS3, and a combination of polysilane treated TiH_2 with 1.0 wt.% Z 6020 polysilane and 2.0 wt.% 2008 grade PMMA. A standard of pure, reagent grade acetone was used for comparison.

The samples were placed in a circular pan 4.75 cm in diameter and 0.95 cm tall. The pan was positioned on a digital balance in a fume hood with a controlled flow rate of 0.5 m/s. Flowing air was used to simulate as closely as possible the environment of a falling sphere. Spheres typically fall from the nozzle to the conveyor at a rate approximately six times as fast as the moving air in the experiment leading to higher evaporation rates in the real scenario.

Readings were taken at 10 second intervals during the first 2 minutes and every minute thereafter for thirty minutes. Evaporation rate was obtained by dividing the mass lost through evaporation by the area of the evaporating surface (the area of the pan). The data is presented in one minute increments.

III.5 Hollow Sphere Fabrication

There are several steps that must be satisfied for the successful formation of highly uniform hollow spheres using the coaxial nozzle process. Because powders of different chemical compositions exhibit different surface characteristics, polymer additives that are satisfactory for some systems will not work with others. Slurry suitability for Ti spheres is dictated by the solids loading and degree of dispersion, the influence of polymer additives on rheology and the evaporation of acetone, and the minimization of impurities soluble in the metal lattice that serve to embrittle the foam. As a result, trials with different dispersants, binders, and if necessary, combinations of these must be investigated.

III.5.1 Slurry Preparation

Slurries are prepared by weighing the batch ingredients on an electronic balance. First, the acetone, polymer additives, and YSZ milling balls are placed into Nalgene bottles. The typical amount of polymer added to the mixture is 3 wt.% of the solids in the slurry. This amount may be higher or lower depending on the dispersion efficiency of the polymer system used. To ensure full dissolution of the polymer, the mixture is milled for fifteen minutes at room temperature. Experience dictates that a slurry with a solids content of between 40 and

50 vol.% is most likely to successfully process into hollow spheres. The slurry is subsequently milled for 24 hours to ensure uniformity and deagglomeration.

III.6 Viscosity Measurements

Before a slurry is blown into hollow spheres, the viscosity of the dispersion is characterized. Thus the effect of polymer additives, slurry solids loading, and shear rate on viscosity can be measured. A Brookfield LV type viscometer with associated cylindrical spindles was used in the viscosity measurements. The rotation rate of the spindles could be changed to yield information about the effect of shear rate on viscosity. The shear rates used were 12.6, 6.3, and 2.5 sec^{-1}. Measurements were calibrated using Brookfield silicone oil viscosity standards.

III.7 Dispersion Stability

Electrokinetic potential, also known as zeta potential (ζ) was measured using a Coulter DELSA 440SX Electrophoretic Mobility unit. This device measures mobility through Laser Doppler Velocimetry (LDV). The motion of individual powder particles is measured in a known electric field and is directly related to the ζ-potential by the Hückel equation..

Samples are made by preparing a dilute suspension in acetone containing no more than 5 vol.% TiH_2 powder. Inside the instrument, the suspension is illuminated by a 5 mW He-Ne laser at a wavelength of 632 nm. The light is scattered at several different angles and compared to a reference beam to determine the Doppler shift. The Doppler shift is a function of angle and particle velocity. The ζ-potential of TiH_2 powder in the presence of several adsorbed polymer additives was evaluated. The ζ-potential was measured at 4 angles; 8.7°, 17.2°, 25.8°, and 34.5°. The values reported are the average of the ζ-potentials obtained at each of the four angles.

III.8 Adsorption Experiments

To construct adsorption isotherms of polysilane on TiH_2 powder, dispersions were prepared with solid contents of 30 vol.%. These lower concentrations were used so that adequate amounts of acetone and polymer would be available for adsorption and so the slurry would flow easily during mixing and so enough supernatant would be available for analysis after centrifuging. The original polysilane concentrations ranged from 0 wt.% to 10 wt.% of the TiH_2 powder.

Adsorption of polysilane onto TiH_2 powder was evaluated by using the treatment method described in III.2. Approximately 10 cm^3 of slurry was placed into Falcon 15 cm^3 conical centrifuge tubes from Becton Dickinson and Company. These samples were centrifuged at between 1000 and 5000 RPM for fifteen minutes. After this time, the supernatant fluid was free of TiH_2 particles. A small amount of the supernatant was withdrawn using a syringe. The index of refraction (n) of these solutions was measured using an Abbe refractometer, model 10450 manufactured by American Optical. Six to ten drops were sufficient to gain accurate results while not significantly changing the experiment. The remaining fluid was returned to the appropriate centrifuge tube.

Standard solutions of acetone with known concentrations of polysilane were prepared to use in the determination of the amount of adsorbed polysilane. This calibration curve can be found in Figure 3.1. The indices of refraction of these solutions were measured together with the slurry samples to eliminate any effects of the refractometer and temperature fluctuations. The polysilane concentrations were measured with respect to the powder in the slurry samples and with respect to the acetone in the calibration standards. It is therefore necessary to calculate the concentration of polysilane with respect to acetone assuming zero adsorption (all polysilane added to the powder is desorbed and in solution). The concentration found using the calibration curve can then be subtracted from this value, yielding the amount of adsorbed polysilane. Dividing by the mass of powder present gives the adsorbed polysilane in mg/g powder. These concentrations are the equilibrium concentrations of adsorption and thus apply to any amount of powder. The adsorption isotherm is plotted as a function of equilibrium concentration.

III.9 Visual Inspection

Two types of analysis were used in the quantitative determination of batch quality. Visual inspection, a non-destructive tool, was used to determine the presence of several types of flaws in green spheres. The frequency of spheres containing tails, dimples, cracks, pinholes, and cracked holes was determined, as well as sphere continuity.

Ideally, each batch of spheres should contain no defects. This expectation is unrealistic however, when considering the large number of variables involved in the sphere formation process and the high frequency of sphere formation. Inspection of a fraction of the batch can be used as a judge of the quality of the entire batch, providing the sample is taken randomly. Lot quality refers to some measurable or countable property of the hollow spheres.

A single-sampling plan was used. This plan is based on the combination of an acceptable quality level (AQL) and an associated sample size. Several sampling plans have become standard in industry. Amongst the most widely used is Military Standard 105D (MIL-STD-105D). This standard has three quality levels, of which level II is normally chosen. Level I uses smaller sample sizes and level III uses larger sample sizes than level II. The master table for single sampling from MIL-STD-105D can be found in Table 3.1 (32).

Typical slurry batch sizes of 150 cm^3 take approximately 5 minutes to be completely processed into hollow spheres. At a frequency of 4,000 spheres/min, this results in the formation of 20,000 spheres from each batch. This corresponds to code letter M from MIL-STD-105D, associated with a lot size between 10,001 and 35,000 and general inspection level II. To satisfy the standard, samples of 315 spheres were taken from each batch for defect evaluation.

Because the net effect of sphere flaws in titanium foams remains unknown, no specific AQL can as yet be set for each defect. Instead, the attempt is made to find the quality level for each defect in each batch and adjust process variables to improve these quality levels.

III.10 Digital Analysis

Digital analysis is a destructive analysis tool that can be used to quantify the wall thickness uniformity of individual fired spheres. Digital analysis can be used regardless of the ductility of the spheres. Approximately twenty titanium spheres were mounted in 1 ¼ inch diameter mounts using spray adhesive and Leco two-part epoxy resin. The spheres were subsequently sectioned and polished to half their original diameter.

A Reichart optical microscope, model MeF3A, was used to obtain bright field images of individual spheres. The contrast between the reflective metallic spheres and the mounting material is high, allowing easy differentiation between the two. A high resolution Hitachi CCD camera, model KP-M2U was attached to a port on the microscope using a C-mount. The microscope was set to the lowest magnification that allowed the sphere to completely fill the field of view of the camera, 2.5x, 5x, or 8x depending on the diameter of the sphere cross section. The signal was captured as a still image using a 16 bit ISA ComputerEyes/1024 video digitizer adapter card. The hardware provided images 640 x 480 pixels in size. These images could be manipulated in Adobe Photoshop and converted to grayscale images if necessary to more easily use the measurement software.

Software code, written in Visual Basic by Dr. Robert Speyer, was used for the measurement of wall thickness. Each pixel in a grayscale image is assigned an intensity value from 0 to 255. Pixels that are entirely black have a value of 0 and those that are entirely white have a value of 255. On the captured video images, sphere walls appear much brighter than the background because of their metallic character. By choosing a threshold brightness value between that of the lowest pixel value of the sphere wall and highest pixel value of the mounting material, it is possible to select only the material in the sphere wall. It is sometimes necessary to edit the image to remove bright portions of the mounting material. The software provides a preview function to prevent the selection of extraneous pixels. Upon completion of the threshold utility, the sphere wall appears entirely in green against a red background.

To conduct measurements, an algorithm first finds the center of mass of the green color. This is taken as the sphere center. The measurement of sphere wall thickness occurs at

1° intervals. A line extends through the red background and begins counting the number of green pixels encountered, stopping the count when the red on the outside of the sphere is reached. Through knowledge of the image magnification, the pixel dimensions can be determined, and from this the true sphere wall thickness can be found. A schematic of this process can be found in Figure 3.2.

III.11 Powder x-ray Diffraction

A θ - 2θ type automated powder x-ray diffractometer, model PW1800 by Philips Electronic Instruments, Inc. was used for crystallographic examination. The machine generates CuKα x-rays at a wavelength of 1.5406 Å which are diffracted by the sample and processed by a Xe gas proportional detector moving in the vertical plane. The diffractometer was used to identify the presence of phases as well as to conduct fine lattice parameter measurements.

III.12 Lattice Parameter Measurements

To determine accurately the hexagonal lattice parameters a_o and c_o for fired titanium, and thus estimate the impurity content, Cohen's method was used (33). The best method of determining lattice parameter involves calculating values of a_o and c_o at each reflection and plotting these against a correction function. Systematic errors associated with the diffractometer can be removed by using the proper extrapolation function. Random errors can be reduced by taking the linear regression of the data. The Nelson-Riley equation (1) defines this extrapolation function.

$$\frac{\Delta d}{d} = k\left(\frac{\cos^2\theta}{\sin\theta} + \frac{\cos^2\theta}{\theta}\right) \tag{1}$$

By squaring Bragg's law (2), taking the logarithm, and rearranging terms, the result is (3).

$$\lambda = 2d\sin\theta \tag{2}$$

$$\ln\sin^2\theta = \ln\left(\frac{\lambda^2}{4}\right) - 2\ln d \tag{3}$$

By taking the derivative of (3), another expression for $\Delta d/d$ can be formulated (4).

$$\frac{\Delta d}{d} = \frac{-\Delta\sin^2\theta}{2\sin^2\theta} \tag{4}$$

This can be substituted into (1) to arrive at the error in ($\sin^2\theta$) with respect to θ (5). D is a new constant that takes into account k and other constants introduced in the mathematics.

$$\Delta \sin^2\theta = D\sin^2 2\theta\left(\frac{1}{\sin\theta}+\frac{1}{\theta}\right) \tag{5}$$

The true value of $(\sin^2\theta)$ for each diffraction line is given by (6). This equation includes the true lattice parameters a_o and c_o.

$$\sin^2\theta = \frac{\lambda^2}{3a_o^{\,2}}\left(h^2+hk+k^2\right)+\frac{\lambda^2}{4c_o^{\,2}}\left(l^2\right) \tag{6}$$

The difference between the observed $(\sin^2\theta)$ and the true $(\sin^2\theta)$ is $(\Delta \sin^2\theta)$, and so it is possible to obtain (7) by substitution. From (7) the true lattice constants can be determined by solving three simultaneous equations using Cramer's rule. For simplification of the mathematics, equation (7) is broken into six separate parts (7a-f).

$$0 = \frac{\lambda^2}{3a_o^{\,2}}\left(h^2+hk+k^2\right)+\frac{\lambda^2}{4c_o^{\,2}}\left(l^2\right)+D\sin^2 2\theta\left(\frac{1}{\sin\theta}+\frac{1}{\theta}\right) \tag{7}$$

$$A = D \tag{7a}$$

$$B = \frac{\lambda^2}{4c_o^{\,2}} \tag{7b}$$

$$C = \frac{\lambda^2}{3a_o^{\,2}} \tag{7c}$$

$$\alpha = \left(h^2 + hk + k^2\right) \quad (7d)$$

$$\gamma = \left(l^2\right) \quad (7e)$$

$$\delta = \sin^2 2\theta\left(\frac{1}{\sin\theta} + \frac{1}{\theta}\right) \quad (7f)$$

By solving the simultaneous equations (8-10) for *A*, *B*, and *C*, it is possible to find the lattice parameters a_o and c_o, using the relations in (11) and (12), respectively.

$$\Sigma\, \alpha \sin^2\theta = C\, \Sigma\, \alpha^2 + B\, \Sigma\, \alpha\gamma + A\, \Sigma\, \alpha\delta \quad (8)$$

$$\Sigma\, \gamma \sin^2\theta = C\, \Sigma\, \alpha\gamma + B\, \Sigma\, \gamma^2 + A\, \Sigma\, \gamma\delta \quad (9)$$

$$\Sigma\, \delta \sin^2\theta = C\, \Sigma\, \alpha\delta + B\, \Sigma\, \gamma\delta + A\, \Sigma\, \delta^2 \quad (10)$$

$$c_o = \sqrt{\frac{\lambda^2}{4B}} \quad (11)$$

$$a_o = \sqrt{\frac{\lambda^2}{3C}} \quad (12)$$

The JCPDS card for Ti, found in Figure 3.3 (a) was used in conjunction with a rapid scan from 15 to 155 °2θ (step size 0.015 °2θ for a 1.25 sec hold) to choose peaks that were well defined and free from other nearby peaks (34). In the lattice parameter analysis, the twelve most intense diffraction peaks from Ti metal were used. A list of the peaks used in the analysis can be found in Figure 3.3 (b). Scans of each peak are made over a 3 °2θ range with a step size of 0.015 °2θ. The hold time varies such that the number of counts generated by each peak is a constant. For example, a peak of 10% relative intensity will have a hold time 10 times greater than the 100% peak. This process yields statistically significantly data for use in the Nelson-Riley equation.

In this investigation, a sample of ductile titanium metal sheet, ASTM grade 2 was used as a standard. Dry pressed pellets, each ¾ of an inch in diameter and pressed at 8000 psi, were made containing pure TiH_2 powder and TiH_2 powder with 3 wt.%, 5 wt.%, and 10 wt.% magnesium powder. No additives of any kind were used in the preparation of the pellets. The pellets were fired in vacuum to 1000 °C and the lattice parameters of the samples determined using the method previously described. Brittle spheres were also analyzed to determine approximate levels of contamination.

III.13 Electron Microscopy

An Hitachi scanning electron microscope (SEM), model.S800 and equipped with a field emission gun electron source, was used for photographing spheres because of the large depth of field of the instrument.

Table 3.1 The master table for single sampling from MIL-STD-105D.

Sample size code letter	Sample size	Acceptable quality levels (normal inspection)																									
		0.010	0.015	0.025	0.040	0.065	0.10	0.15	0.25	0.40	0.65	1.0	1.5	2.5	4.0	6.5	10	15	25	40	65	100	150	250	400	650	1000
		Ac Re	Ac Re	Ac Re	Ac Re	Ac Re	Ac Re	Ac Re	Ac Re	Ac Re	Ac Re	Ac Re	Ac Re	Ac Re	Ac Re	Ac Re	Ac Re	Ac Re	Ac Re	Ac Re	Ac Re	Ac Re	Ac Re	Ac Re	Ac Re	Ac Re	Ac Re
A	2	↓	↓	↓	↓	↓	↓	↓	↓	↓	↓	↓	↓	↓	↓	0 1	↓	↓	1 2	2 3	3 4	5 6	7 8	10 11	14 15	21 22	30 31
B	2	↓	↓	↓	↓	↓	↓	↓	↓	↓	↓	↓	↓	↓	0 1	↑	↓	1 2	2 3	3 4	5 6	7 8	10 11	14 15	21 22	30 31	44 45
C	5	↓	↓	↓	↓	↓	↓	↓	↓	↓	↓	↓	↓	0 1	↑	↓	1 2	2 3	3 4	5 6	7 8	10 11	14 15	21 22	30 31	44 45	↑
D	8	↓	↓	↓	↓	↓	↓	↓	↓	↓	↓	↓	0 1	↑	↓	1 2	2 3	3 4	5 6	7 8	10 11	14 15	21 22	30 31	44 45	↑	↑
E	13	↓	↓	↓	↓	↓	↓	↓	↓	↓	↓	0 1	↑	↓	1 2	2 3	3 4	5 6	7 8	10 11	14 15	21 22	30 31	44 45	↑	↑	↑
F	20	↓	↓	↓	↓	↓	↓	↓	↓	↓	0 1	↑	↓	1 2	2 3	3 4	5 6	7 8	10 11	14 15	21 22	↑	↑	↑	↑	↑	↑
G	32	↓	↓	↓	↓	↓	↓	↓	↓	0 1	↑	↓	1 2	2 3	3 4	5 6	7 8	10 11	14 15	21 22	↑	↑	↑	↑	↑	↑	↑
H	50	↓	↓	↓	↓	↓	↓	↓	0 1	↑	↓	1 2	2 3	3 4	5 6	7 8	10 11	14 15	21 22	↑	↑	↑	↑	↑	↑	↑	↑
J	80	↓	↓	↓	↓	↓	↓	0 1	↑	↓	1 2	2 3	3 4	5 6	7 8	10 11	14 15	21 22	↑	↑	↑	↑	↑	↑	↑	↑	↑
K	125	↓	↓	↓	↓	↓	0 1	↑	↓	1 2	2 3	3 4	5 6	7 8	10 11	14 15	21 22	↑	↑	↑	↑	↑	↑	↑	↑	↑	↑
L	200	↓	↓	↓	↓	0 1	↑	↓	1 2	2 3	3 4	5 6	7 8	10 11	14 15	21 22	↑	↑	↑	↑	↑	↑	↑	↑	↑	↑	↑
M	315	↓	↓	↓	0 1	↑	↓	1 2	2 3	3 4	5 6	7 8	10 11	14 15	21 22	↑	↑	↑	↑	↑	↑	↑	↑	↑	↑	↑	↑
N	500	↓	↓	0 1	↑	↓	1 2	2 3	3 4	5 6	7 8	10 11	14 15	21 22	↑	↑	↑	↑	↑	↑	↑	↑	↑	↑	↑	↑	↑
P	800	↓	0 1	↑	↓	1 2	2 3	3 4	5 6	7 8	10 11	14 15	21 22	↑	↑	↑	↑	↑	↑	↑	↑	↑	↑	↑	↑	↑	↑
Q	1250	0 1	↑	↓	1 2	2 3	3 4	5 6	7 8	10 11	14 15	21 22	↑	↑	↑	↑	↑	↑	↑	↑	↑	↑	↑	↑	↑	↑	↑
R	2000	↑	↑	1 2	2 3	3 4	5 6	7 8	10 11	14 15	21 22	↑	↑	↑	↑	↑	↑	↑	↑	↑	↑	↑	↑	↑	↑	↑	↑

↓ = Use first sampling plan below arrow. If sample size equals, or exceeds, lot or batch size, do 100 percent inspection.

↑ = Use first sampling plan above arrow.

Ac = Acceptance number.
Re = Rejection number.

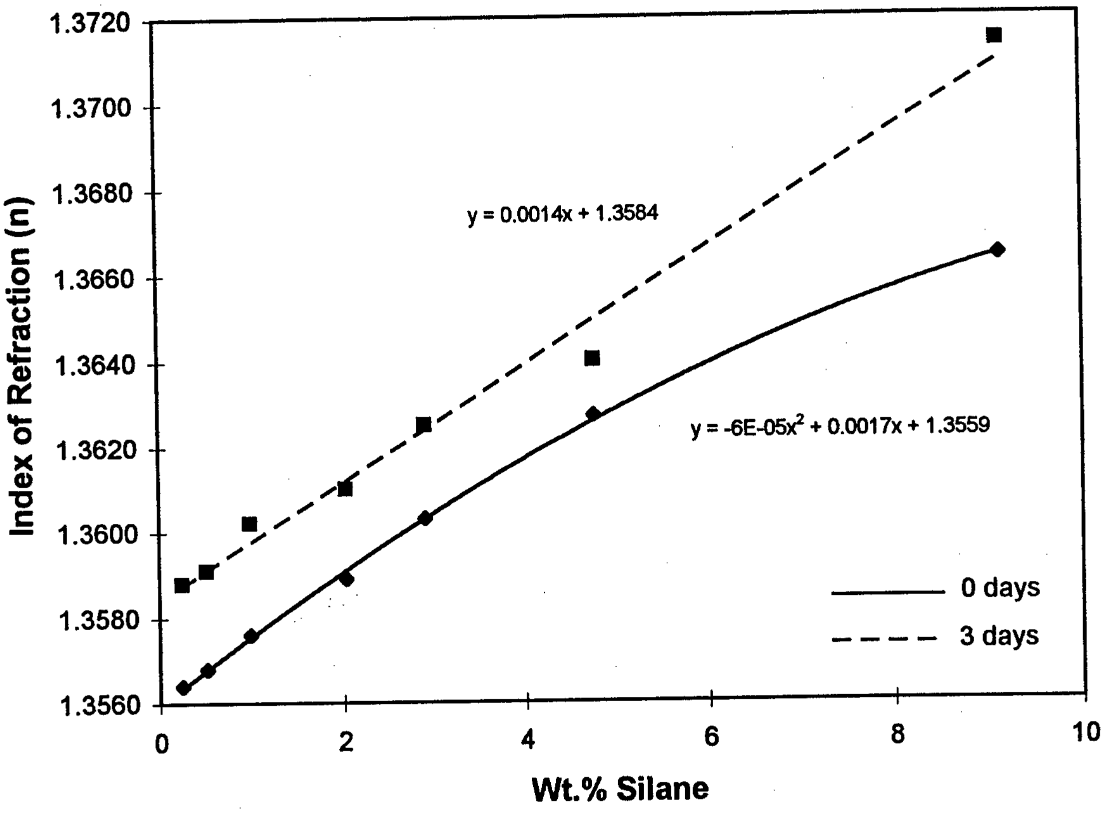

Figure 3.1 Calibration relationship for index of refraction and the concentration of polysilane in acetone solution.

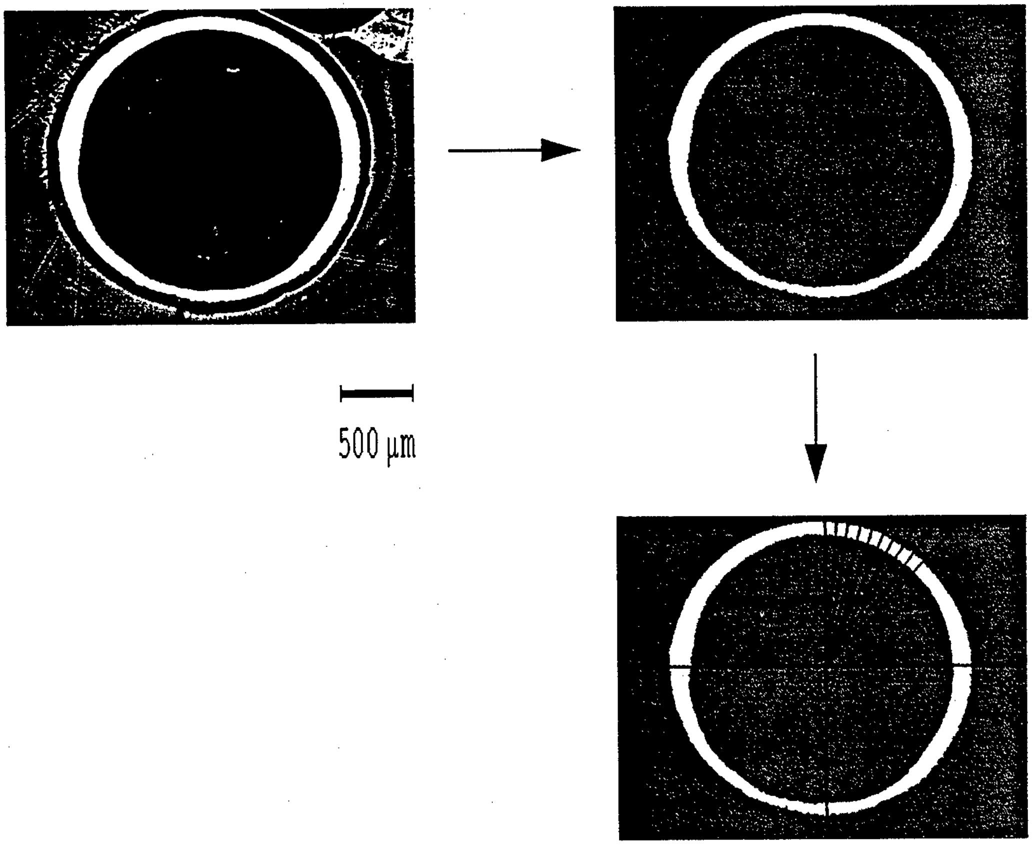

Figure 3.2 A schematic of the process used to determine sphere wall thickness.

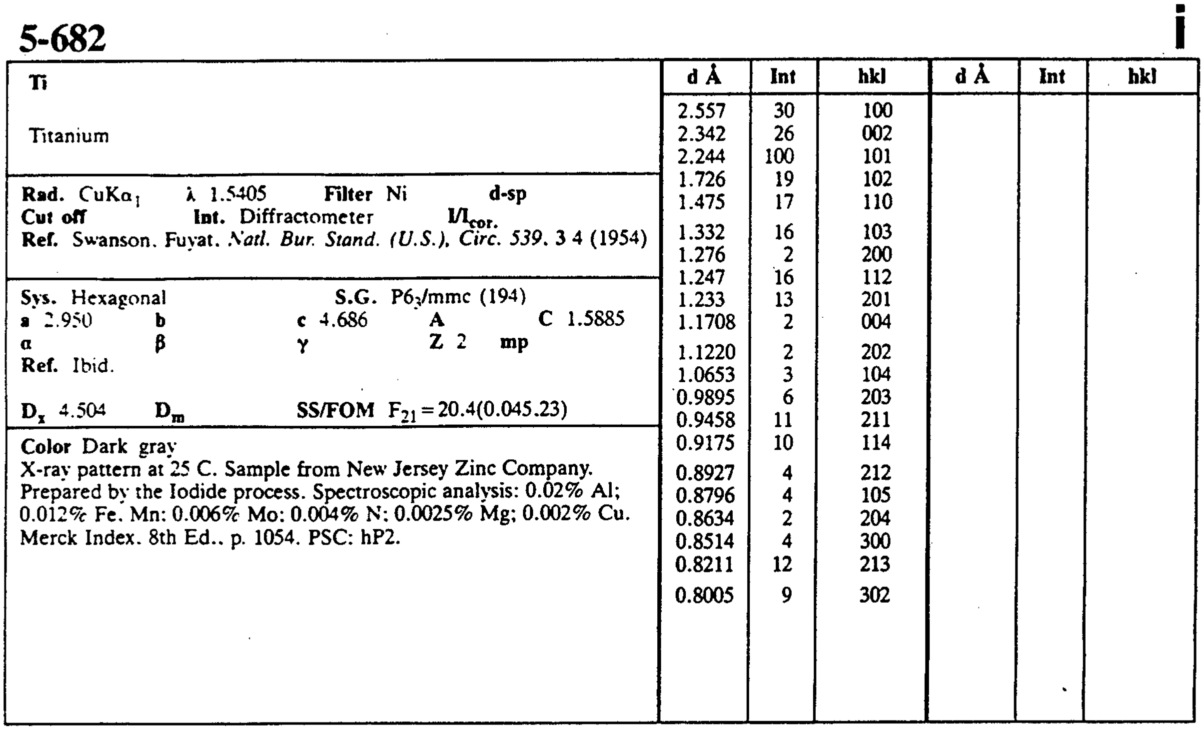

5-682 i

Ti

Titanium

Rad. $CuK\alpha_1$ **λ** 1.5405 **Filter** Ni **d-sp**
Cut off **Int.** Diffractometer **$I/I_{cor.}$**
Ref. Swanson. Fuyat. *Natl. Bur. Stand. (U.S.), Circ. 539*. 3 4 (1954)

Sys. Hexagonal **S.G.** $P6_3/mmc$ (194)
a 2.950 **b** **c** 4.686 **A** **C** 1.5885
α **β** **γ** **Z** 2 **mp**
Ref. Ibid.

D_x 4.504 **D_m** **SS/FOM** $F_{21} = 20.4(0.045.23)$

Color Dark gray
X-ray pattern at 25 C. Sample from New Jersey Zinc Company. Prepared by the Iodide process. Spectroscopic analysis: 0.02% Al; 0.012% Fe. Mn: 0.006% Mo: 0.004% N: 0.0025% Mg; 0.002% Cu. Merck Index. 8th Ed.. p. 1054. PSC: hP2.

d Å	Int	hkl	d Å	Int	hkl
2.557	30	100			
2.342	26	002			
2.244	100	101			
1.726	19	102			
1.475	17	110			
1.332	16	103			
1.276	2	200			
1.247	16	112			
1.233	13	201			
1.1708	2	004			
1.1220	2	202			
1.0653	3	104			
0.9895	6	203			
0.9458	11	211			
0.9175	10	114			
0.8927	4	212			
0.8796	4	105			
0.8634	2	204			
0.8514	4	300			
0.8211	12	213			
0.8005	9	302			

a

b

d (Å)	Intensity	h k l
2.557	30	1 0 0
2.342	26	0 0 2
2.244	100	1 0 1
1.726	19	1 0 2
1.475	17	1 1 0
1.332	16	1 0 3
1.247	16	1 1 2
1.233	13	2 0 1
0.9458	11	2 1 1
0.9175	10	1 1 4
0.8211	12	2 1 3
0.8005	9	3 0 2

Figure 3.3 (a) The JCPDS card for Ti metal and (b) the peaks used in the lattice parameter measurement.

CHAPTER IV

RESULTS AND DISCUSSION

Previous work to fabricate titanium hollow spheres (19) characterized precursor powders of TiH_2, Ti-6Al-V hydride, vanadium hydride, and master alloys 60Al-40V and 35Al-65V. XRD, SEM, chemical analysis, particle size, density, surface area measurements, and thermal analysis techniques were used in the characterization of the spheres. Various polymer systems were evaluated for their effectiveness in dispersing TiH_2-acetone slurries.

For this study, many of these techniques were used in conjunction with viscosity measurements, evaporation rate data, zeta potential, adsorption behavior, uniformity analysis, and lattice parameter measurements in an effort to produce uniform geometry TiH_2 powder hollow spheres and subsequently, ductile titanium. The data from these experiments was used to formulate an ideal TiH_2-acetone precursor slurry and obtain uniform hollow Ti spheres.

IV.1 Powder Characterization

Previous work determined dry ball milling to be the most efficient method of reducing the particle size of TiH_2 powder. This method is beneficial because milling in a protective Ar atmosphere prevents the introduction of chemical contaminants, particularly oxygen and nitrogen. The brittle nature of TiH_2 allows it to be fractured easily on impact. The hydride required finer grinding because as received TiH_2 material had a particle size distribution between 2 and 100 μm with an average particle diameter of 27 μm. The coaxial nozzle process requires a much smaller particle size range and average particle size than those found in the commercially available titanium hydride. For optimum performance, the bulk of the particle size distribution should be between 1 and 10 μm and an average diameter of between 4 and 7 μm is required. The hydride was dry ball milled for a wide time range and a comparison of TiH_2 particle size distributions with milling time can be found in Figure 4.1. The distributions in the figure, labeled 1 to 6 from right to left, correspond to 24 hour milling increments. After the first 24 hours, particle size distributions changed slowly with time, as shown in Figure 4.2. Therefore, 64 hours was established as the grinding time for future work. This provided a reproducible and sufficiently small particle size for sphere formation.

IV.2 Dispersion of TiH_2 in Acetone

The viscosity of the acetone slurry to be processed into hollow spheres is one of the most important variables in the process. The viscosity of TiH_2 powder dispersed in acetone with a number of polymer systems was studied. The polymers investigated included poly vinyl butyral (PVB), ethyl cellulose (EC), poly-methyl methacrylate (PMMA), Pavebond, PS3, and polysilane.

PS3 was used in previous work (19) to disperse TiH_2, resulting in viscosities below 100 mPa·sec at concentrations of 5.0 wt.% and slurry solids contents as high as 55 vol.%. PMMA at a concentration of 3.0 wt.% did not disperse TiH_2, producing a viscosity minimum of 330 mPa·sec at the relatively low solids content of 35 vol.%. However, by adding 0.70 wt.% PS3 and 3.0 wt.% 2008 PMMA to a 52 vol.% TiH_2 slurry, the viscosity was reduced to 100 mPa·sec and it was possible to form hollow spheres. These spheres remained moist on the conveyor belt, causing them to sag and deform. The diameter and wall thickness uniformity of the sphere batch of this composition was relatively poor. Because of the acetone evaporation problem caused by PS3, a search was made for a dispersant which did not affect drying.

TiH_2 is difficult to disperse in acetone because of the negative surface charges involved. The negative charge on the surface of TiH_2 may be due to hydrogen vacancies caused by nonstoichiometry. This results in the inability of several anionic polymers to disperse TiH_2 powder. The negative surface charge in acetone was demonstrated by the measurement of negative ζ-potentials in the -100 mV range. Furthermore, the surface potentials reported for the chemisorption of H_2 on the transition metals are all negative (35). Large potentials arise from the dielectric constant of acetone, which is approximately 4 times lower than that of water. Experience with acetone slurries of materials having negative surface charges is also minimal, as powders used so far in the coaxial nozzle process have all been positively charged.

The negative charge present on the surface of TiH_2 in acetone was reversed through silylation. In this process, a polysilane coupling agent is covalently bonded to the surface of the hydride through a hydrolysis reaction. The polysilane reacts with $(OH)^-$ groups in solution and on the surface of the TiH_2 powder, forming methanol and water. The oxygen is then free to bond the polymer molecule to the surface of the powder via the silane group as can be seen in Figure 4.3.

After treating the TiH_2 powder with polysilane, the two nitrogen groups lend a positive charge to the polymer molecule extended into the acetone. Thus, the surface charge of the particle-polysilane complex is positive. This allows dispersion of particles having a positive surface charge with polymers such as 2008 PMMA. By treating TiH_2 powder with 1.0 wt.% polysilane coupling agent and adding 3.0 wt.% 2008 PMMA, a slurry with a solids loading of 45 vol.% was made having a viscosity of 36.8 mPa·sec. This slurry also formed highly uniform hollow spheres and the spheres dried well in free fall from the nozzle. A comparison of the viscosity of different concentrations of TiH_2 dispersed with 1.0 wt.% polysilane treated powder and 3.0 wt.% 2008 PMMA with slurries dispersed solely with 2008 PMMA and PS3 can be found in Figure 4.4.

In the search for a suitable dispersant, alternatives to polysilane were screened by preparing small scale settling experiments. Dilute suspensions were prepared with several polymer systems and the settling rate qualitatively studied. Longer settling times for a dilute suspension suggest that the polymer system may be capable of dispersing a concentrated slurry. From these settling experiments, it can be qualitatively determined which polymers have the possibility of dispersing concentrated powder slurries. The composition of the suspensions prepared in this investigation and their relative rank is presented in Table 4.1.

It was found that of the polymer systems investigated, EC and EC with Pavebond had the greatest potential to disperse TiH_2. Unfortunately when tested on concentrated slurries, none of the polymer systems showing dispersing potential provided low viscosity systems using ethyl cellulose. At a solids content of 40 vol.%, a minimum viscosity of 2000 mPa·sec was observed at a concentration of 0.45 wt.% EC. The change in viscosity over a range of EC concentrations for a 35 vol.% TiH_2 slurry can be found in Figure 4.5.

Pavebond, an asphalt additive, was completely ineffective in the dispersion of TiH_2. Pavebond has been used successfully in dispersing oxides such as SiO_2 in acetone. A dispersion with a solids content of 35 vol.% was prepared and the concentration of Pavebond changed between 0.40 wt.% and 2.5 wt.%. The viscosity held constant at near 1000 mPa·sec throughout the entire range.

From the settling rate experiment, PVB also appeared to be a viable dispersant for TiH_2. At a solids loading of 35 vol.%, a viscosity low enough to form hollow spheres was attained. However, the spheres blown from this slurry had too high an acetone content to allow drying following formation. Increasing the solids loading to 40 vol.% increased the viscosity to a high enough value to prevent the formation of hollow spheres. The change in viscosity over a range of PVB concentrations for 35 vol.% and 40 vol.% TiH_2 slurries can be found in Figure 4.6. An attempt to disperse a 42.7 vol.% slurry with 2.0 wt.%

2008 PMMA and 1.0 wt.% PVB resulted in a viscosity of 550 mPa·sec, which was also too high to form hollow spheres.

It is important to note that each of these slurries exhibits pseudoplastic behavior, i.e. increasing shear rates reduce the viscosity. Pseudoplasticity arises when laminar flow orients the slurry particles in such a manner that the resistance to shear is reduced. This is desirable for forming spheres as dilatent slurries will clog the nozzle. Also, after sphere formation, there is a low shear rate and the higher, low shear rate viscosity helps to stabilize the sphere geometry as it dries in flight. The shear thinning response of TiH_2 dispersed with 1.0 wt.% polysilane treated powder and 3.0 wt.% 2008 PMMA at three shear rates, 12.6, 6.30, and 2.52 sec^{-1} can be found in Figure 4.7.

IV.3 Evaporation Rates

Following the evaluation of viscosity, it was necessary to evaluate the characteristics of the evaporation of acetone from a slurry. Hollow spheres must evolve a tough skin after formation and before contacting the collection apparatus or the spheres will deform or be otherwise damaged.

Evaporation rates were measured as a function of time for acetone based TiH_2 slurries with a solids loading of 35 vol.% and dispersed with combinations of 2008 PMMA, PS3, and Z 6020 polysilane. The data is presented as fraction acetone remaining as a function of time in Figure 4.8 and converted to the dependence of evaporation rate on the fraction acetone remaining in Figure 4.9. It is possible to speculate why slurries prepared with PS3 do not harden rapidly into rigid shells like those prepared with PMMA or PMMA with polysilane dispersion. When the curves are extrapolated to zero time (fraction acetone remaining = 1), during the critical initial drying stage, acetone evaporated from the slurry dispersed with PS3 at rates approaching that of pure acetone. For slurries containing solely PMMA and polysilane treated PMMA, a significantly lower evaporation rate is observed early in the process. This lower evaporation rate can be attributed to the rapid formation of a polymer skin. Transport of acetone through the skin becomes the rate limiting step and slows the process enough to maintain a stiff, tack free PMMA surface. Thus, acetone evaporates from the surface at a faster rate than transport through the surface skin. Slurries dispersed with PMMA do require a longer total drying time but a stable, supporting polymer shell is maintained from early in the drying process until complete evaporation occurs. Addition of small quantities of PS3 increases the initial evaporation rate significantly, is assumed to prevent the formation of a continuous PMMA shell that acts as a barrier to transport, and results in the collapse of the hollow spheres on landing.

To demonstrate that polysilane aided dispersion of TiH_2 is usable in hollow sphere formation, slurries were prepared with TiH_2 treated with 0.25 wt.% to 1.0 wt.% polysilane and dispersed in acetone-PMMA solutions. The spheres formed well from the coaxial nozzle and drying in free flight was not noticeably different from that of slurries containing only PMMA as the dispersant and binder.

IV.4 Zeta Potential

Electrophoretic mobility can be used as a measure of the colloidal stability of the suspensions used to form hollow spheres. The ζ-potential can be obtained from the mobility by using the Hückel equation. As explained previously, the surface potential of TiH_2 powder in acetone is strongly negative. Zeta potential measurements confirm a negative surface, with measured values of -117 mV for TiH_2 in acetone with no polymer additives.

By treating the surface of TiH_2 powder with polysilane, a charge reversal can be realized. A dilute suspension of 0.23 wt.% TiH_2 powder treated with 0.25 wt.% polysilane was sufficient to reverse the surface charge. Previous experience with the TiH_2 system (19) has shown that ζ-potentials between -25 and 25 mV will result in flocculation. Of the samples treated with 1.0 wt.% polysilane, the average ζ-potential was higher than 50 mV in all suspensions with particle concentrations greater than 0.20 wt.%, as shown in Figure 4.10. For the samples treated with 0.25 wt.% polysilane, the ζ-potential was lower by between 25 and 60%. Although the average ζ-potential may be in the dispersed range, there is reduced stability when an increasing fraction of particles enter the low potential, flocculated range. For the powder with the smaller polysilane content, addition of a small amount of powder to acetone may result in desorption of polysilane to less than a monolayer coverage, thereby reducing the ζ-potential. This is consistent with the increasing potential with wt.% TiH_2 for the lower polysilane concentration and a constant, high potential for the higher polysilane content powder regardless of the amount of hydride added to acetone.

The ζ-potentials of two powder samples that showed the largest charging can be found in Figures 4.11 and 4.12. Both samples contained pure acetone and 1.0 wt.% TiH_2, with the former having a treatment of 0.25 wt.% polysilane and the latter having a treatment of 1.0 wt.% polysilane. As can be seen in the figures, the particles in each suspension show a range of potentials from below 25 mV in the 0.25 wt.% case to greater than 100 mV in both cases. The powder treated with 0.25 wt.% shows lower potentials and a significantly greater range of potentials. Because there were fewer particles with low ζ-potentials and there was a narrower, higher potential distribution than with 0.25 wt.% polysilane, 1.0 wt.% polysilane was used in all subsequent trials.

IV.5 Adsorption Isotherms

The amount of polysilane associated with monolayer coverage of TiH_2 can be predicted using estimations of the surface area of adsorption. This value can be compared to measured adsorption isotherms (36). The average area occupied by the adsorbing molecule, *a*, can be found using (1) where *M* is the molecular weight of the

$$a = \left(\frac{M}{\rho \cdot N_A} \right)^{\frac{2}{3}} \tag{1}$$

polysilane, ρ is the density of the polysilane, and N_A is Avagadro's number (6.023×10^{23} mol^{-1}). The average surface area occupied by a single polysilane molecule was calculated to be 4.383×10^{-15} cm^2. The weight of polysilane present in a monolayer can then be found by solving for W in (2) with knowledge of a and information about S,

$$W = \frac{M \cdot S}{N_A \cdot a} \tag{2}$$

the specific surface area of the TiH_2 powder. Earlier work with this material found that for TiH_2 powder having an average particle size of 6 μm, the specific surface area was 1.6 m^2/g. The amount of polysilane in the monolayer can thus be predicted at 1.091 mg/g TiH_2.

In order to make a quantitative determination of adsorbed polysilane, calibration curves showing the relationship between index of refraction and the concentration of polysilane in acetone solution were prepared, as shown in Figure 3.1. There is an interaction between the polysilane and acetone that causes a darkening of color and an increase in the index of refraction over time. The nature of this reaction is as yet unknown. All samples must therefore be prepared simultaneously. Data was taken within two hours of sample preparation and following three days of storage at room temperature.

From the adsorption isotherm data presented in Figure 4.13, it is evident that polysilane has a strong affinity for TiH_2 surfaces at low equilibrium concentrations of polysilane in solution. This is confirmed by ζ-potential measurements that suggest small concentrations of polysilane act to reverse the charge of TiH_2. The isotherms are initially similar to a type II BET isotherm immediately after slurry preparation, with monolayer coverage at approximately 1.0 mg polysilane/g TiH_2 at an equilibrium polysilane concentration of approximately 5.0 wt.%. This agrees well with the calculated amount of polysilane present in a monolayer, 1.091 mg/g TiH_2. At higher polysilane concentrations, multilayer adsorption appears to be occurring, as is typical of type II behavior. After three days, the isotherm shifts closer to type I behavior with approximately the same monolayer coverage. However, there does not appear to be further adsorption above monolayer coverage except at the highest concentration. The calculated monolayer value is consistent with this data as well.

IV.6 Sphere Defects

One objective of this study was to quantify sphere defects as a starting point to improve sphere quality. There are three general types of defective spheres that can be found in a batch of even the highest quality. These are (1) defects that do not compromise the integrity of the sphere, (2) defects that cause the surface of the sphere to be pierced, and (3) defects that do not contribute to mechanical properties and do not exhibit the characteristics of hollow spheres. They are present as a result of interactions between sphere blowing parameters, slurry characteristics, and the downstream environment. By recognizing these flaws, it is possible to modify processing parameters and produce better sphere batches.

Defects in spheres can be evaluated with either of two methods, a non-destructive visual inspection and a computer assisted digital analysis.

IV.6.1 Defects in Continuous Spheres

Defects that are present in spheres but that do not break the surface include tails and dimples, out of roundness, and sphere wall thickness uniformity. Tails and dimples can be observed directly and nondestructively by inspecting spheres visually. While roundness can be evaluated by inspection, good quantitative results can only be obtained through cross sectioning and digital image analysis.

IV.6.1(a) Defects Requiring Visual Inspection

Tails are an artifact of the blowing process. As spheres form, material concentrates at the pinch off points. Depending on the viscosity and drying characteristics of the slurry, this material can be frozen into the sphere before it has the opportunity to uniformly distribute. A micrograph of the tail defect can be found in Figure 4.14. A schematic of tail formation is illustrated in Figure 4.15.

Pressure differences between the inside of the sphere and the environment result in the formation of dimples, essentially a dent in the sphere. Ripples on the sphere surface are a less severe manifestation of this flaw. The sharp edges caused by dimpling are often accompanied by cracking. A micrograph of the dimple defect can be found in Figure 4.16.

IV.6.1(b) Requiring Digital Analysis

Due to aerodynamic forces present as hollow spheres drop from the nozzle to the collection apparatus, a decentering of the central air bubble is possible. This may result from drag, rotation, or ringing oscillation. If the sphere hardens in this state, the wall thickness in the equatorial region of the sphere can be three or more times as thick as the polar endcaps. Severe decentering may cause the polar endcaps to be broken, causing pinhole defects as described below. The thin polar endcaps are also more likely to fracture on collection or during handling. A schematic of deviation from wall thickness uniformity can be found in Figure 4.17.

Out of roundness implies that the hollow shell takes on an oblate, non-spherical form. This defect generally is found in spheres that come from slurries that have a high initial viscosity. The spheres dry before thermodynamic forces can act to reduce surface energy and increase the sphericity of hollow shells. Out of roundness can also be attributed to contact with the apparatus if case hardening is slow. Rapid deceleration will cause formation of an oblate spheroid due to compressive deformation on one axis.

IV.6.2 Defects in Discontinuous Spheres

Defects that cause the surface of the sphere to be compromised include cracks, pinholes, cracked holes, and blowouts. These defects can be observed directly and nondestructively by inspecting spheres visually. Cracks, as described earlier, can result from extreme dimpling or from collision with the collection apparatus. These defects typically arise during sphere formation and not from rough handling. However, cracks increase the likelihood of sphere fracture. A micrograph of the crack defect can be found in Figure 4.18.

Pinholes may be formed in one of two ways. First, the joint between tail and hollow sphere is a stress concentrator. Fracture at this joint will result in a circular hole in the sphere. It is also possible for slow evaporation to cause a decentering of the central air bubble. When the spherical air bubble contacts the wall of the sphere, a circular flaw will form. An illustration of this route to pinhole formation can be found in Figure 4.17. A micrograph of the pinhole defect can be found in Figure 4.19.

Spheres containing cracked holes have a fraction of the sphere surface removed, either through impact during collection or rough handling. These defects typically arise after sphere formation and are caused by the presence of thin polar endcaps that are more susceptible to fracture. A micrograph of the cracked hole defect can be found in Figure 4.20.

Blowouts are often unrecognizable as spheres. They typically arise at the beginning of the blowing process as conditions tend towards steady state from instability, or when the nozzle orifice becomes obstructed with coagulated material.

IV.6.3 Other defects

The third type of defect includes streamers, satellite spheres, and broken tails. Pieces that have been broken in flight or by handling, for example, from cracked holes, also fall into this category. Streamers arise when strings of slurry connecting spheres harden and are collected. Satellite spheres are a result of these streamers becoming spherical because of the thermodynamic driving force for the reduction of surface area. Satellite spheres are typically much smaller than the spheres being blown. A schematic of the formation of streamers and satellite spheres can be found in Figure 4.15.

IV.7 Sphere Uniformity: Visual Inspection

Visual inspection was used to determine the frequency of spheres containing tails, dimples, cracks, pinholes, and cracked holes, as well as the continuity or discontinuity of the sphere. Spheres from a slurry with a solids loading of 52 vol.% TiH_2 dispersed with 3.0 wt.% PMMA and 0.70 wt.% PS3 was compared to spheres from a slurry with a solids loading of 44 vol.% TiH_2 treated with 1.0 wt.% polysilane and dispersed with 3.0 wt.% PMMA. These slurries are the best found in previous investigations with PS3 dispersion and the best associated with the present work with polysilane dispersion.

AQLs, or Acceptable Quality Levels, were measured for sphere batches made with PS3 and polysilane. These values will become much more important in the future, when the effect of sphere defects on foam mechanical properties is known. This knowledge would allow the establishment of an acceptance number. An acceptance number is a defect level above which a batch is discarded and below which a batch is accepted. Acceptance sampling is a test of whether the proportion of defective items in the batch is some specified value p_0 against the alternative that it equals p_1. In this sampling method, p_0 is the AQL and p_1 is the Lot Tolerance Percent Defective (LTPD). The method is based on a specific sample size, AQL, and/or LTPD. Assuming the least stringent AQL in the standard, it was found that spheres made with PS3 failed in 4 of the 6 defect categories whereas spheres made with polysilane failed 3 of the 6 defect categories. It should be noted that the quality levels associated with MIL-STD-105D are extremely high.

The polysilane dispersion formulation caused a reduction in each defect studied, except cracked holes, due to improved drying characteristics. A photograph of a representative sample of spheres from this batch can be found in Figure 4.21. The frequency of tails was reduced 67%, pinholes were reduced 64%, dimples were reduced 34%, cracks were reduced 28%, and blowouts were reduced 22%. The frequency of completely continuous spheres increased 33%. A graph comparing the defect frequency of the two batches can be found in Figure 4.22.

IV.8 Wall Thickness Uniformity: Digital Analysis

By taking cross sections of fired hollow spheres, it is possible to make quantitative determinations of wall thickness uniformity. Thickness uniformity is an important consideration when forming spheres having maximum mechanical properties. The severity of defects such as thick equatorial stripes can be easily identified and a quality comparison between batches can be made.

In this study, the same two batch compositions used in IV.7 above were fired at 1100 °C for 30 minutes with a heating rate of 7 °C/min. The resulting Ti spheres were mounted, cross-sectioned, and polished. Six spheres were taken from each batch and analyzed with the program.

Figures 4.23 (a) and 4.24 (a) show the frequency of wall thickness for two spheres with PS3 dispersion. The solids loading of the slurries used to form these spheres was

52 vol.% TiH_2 dispersed with 3.0 wt.% PMMA and 0.70 wt.% PS3. Both profiles are broad and irregular indicating vastly different thickness in each sphere. Micrographs of the spheres associated with the measurements can be found in Figures 4.23 (b) and 4.24 (b), respectively.

The data for individual spheres corresponds well to a combination of the data for all six spheres from the batch. Figure 4.25 shows this combination. There is a broad bimodal distribution present indicating a wide range of thicknesses as well as the thick stripe defect. There is a lack of repeatability in the sphere wall thickness.

By decreasing the solids loading to 44 vol.% and dispersing with a combination of polysilane and PMMA instead of PS3, it was possible to greatly improve wall thickness uniformity. Figures 4.26 (a) and 4.27 (a) show the frequency of the appearance of a particular wall thickness measurement for each of two spheres where polysilane was used in place of PS3. Both profiles are narrow and sharply defined indicating the presence of narrow thickness ranges present within the spheres from this batch. There are readily apparent, sharply defined, and closely spaced bimodal distributions present, implying that there is a thick stripe effect but that the defect is not severe. Micrographs of the spheres associated with the measurements can be found in Figures 4.26 (b) and 4.27 (b), respectively.

The data for these individual spheres also corresponds well to a combination of the data for all six spheres from the batch, as shown in Figure 4.28. There is a narrow, closely spaced bimodal distribution present, and a narrow range of thickness values in the bulk.

This narrow range indicates the repeatability of this batch formulation. Spheres formed from this batch appear essentially the same.

Visual inspection and digital analysis both confirm that the dispersion of TiH_2 with polysilane and 2008 PMMA is highly effective in producing more uniform, more repeatable, and higher quality Ti spheres.

IV.9 Lattice Parameter Measurements

Little is presently known about the mechanical properties of Ti spheres and foams because of the purity control problem associated with dehydriding titanium. Control of the process and the reduction of impurities in titanium should improve mechanical properties and result in ductile instead of brittle foams. Form Table 2.1, target values for impurity levels in titanium that retain good mechanical properties can be found. A Grade 4 ASTM No. B265 alloy, containing at least 99.0% Ti and a maximum of 0.40% O, 0.05% N, 0.08% C, and 0.015% H, has good corrosion resistance and high strength.

Diffusion of interstitial impurities through the titanium lattice is of special import when considering embrittlement of the alloy. Diffusion is dependent on the size of the atom diffusing, available space in the structure, solubility, and temperature. The diffusion phenomena can be modeled using the Arrhenius relation (3) because the process is thermally activated.

$$D = D_o \exp\left(\frac{-Q}{RT}\right) \tag{3}$$

The diffusivity, D includes the influence of temperature on diffusion and the propensity for the atom to move through the lattice due to spatial considerations (37). It can be seen from data in the literature (38) that the diffusivity of oxygen in a titanium matrix increases approximately one order of magnitude after the transformation from α- to β-phase. Of course, oxygen itself has a direct influence on this transition for reasons previously described. The trends associated with the diffusivity of oxygen can be found in Figure 4.29. Values of log D at typical processing temperatures of 1100 °C are for the α-phase, -13.3 m^2/sec and for β-phase -12.1 m^2/sec.

The Van-Ostrand Dewey equation (4) is an expression for Fick's second law that can be used to determine an effective penetration depth of an impurity into a lattice. In this model, D is not allowed to vary with concentration and the source of diffusing atoms is continuously replenished.

$$\frac{C(x,t) - C_o}{C_s - C_o} = 1 - erf \frac{x}{2\sqrt{Dt}} \tag{4}$$

In (2), $C(x,t)$ is the concentration at position x at time t. C_s is the concentration of the diffusing material at the surface, and C_o is the initial bulk concentration. The relation ($C_o + C_s / 2$) can be substituted for $C(x,t)$ because the effective penetration is the depth at which the concentration of the diffusing species equals the average of the initial concentration and the surface concentration. It is also necessary to make the approximation erf (½) ~ ½, and introduce the geometrical constant γ. A simple equation for effective penetration depth can then be realized that contains only D, the diffusivity and t, the time (5). The parameter γ is given as unity for plate structures.

$$x_{eff} = \gamma\sqrt{Dt} \tag{5}$$

During a typical soak for the processing of titanium hollow spheres (1100 °C for 30 minutes), oxygen effectively penetrates 97 μm. This estimation does not consider the contribution of the heating and cooling cycle on diffusion, which increases the penetration greater than two fold. This is substantially greater than the 50 μm average sphere thickness, indicating that oxygen is diffusing completely through titanium sphere walls. The combination of the high solubility of oxygen in α-Ti (15.5 wt.%, 30 at.%) and significant diffusion rates explains why Ti spheres do not form an oxide scale at the surface and instead become brittle throughout the bulk of the material.

Magnesium is being used as an addition to titanium because of the potential for Mg to reduce the impurity oxides of titanium present in fired hollow spheres. The reactions outlined below show a thermodynamically favorable route (5 → 7 → 8) from high order titanium oxides to titanium metal. The free energies of the reactions are expressed at room temperature. As the temperature increases, the reactions become increasingly favorable.

Several samples, including a standard of ASTM Grade 2 Ti, pellets composed of fired TiH_2 powder containing no additives, and pellets composed of fired TiH_2 powder with additions of Mg were examined with an x-ray diffractometer to determine the lattice constants of the material. Lattice parameter is an indication of the amount of impurity in Ti, with larger values of c_o corresponding to higher impurity contents.

$$Ti_2O_3 + Mg \rightarrow Ti + TiO_2 + MgO \qquad -5.9\text{ J/mol} \qquad (5)$$

or

$$Ti_2O_3 + Mg \rightarrow 2\ TiO + MgO \qquad +29.9\text{ J/mol} \qquad (6)$$

$$TiO_2 + Mg \rightarrow TiO + MgO \qquad -41.8\text{ J/mol} \qquad (7)$$

$$TiO + Mg \rightarrow Ti + Mg \qquad -17.8\text{ J/mol} \qquad (8)$$

ASTM Grade 2 Ti standard is limited to a maximum impurity concentration as follows:

Nitrogen	0.03%
Carbon	0.08%
Oxygen	0.25%

The c_o lattice parameter of this material was determined to be 4.6837 Å. This compares favorably to the reported lattice parameter 4.683 Å which has been regressed to zero impurity content. The equivalent impurity content of the ASTM Grade 2 Ti, based on this lattice parameter and assuming all impurity as oxygen, was less than 0.05%. The standard also exhibited a large degree of ductility.

Several other samples were tested for lattice parameter. A sample of material that had been through the sphere formation process and fired at 1100 °C for 30 minutes and a heating rate of 7 °C/min was tested. This material contained 0.25 wt.% polysilane and 4.8 wt.% PMMA. X-ray analysis showed the c_o lattice parameter of this material to be 4.7137 Å and a_o to be 2.9591 Å. This corresponds to an equivalent impurity content of approximately 1.8%. A sample of raw powder with no polymeric additives and an addition of 3 wt.% Mg was found to have a c_o of 4.7094 Å and an a_o of 2.9542 Å. This corresponds to an equivalent impurity content of 1.7% Clearly, more control of the impurity content of Ti is required. This can likely be achieved by gettering impurity gasses more efficiently and firing in a cleaner atmosphere.

Table 4.1 Composition and stability of TiH_2-acetone suspension in the presence of dispersing additives.

All compositions contained 1 vol.% (0.160 g) TiH2 powder and 2.640 g Acetone

Rank*	Polymer System	Composition
1	EC	0.010 g EC
2	EC + Pavebond	0.010 g EC 0.005 g Pavebond
3	2008 PMMA	0.010 g 2008 PMMA
4	PVB	0.010 g PVB
5	PVB + Pavebond	0.010 g PVB 0.005 g Pavebond
6	2008 PMMA + PS3	0.009 g 2008 PMMA 0.001 g PS3
7	2008 PMMA + Pavebond	0.010 g 2008 PMMA 0.005 g Pavebond
8	2008 PMMA + Pavebond + PS3	0.010 g 2008 PMMA 0.005 g Pavebond 0.001 g PS3

* Smaller numbers indicate longer settling time.

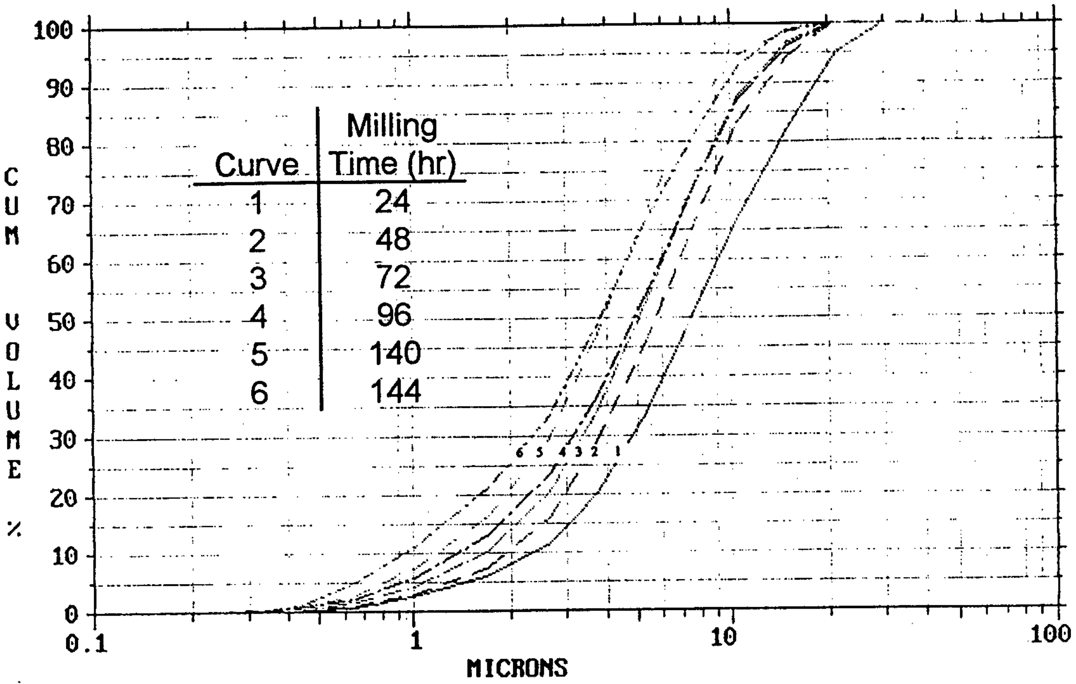

Figure 4.1 TiH$_2$ particle size distribution as a function of milling time.

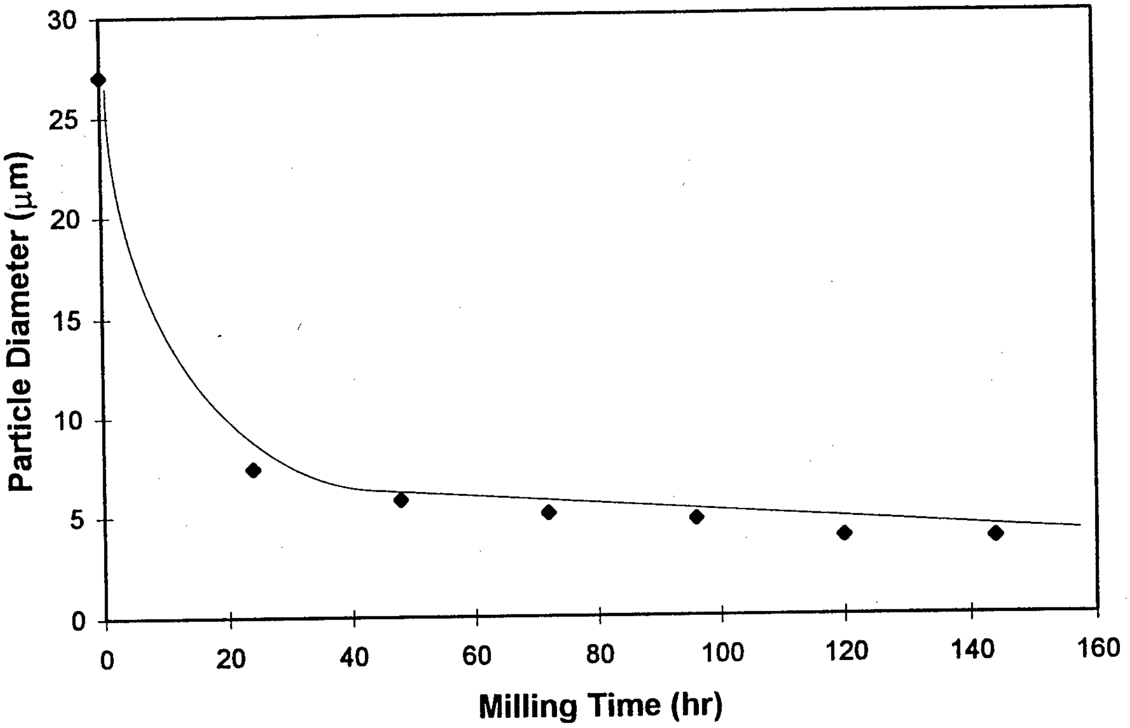

Figure 4.2 Average particle size of dry ball milled TiH_2 powder as a function of milling time.

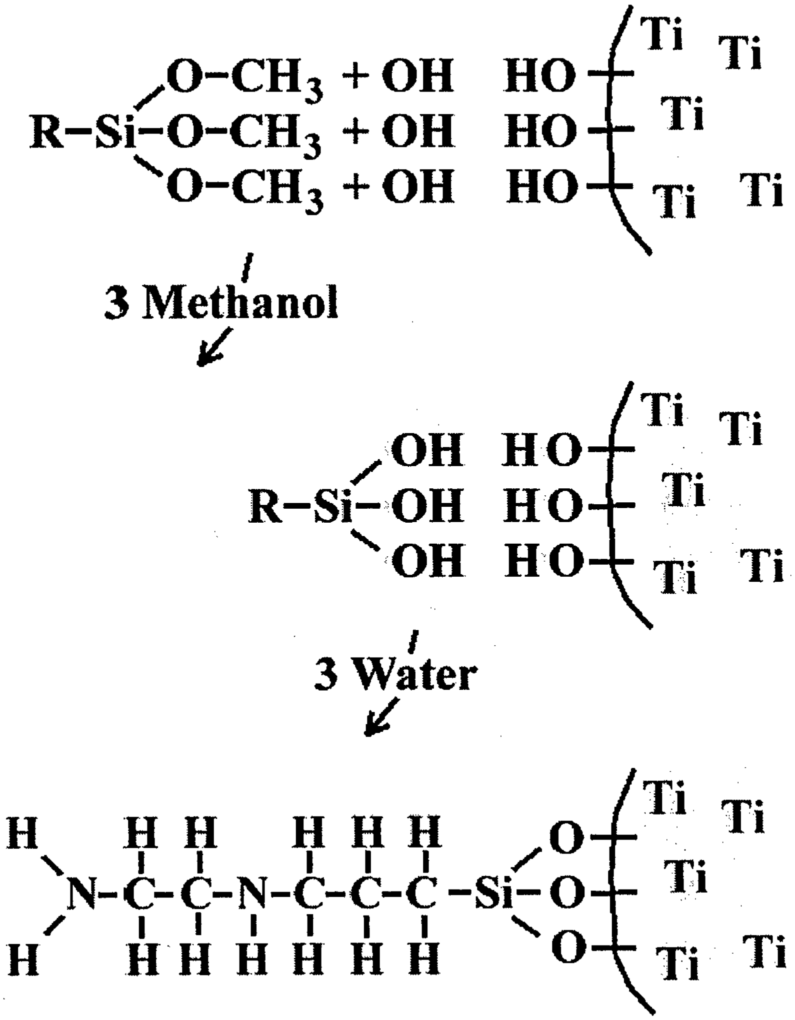

Figure 4.3 Schematic of the bonding of polysilane to TiH_2 powder.

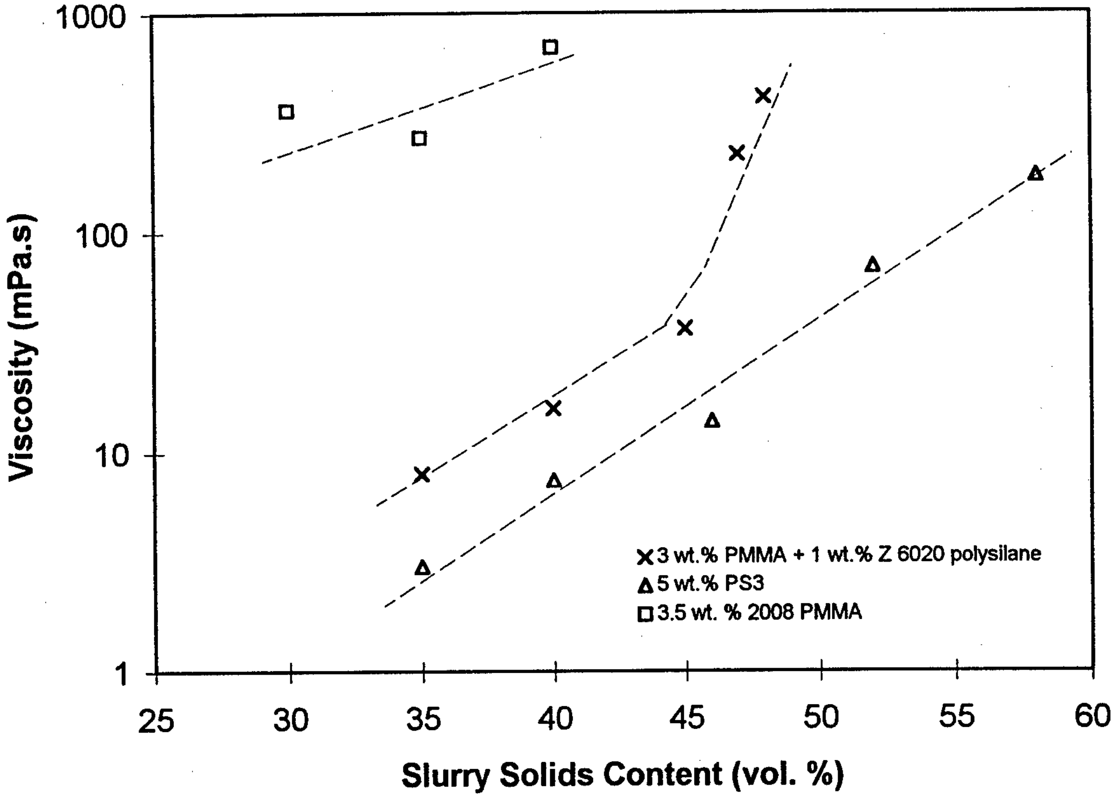

Figure 4.4 The viscosity of various concentrations of TiH_2 dispersed with 1.0 wt.% polysilane treated powder and 3.0 wt.% 2008 PMMA as compared to those slurries dispersed solely with 2008 PMMA and solely with PS3.

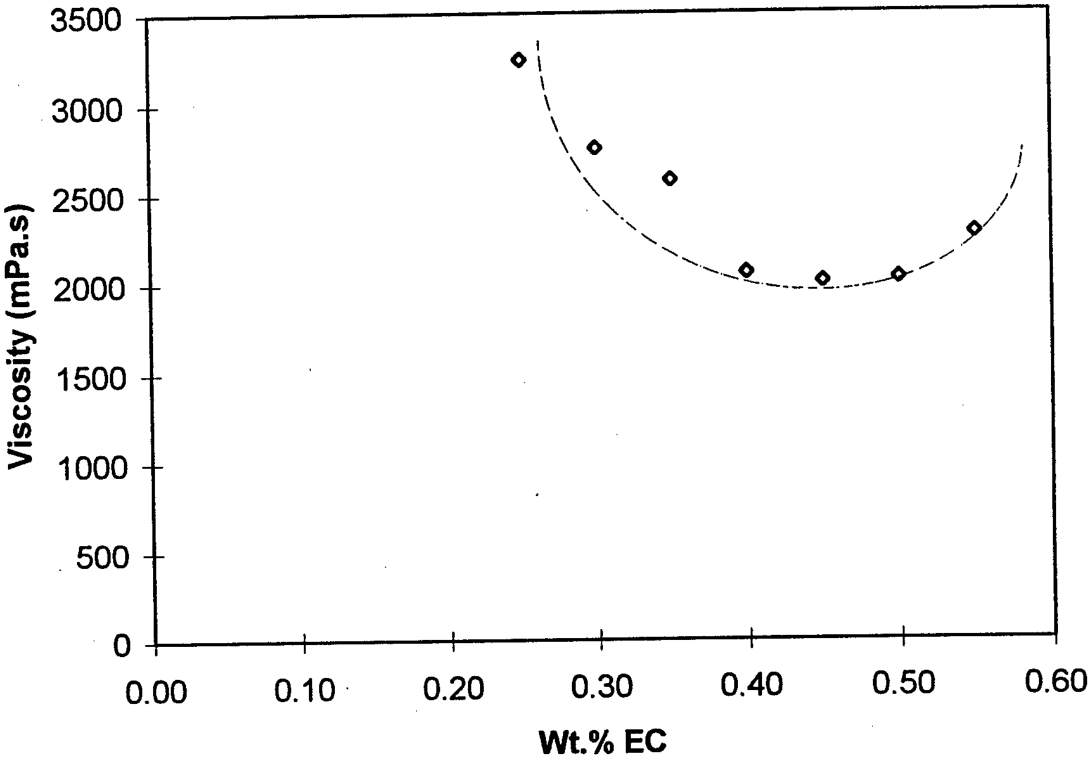

Figure 4.5 The change in viscosity over a range of ethyl cellulose concentrations for 35 vol.% TiH_2 slurry.

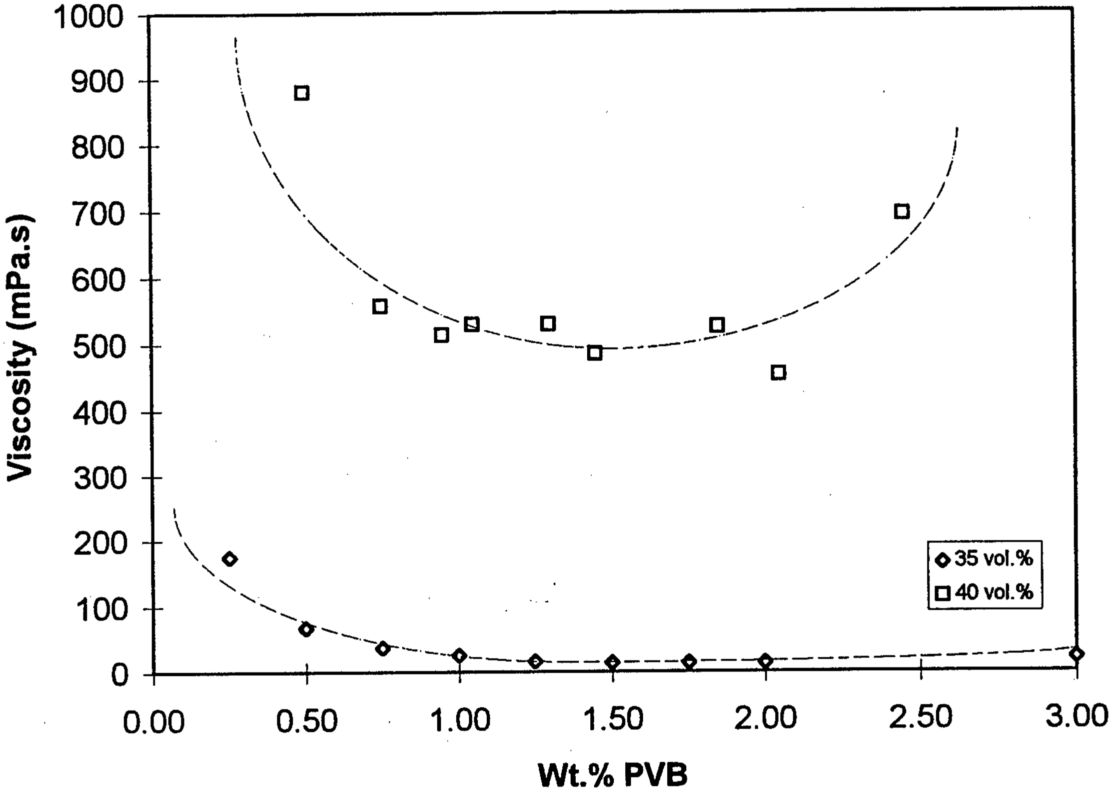

Figure 4.6 The change in viscosity over a range of poly vinyl butyral concentrations for 35 vol.% and 40 vol.% TiH_2 slurries.

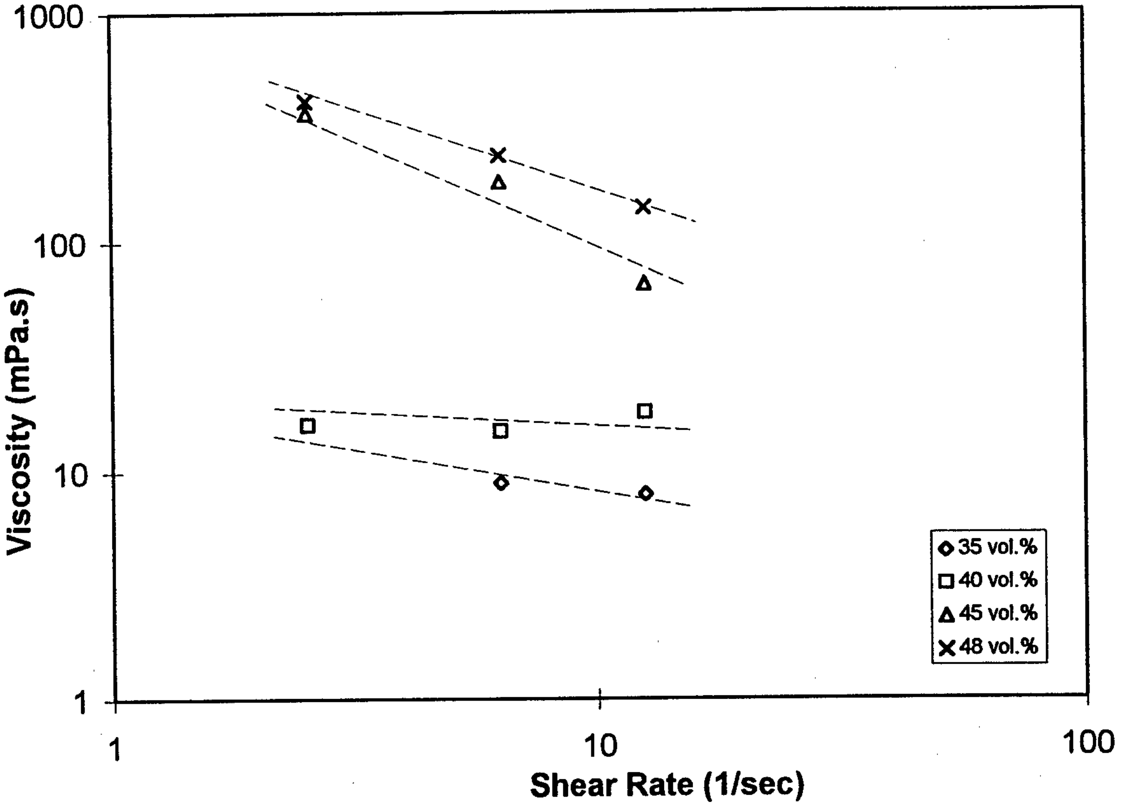

Figure 4.7 Shear thinning response of TiH_2 dispersed with 1.0 wt.% polysilane treated powder and 3.0 wt.% 2008 PMMA. Measurements were taken at shear rates 12.6, 6.30, and 2.52 sec^{-1}.

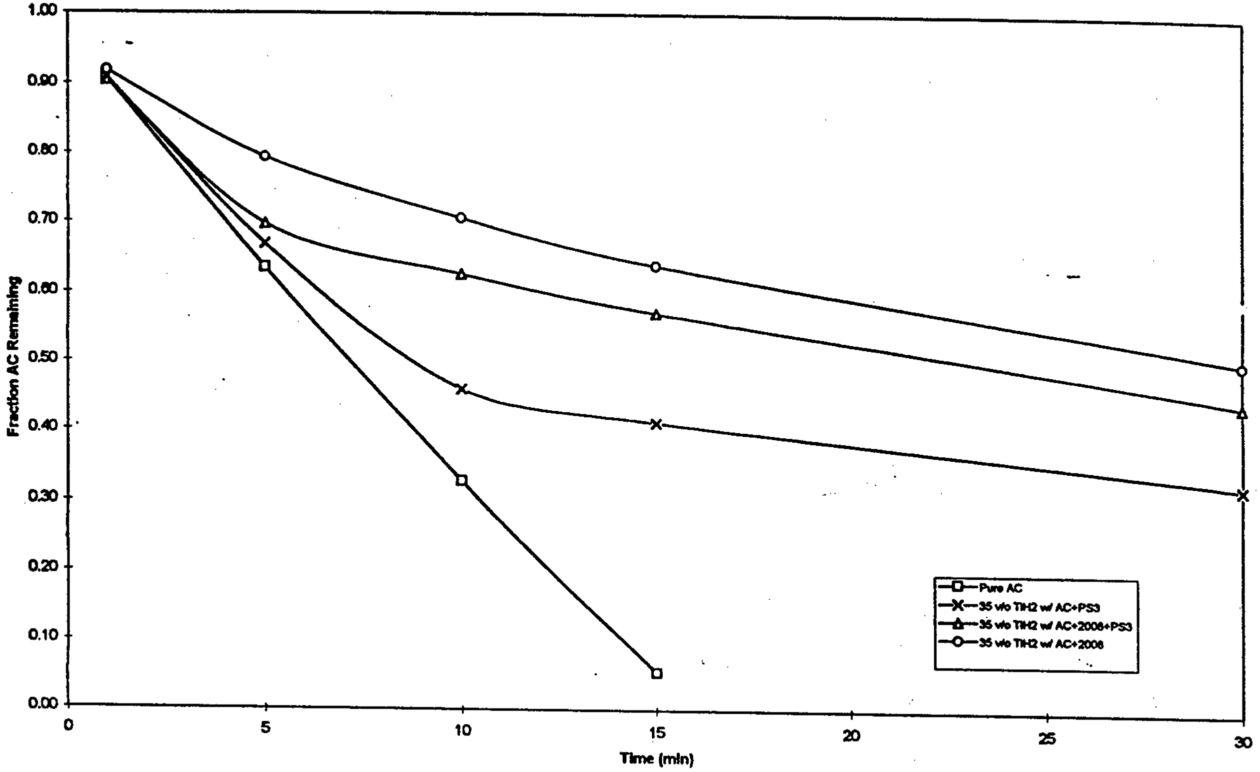

Figure 4.8 Acetone evaporation rates for 35 vol.% TiH_2-acetone slurries with additions of 2008 PMMA, PS3, and Z 6020 polysilane.

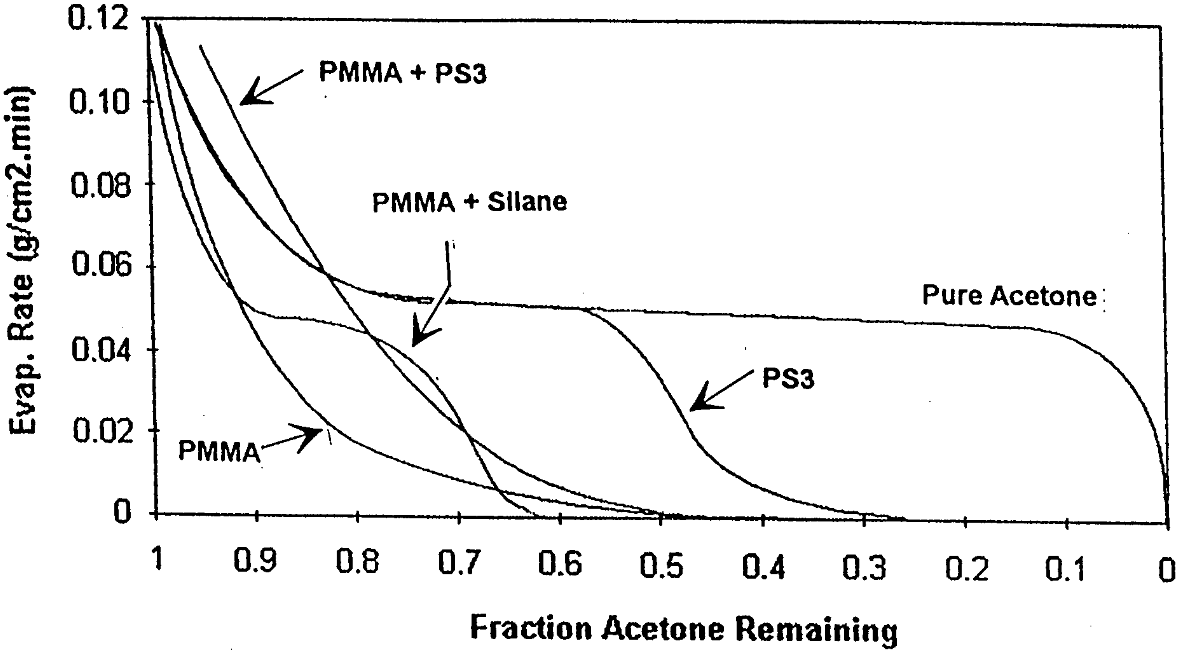

Figure 4.9 Fraction acetone remaining for 35 vol.% TiH_2-acetone slurries with additions of 2008 PMMA and PS3.

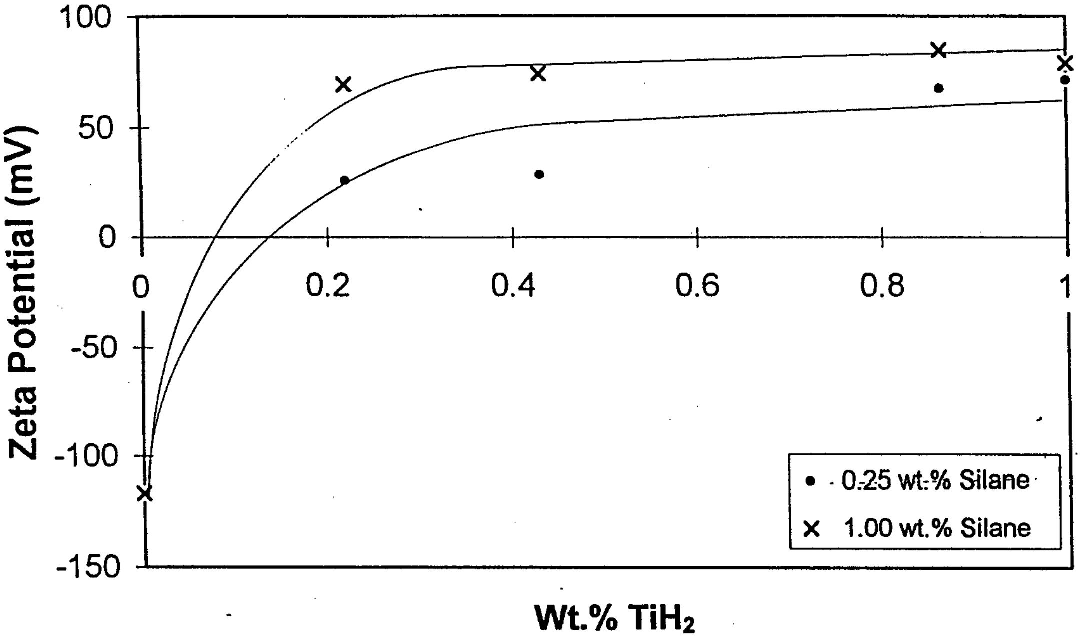

Figure 4.10 A comparison of the ζ-potentials for 0.25 wt.% and 1.0 wt.% polysilane treated TiH_2 powder.

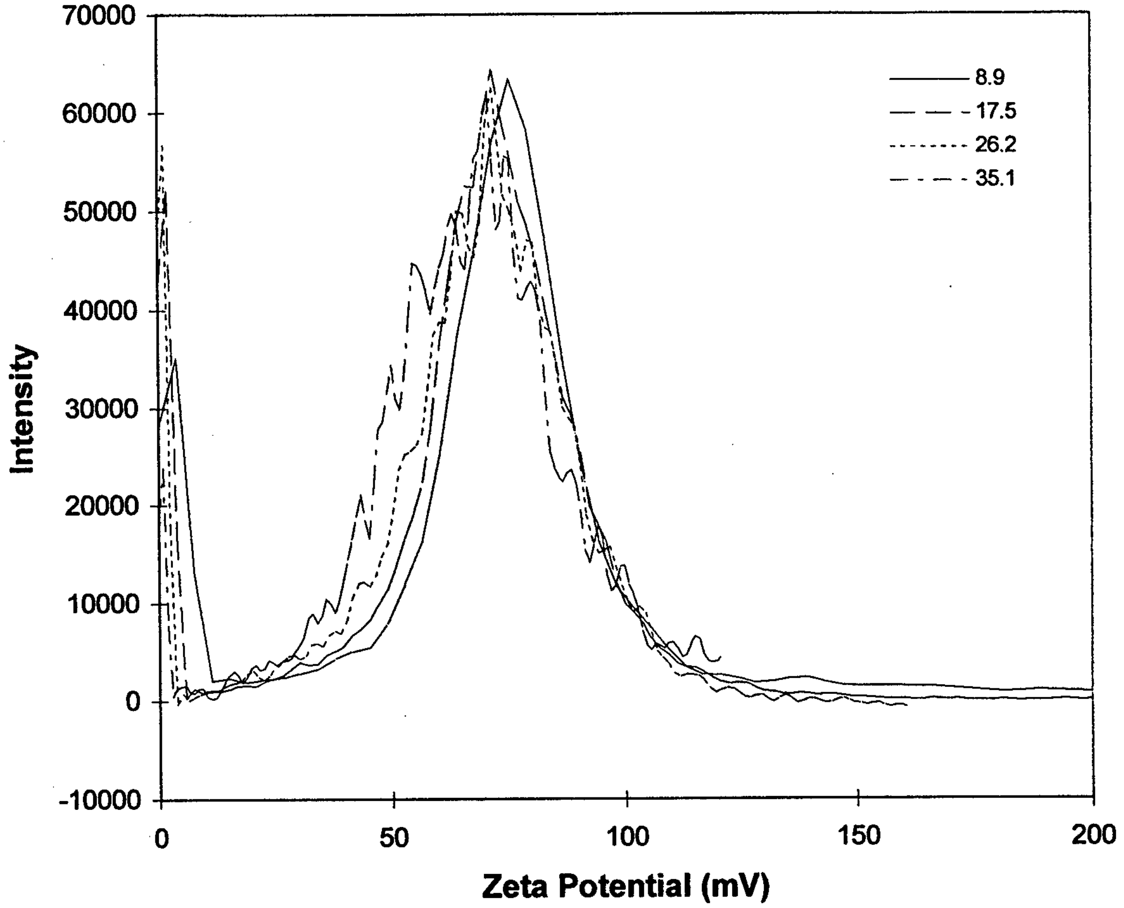

Figure 4.11 The ζ-potential of TiH_2 powder treated with 0.25 wt.% polysilane.

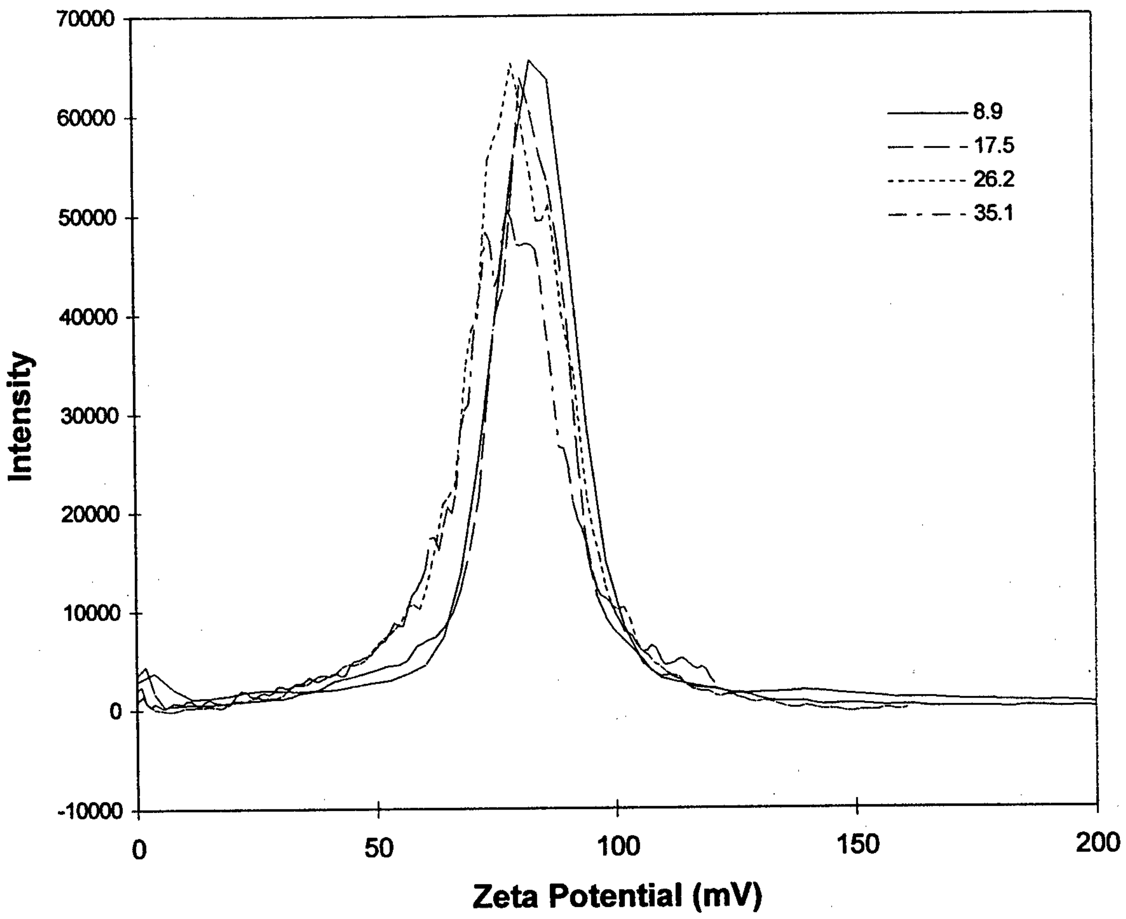

Figure 4.12 The ζ-potential of TiH_2 powder treated with 1.0 wt.% polysilane.

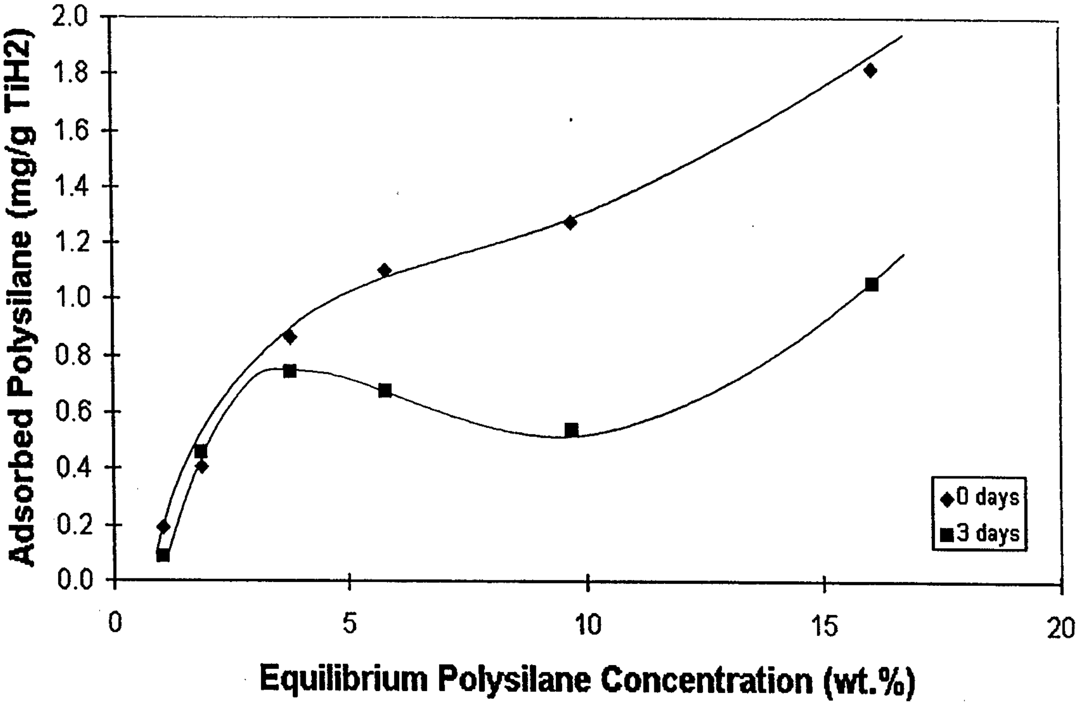

Figure 4.13 Adsorption isotherm for polysilane treated TiH_2 in acetone.

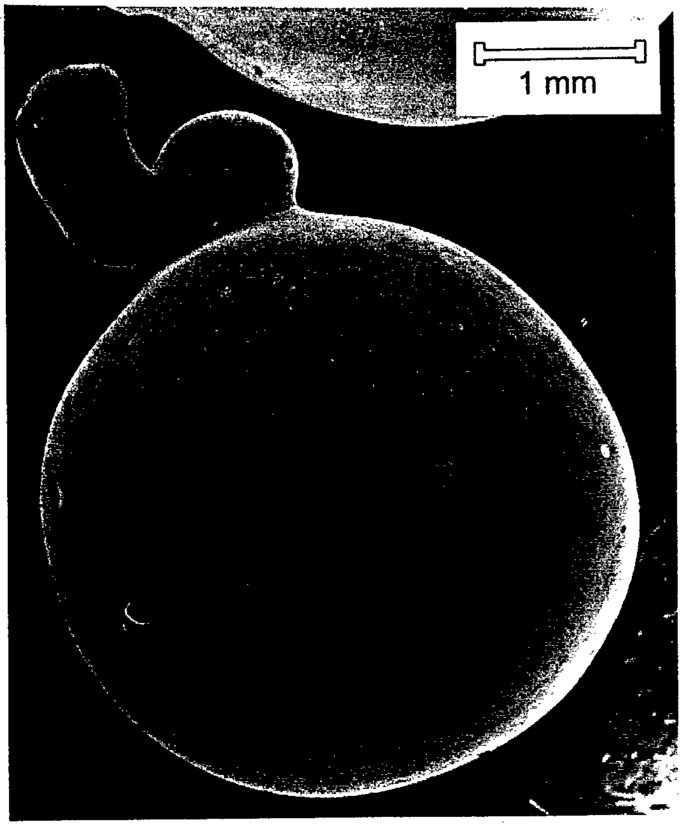

Figure 4.14 Micrograph of a hollow sphere tail defect.

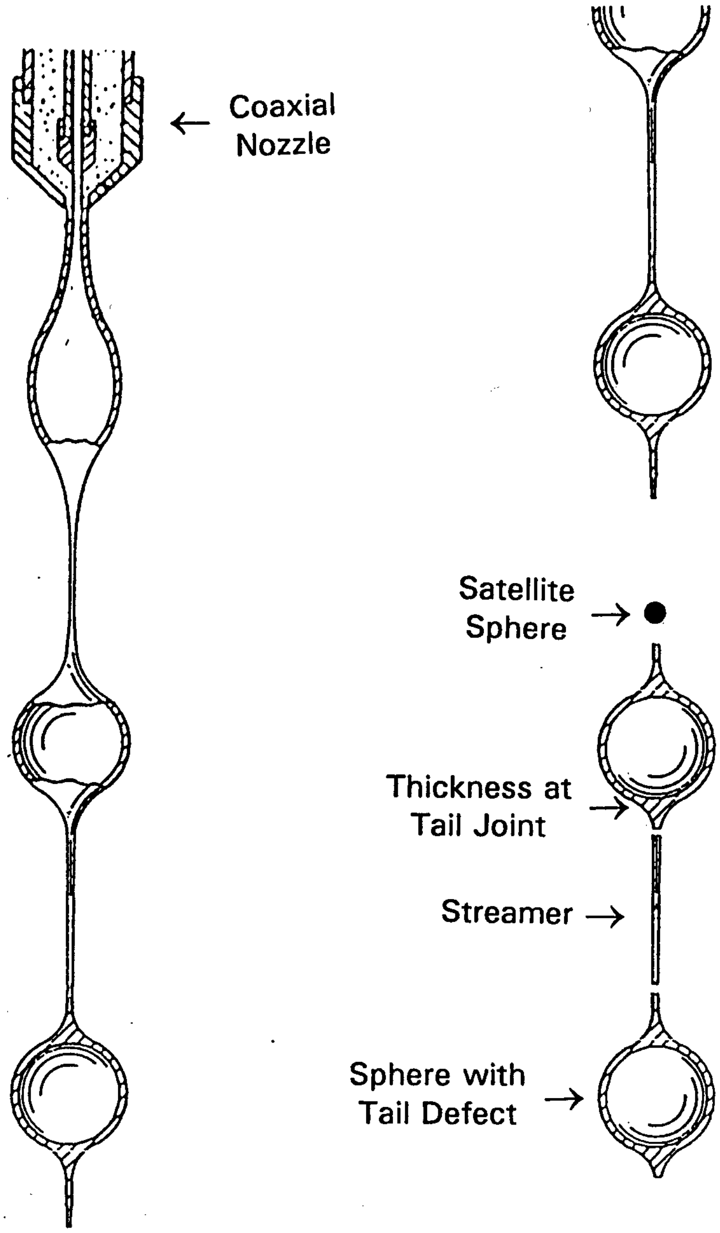

Figure 4.15 Schematic of tail, streamer, and satellite sphere formation.

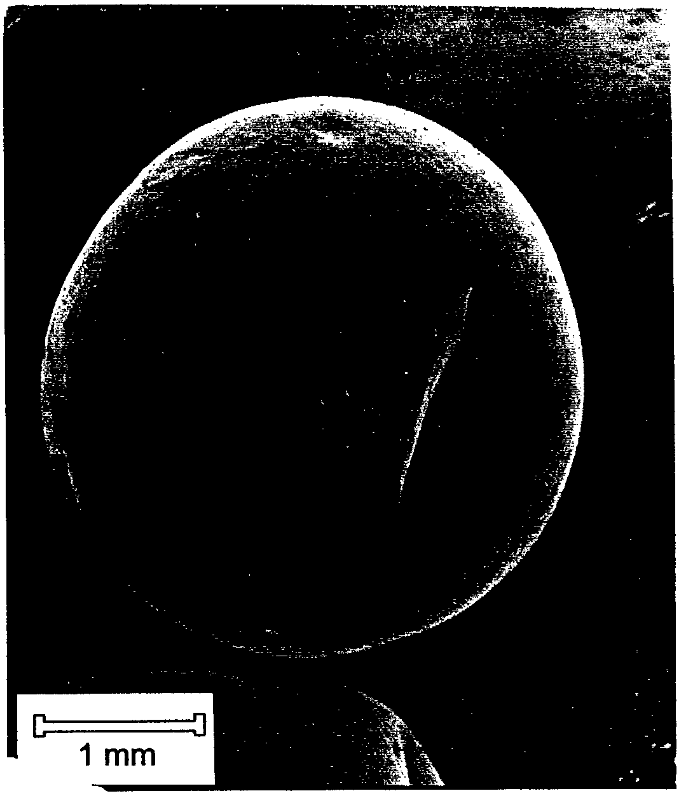

Figure 4.16 Micrograph of the hollow sphere dimple defect.

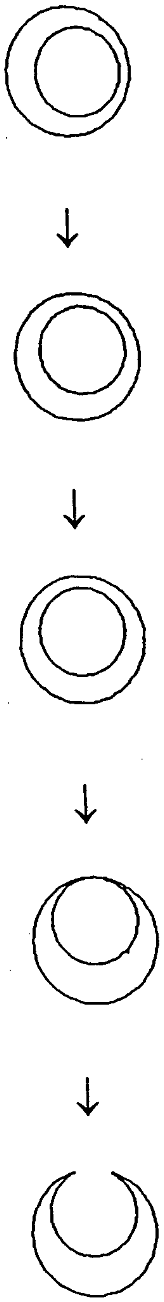

Hollow Sphere
as formed, decentered

Combination of aerodynamic drag, buoyant forces, and gravity can cause the sphere to harden before centering of the gas bubble.

Rotation causes material to be located preferentially in the equatorial regions of the sphere, resulting in thin polar endcaps.

Extreme motion of the central bubble before hardening results in thin areas subject to fracture.

When the bubble breaks through the sphere wall, a pinhole is formed.

Figure 4.17 Schematic of pinhole formation and a route to deviation from wall thickness uniformity

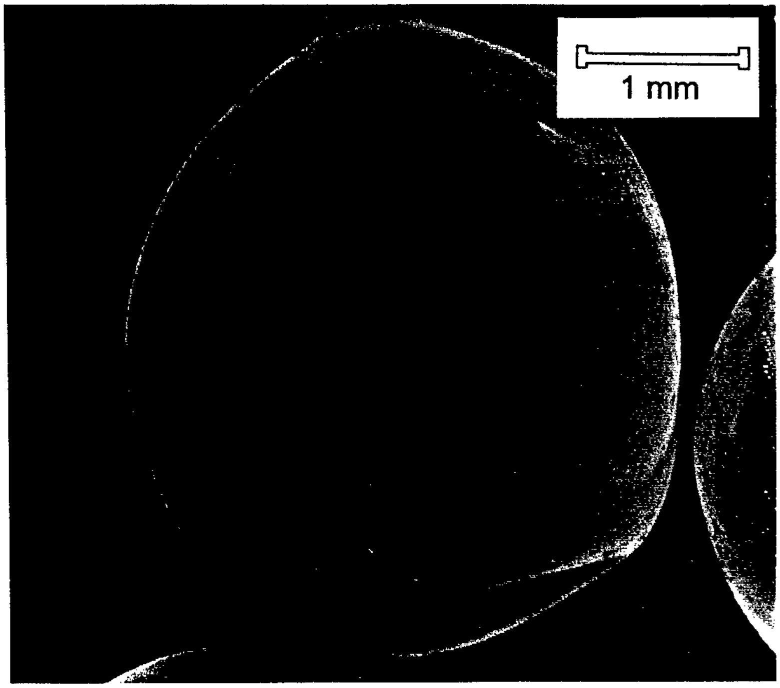

Figure 4.18 Micrograph of the crack defect.

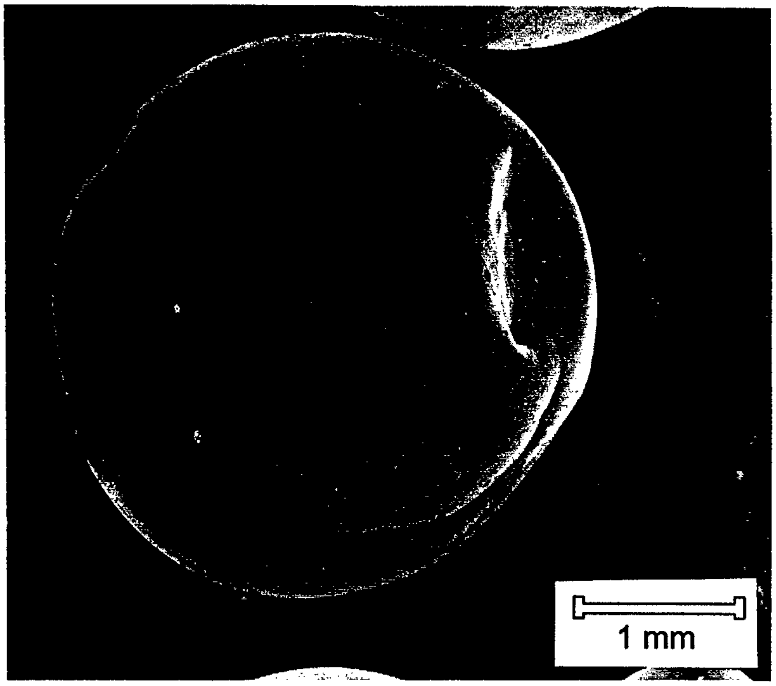

Figure 4.19 Micrograph of the pinhole defect.

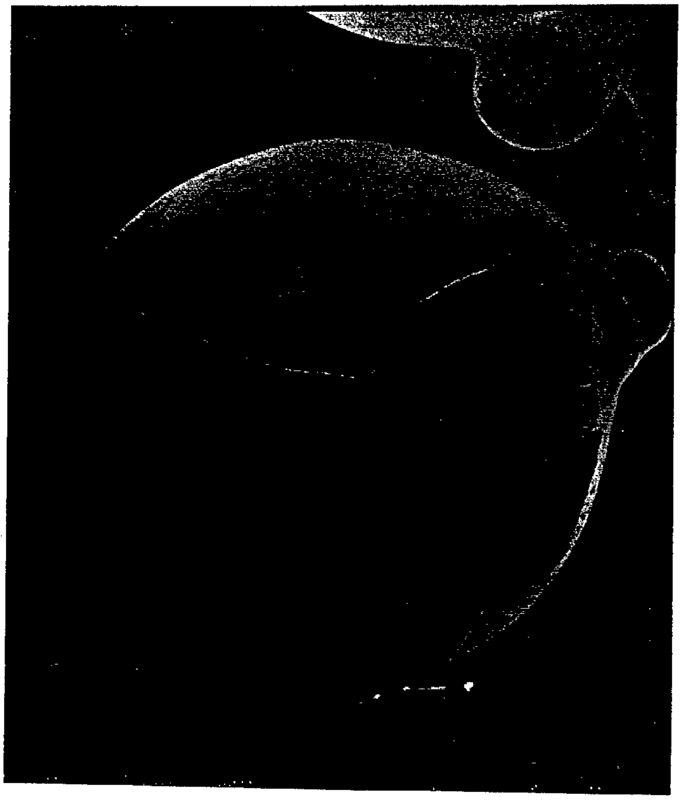

Figure 4.20 Micrograph of the cracked hole defect.

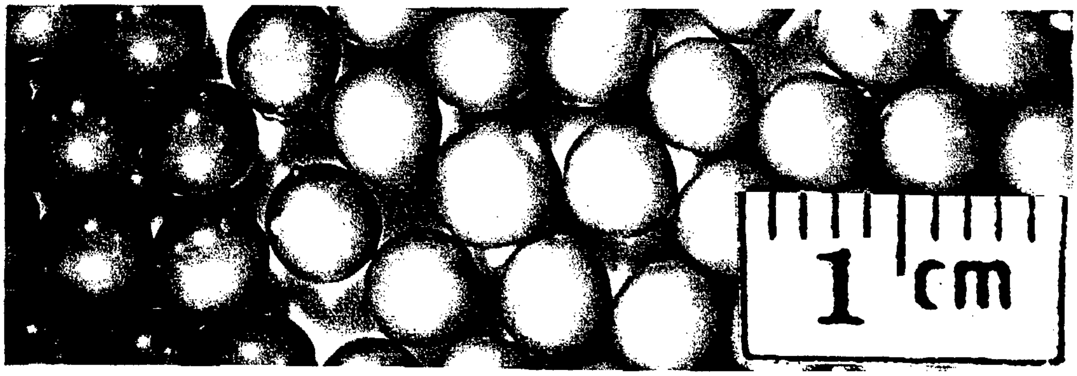

Figure 4.21 Photograph of a representative sample of spheres processed from a slurry with a solids loading of 44 vol.% TiH_2 treated with 1.0 wt.% polysilane and dispersed with 3.0 wt.% PMMA.

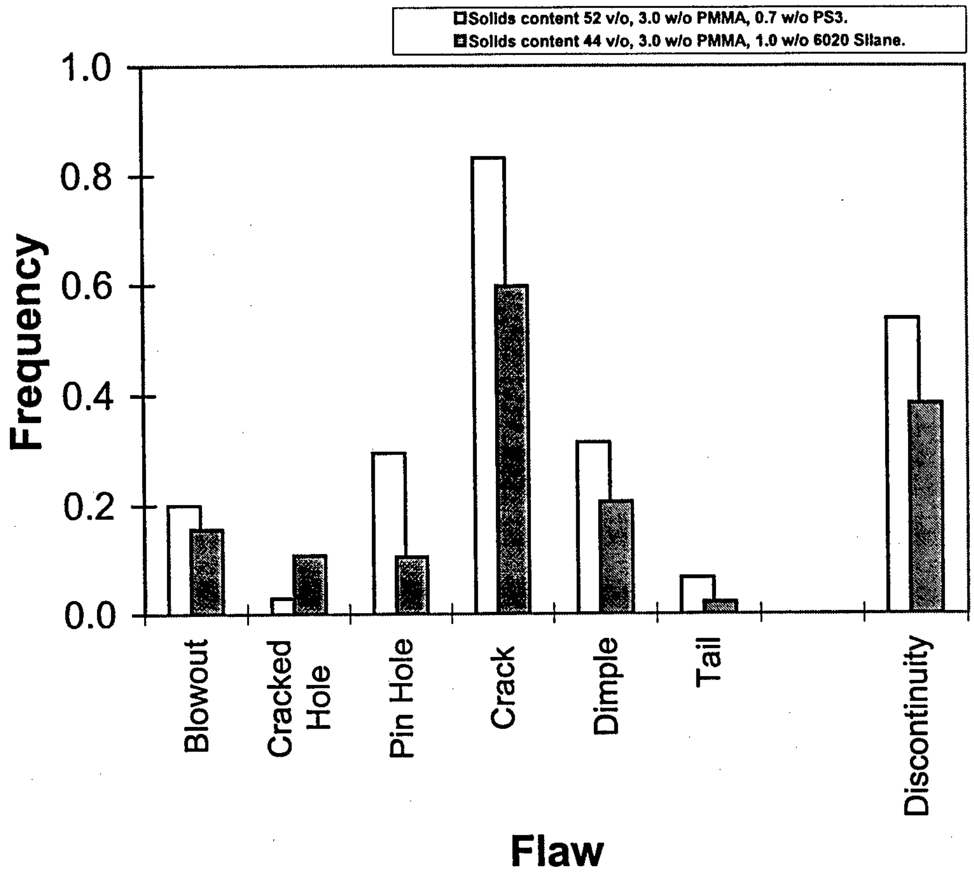

Figure 4.22 Comparison of the defect frequency associated with spheres made from two slurry compositions. A slurry with a solids loading of 52 vol.% TiH_2 dispersed with 3.0 wt.% PMMA and 0.70 wt.% PS3 was compared to a slurry with a solids loading of 44 vol.% TiH_2 treated with 1.0 wt.% polysilane and dispersed with 3.0 wt.% PMMA.

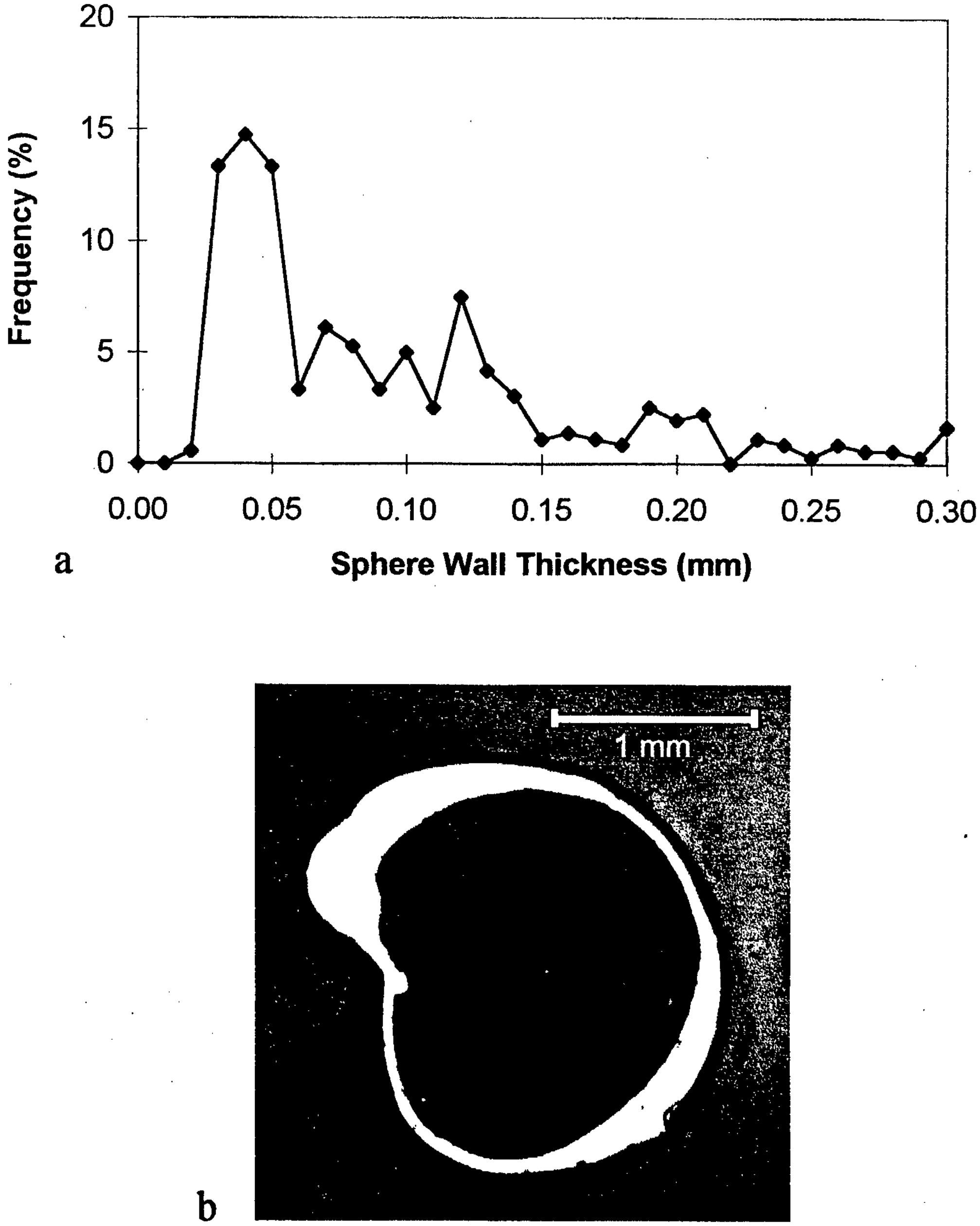

Figure 4.23 (a) The frequency of wall thicknesses present for an individual sphere made with PS3 (b) a cross section of the sphere.

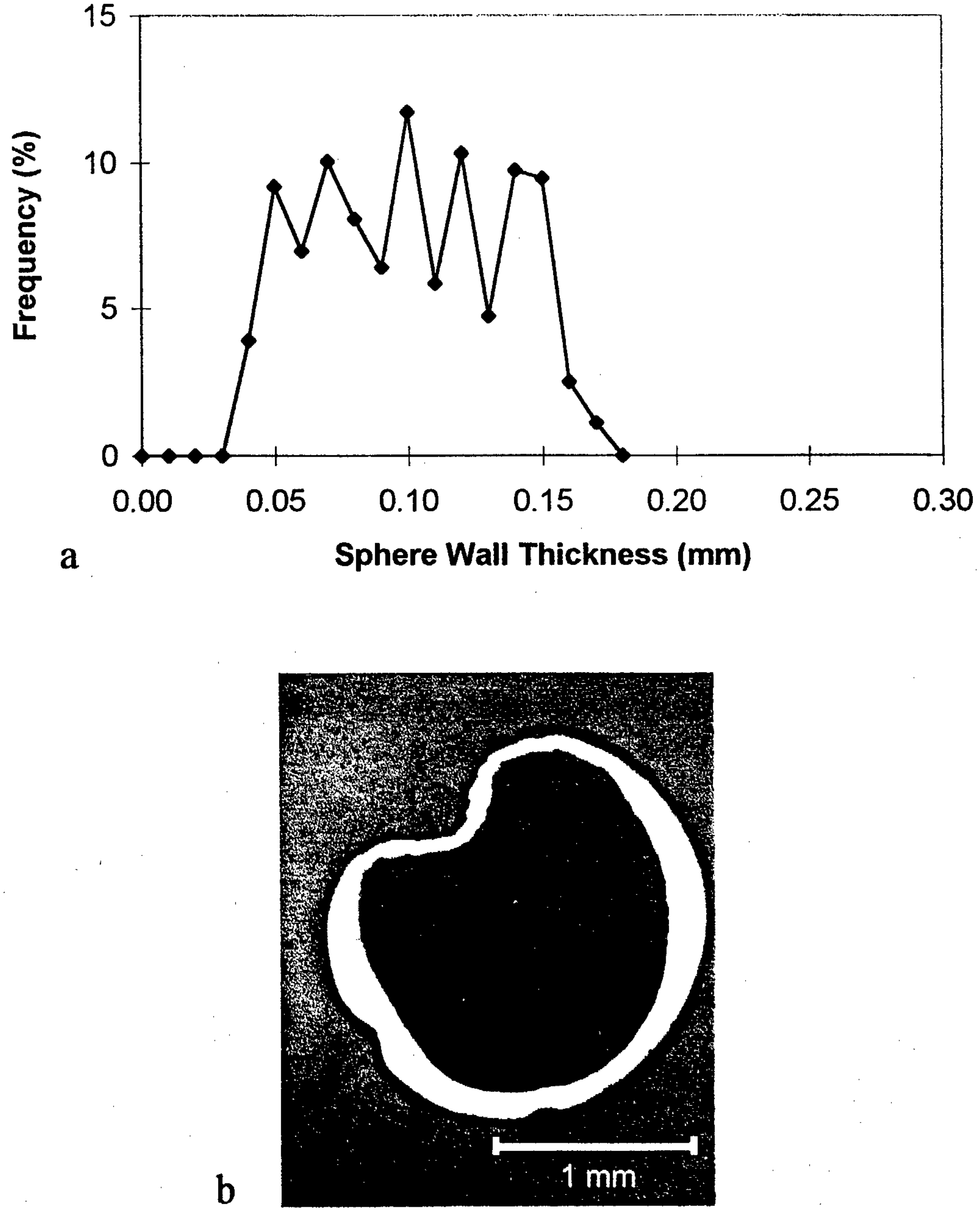

Figure 4.24 (a) The frequency of wall thicknesses present for an individual sphere made with PS3 (b) a cross section of the sphere.

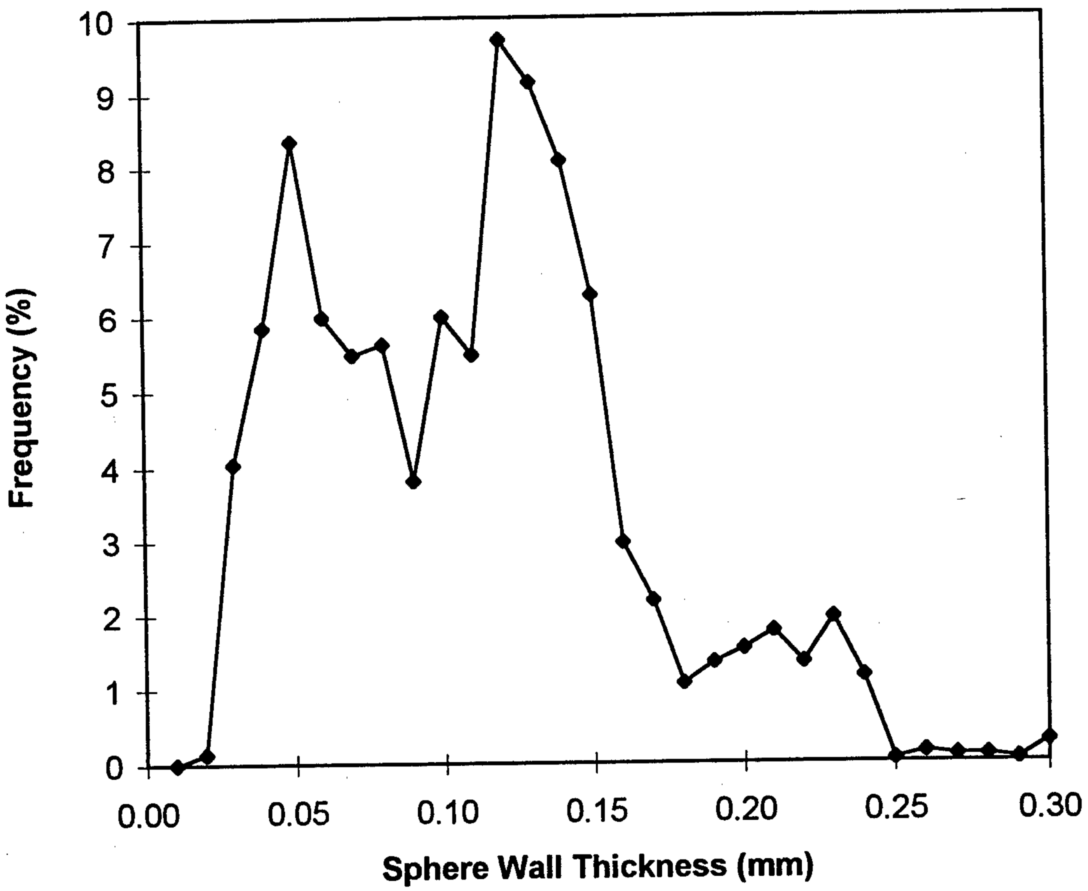

Figure 4.25 The frequency of wall thicknesses present for six spheres made with PS3.

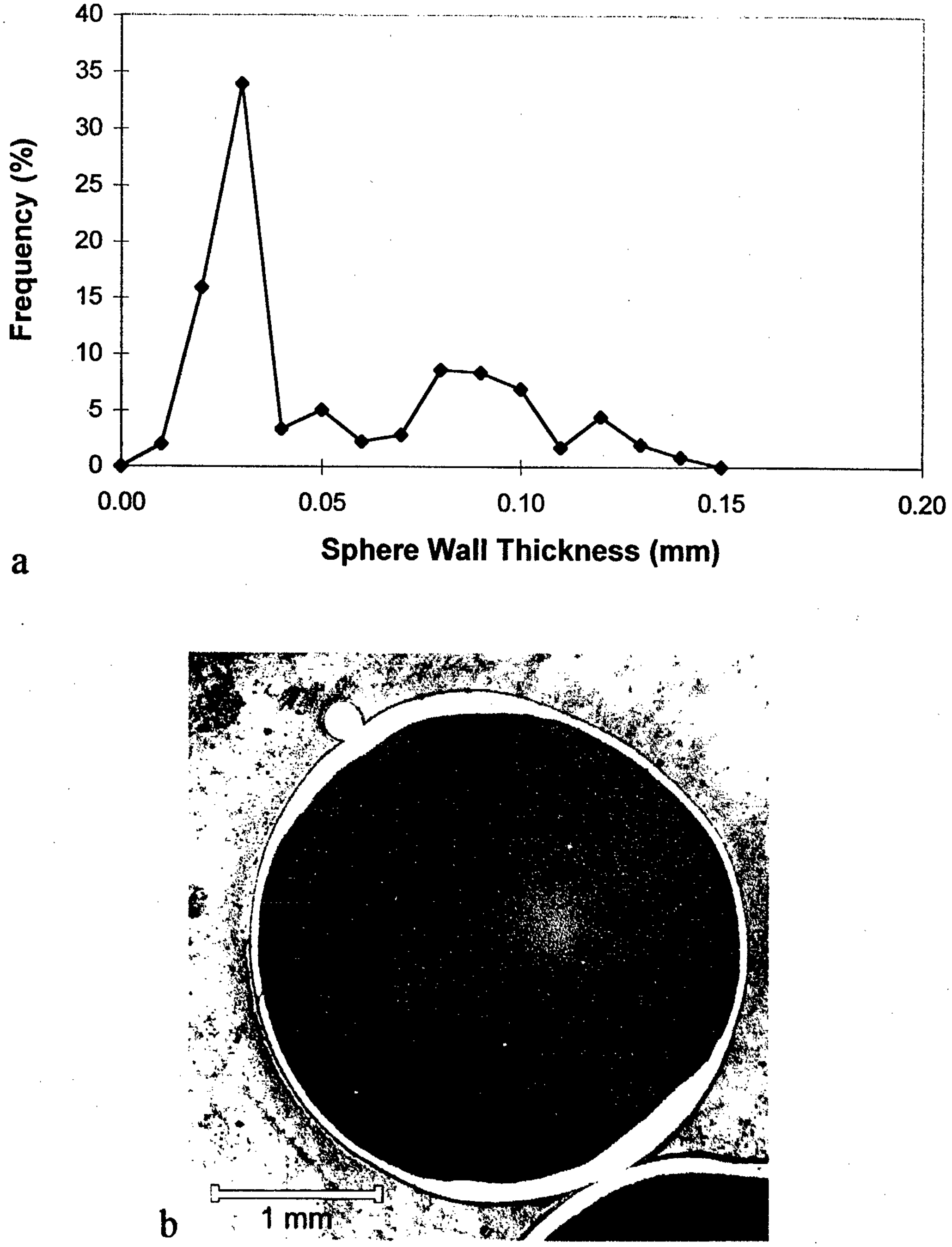

Figure 4.26 (a) The frequency of wall thicknesses present for an individual sphere made with polysilane (b) a cross section of the sphere.

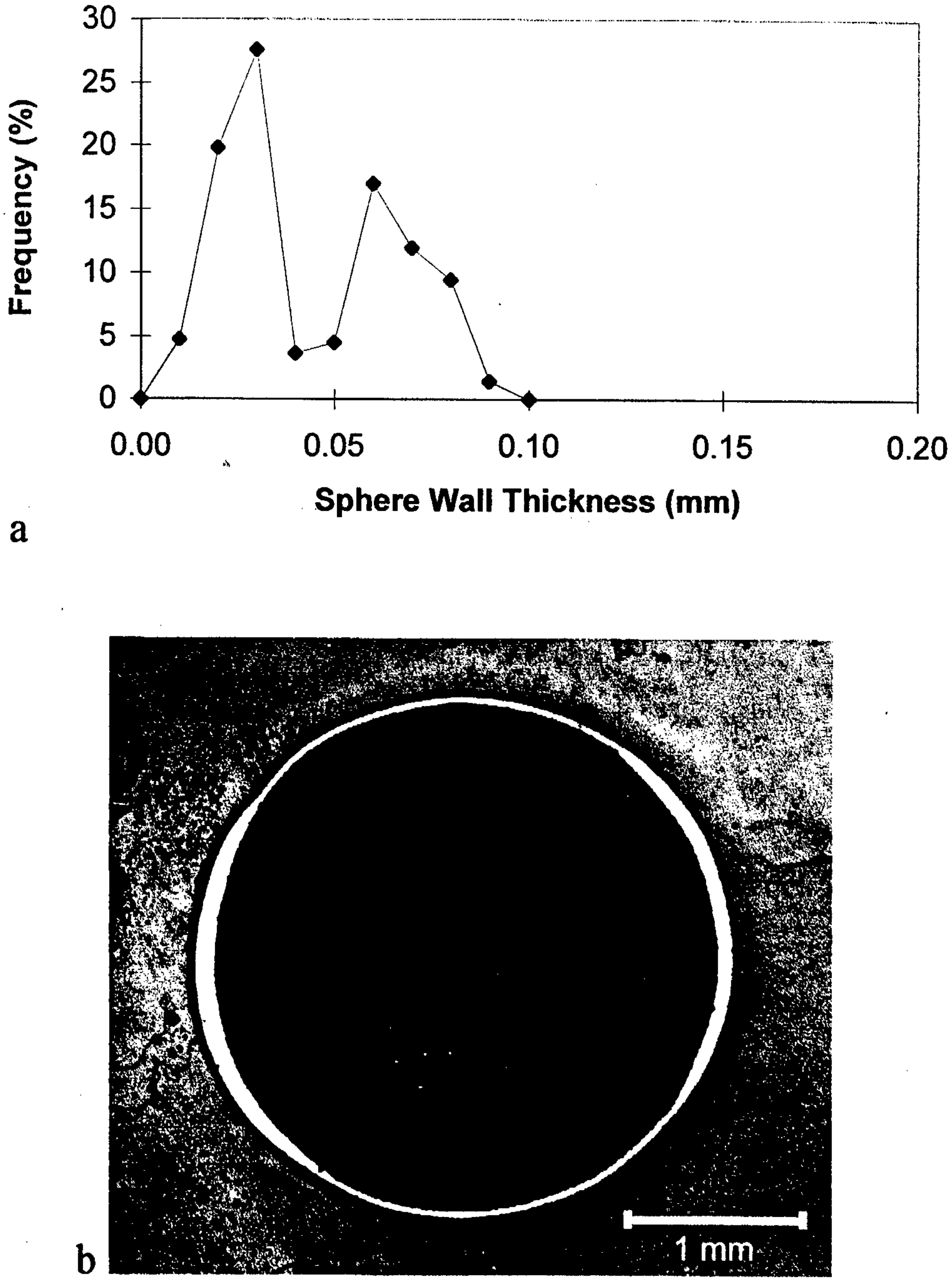

Figure 4.27 (a) The frequency of wall thicknesses present for an individual sphere made with polysilane (b) a micrograph of the sphere.

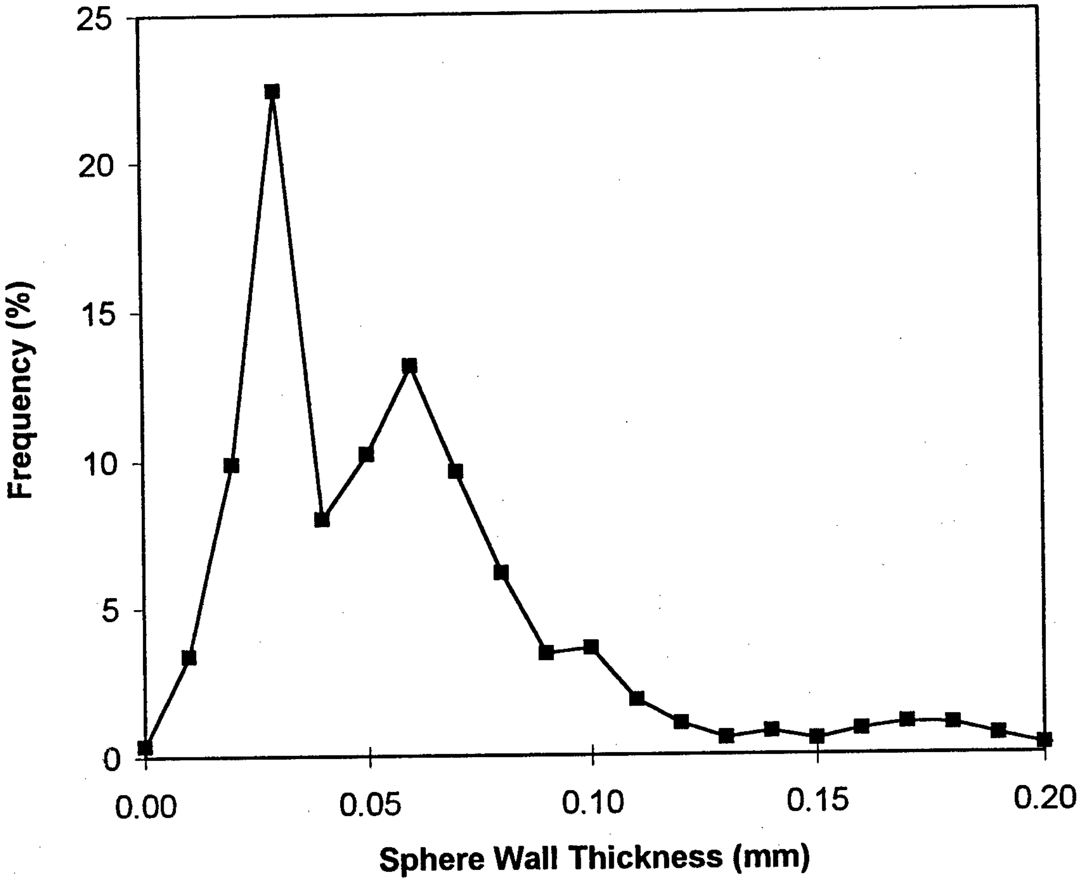

Figure 4.28 The frequency of wall thicknesses present for six spheres made with polysilane.

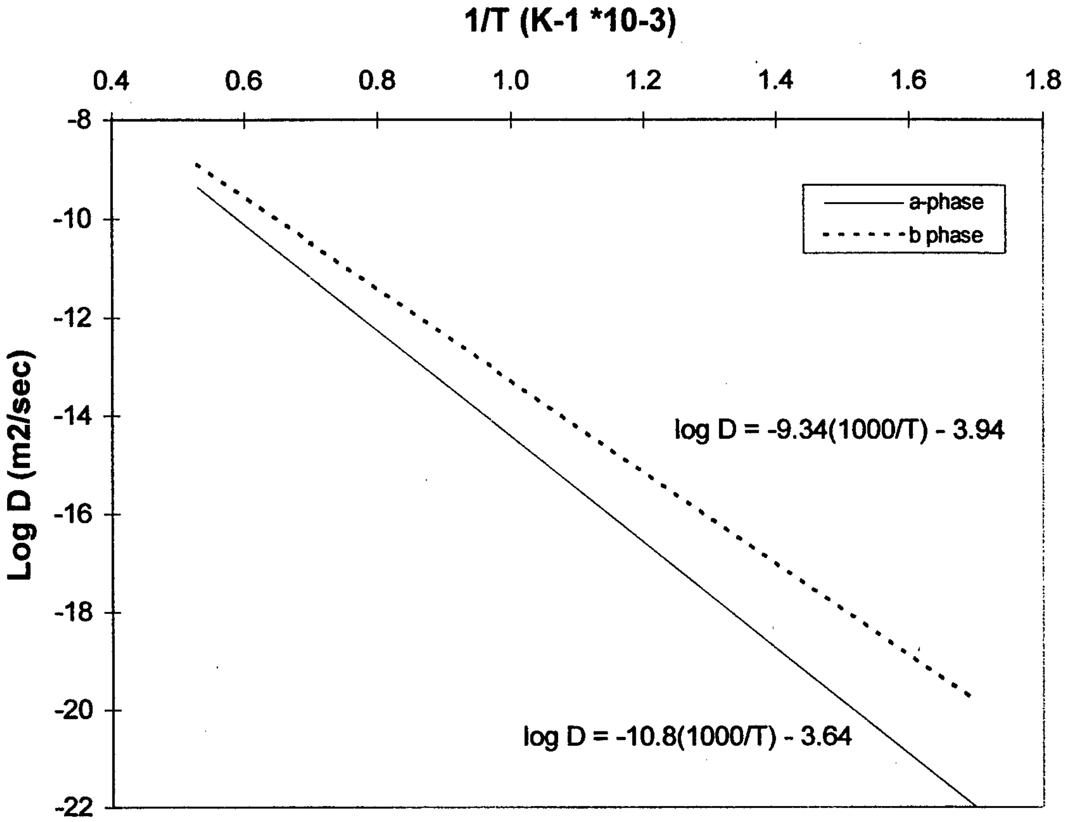

Figure 4.29 The diffusivity of oxygen in titanium with respect to temperature.

CHAPTER V

CONCLUSIONS AND RECOMMENDATIONS

1. TiH_2 is negatively charged in acetone as demonstrated by the measurement of negative ζ-potentials and the inability of several anionic polymers to disperse TiH_2 powder. The negative charge on the surface of TiH_2 is likely caused by hydrogen vacancies resulting from significant nonstoichiometry. Surface potentials in acetone are caused by normal charge levels in a low dialectric constant material. The dialectric constant of acetone is approximately 4 times lower than that of water.

2. Amine modified polysilane adsorbs on the surface of TiH_2 powder in a hydrolyzed state. Small quantities of polysilane adsorbed onto TiH_2 in acetone reverses the surface charge of the hydride producing large positive potentials to allow dispersion in the presence of nonionic polymers such as PMMA.

3. Further study of the adsorption of polymers onto TiH_2 surfaces should focus on the measurement of polysilane and PMMA combinations in acetone. Other polymer

combinations may also require measurement. IR spectroscopy can be used to quantitatively analyze the adsorption of polymer mixtures.

4. During the critical initial drying stage, acetone evaporates from a slurry dispersed with PS3 at rates approaching that of pure acetone. For TiH_2 slurries containing solely PMMA and PMMA with polysilane treated TiH_2, a significantly lower evaporation rate is observed early in the process. This lower evaporation rate can be attributed to the rapid formation of a polymer skin. Surface evaporation is limited by transport through the skin which becomes the rate limiting step and slows the process enough to maintain a stiff, tack free PMMA surface.

5. Of those tested, the only combination of polymers that resulted in favorable viscosity and evaporation rates when used in TiH_2 slurries were polysilane and PMMA. Both visual inspection and digital analysis found spheres made from slurries dispersed with polysilane and PMMA to be significantly more uniform than the next best alternative. The batch with the highest measured uniformity was formed from a slurry with a solids loading of 44 vol.% TiH_2 treated with 1.0 wt.% polysilane and dispersed with 3.0 wt.% PMMA.

6. Magnesium offers the potential of reducing impurity oxides of titanium that embrittle Ti spheres. The diffusion of oxygen through titanium and the solubility of oxygen in titanium are such that during a typical firing cycle, oxygen is able to diffuse completely

through the sphere wall. More study on the use of magnesium as a getterer should be conducted.

7. Preliminary work regarding AQLs (acceptable quality levels) has been conducted. To give these values true meaning, it is necessary to assign AQLs to flaw types based on their effects on mechanical properties. In this way, batches can be designated as sufficient or insufficient quality from which to form a foam. Processing of TiH_2 spheres has not yet reached the point where ductile spheres can be realized. When ductile spheres are formed, a study should be undertaken identifying the impact of each flaw type on the mechanical response of foams. In this way, batches can be either accepted or rejected for use in quality foams.

8. A study involving the firing of TiH_2, starting with no additives and progressing to TiH_2 with the reducing agent Mg, to TiH_2 with varying concentrations of the polymers typically added to disperse the slurry, and finally culminating in the firing of hollow spheres should be undertaken. Firing should be conducted in an atmosphere of the highest possible purity and in a clean furnace and at a variety of temperatures to see if it is possible to form ductile spheres from TiH_2 precursors.

1. Lord Rayleigh, "On the Instability of Jets", *Proc. Lond. Math. Soc.*, 10(4), 1878.

2. A. R. Gardner, *Production Engineer*, 38(141), 1967.

3. J. M. Kendall, M. C. Lee, and T. G. Wang, "Metal Shell Technology Based Upon Hollow Jet Instability", *J. Vac. Sci. Technol.*, 20(4), April, 1982, pp. 1091-1093.

4. M. C. Lee, "Metal Shell Technology", *SAMPE Journal*, Nov./Dec., 1983, pp. 7-11.

5. N. E. Baxter, T. H. Sanders, Jr., A. R. Nagel, C. Uslu, K. J. Lee, and J. K. Cochran, "Metallic Foams from Alloy Hollow Spheres", Synthesis/Processing of Lightweight Metallic Materials II, C.M. Ward-Close, et al., ed., TMS, Warrendale, Pa., 1997, pp. 417-430.

6. I. J. Polmear, Light Alloys, 3rd. Ed., p. 10, Arnold Press, London, 1996.

7. W. F. Smith, Structure and Properties of Engineering Alloys, McGraw Hill, New York, pp. 433-484, 1993.

8. W. B. Pearson, A Handbook of Lattice Spacings and Structures of Metals and Alloys, Permagon Press, Oxford, England, 1967.

9. J. Barksdale, “Titanium: It’s Occurance, Chemistry and Technology”, The Ronald Press Co., New York, pp. 48-50, 1949.

10. T. Massalaki, Binary Alloy Phase Diagrams, Vol. 3, 2nd Ed., ASM International, p. 2926, 1990.

11. M. Pajunen and J. Kivilahti, “Thermodynamic Analysis of the Titanium-Oxygen System”, *Z. Metallkd.*, Vol. 83, No. 1, pp. 17-20, 1992.

12. H. Conrad, "Effect of Interstitial Solutes on Titanium", *Prog. Mat. Sci.*, Vol. 26, pp. 123-147, 1981.

13. Z. Trojanova, V. Kukacka, and V. Moskalenko, “Hardening and softening in pure alpha titanium and commercial titanium at 450-950K”, *Kovove Materialy*, Vol. 28, No. 6, pp. 698-706, 1990.

14. A. McQuillan and M. McQuillan, Metallurgy of the Rarer Metals: Titanium, Butterworths Scientific Publications, London, pp. 402-427, 1956.

15. N. Gokcen, Statistical Thermodynamics of Alloys, Plenum Press, New York, pp. 149-193.

16. Z. Liu and G. Welsch, "Literature Survey on Diffusivities of Oxygen, Aluminum, and Vanadium in Alpha Titanium, Beta Titanium, and Rutile"

17. H. Conrad, "Effect of Interstitial Solutes on Titanium", *Prog. Mat. Sci.*, Vol. 26, pp. 131-147, 1981.

18. K. Wiedemann, R. Shenoy, and J. Unnam, "Microhardness and lattice parameter calibrations of the oxygen solid solutions of unalloyed α-titanium and Ti-6Al-2Sn-4Zr-2Mo", *Met. Trans. A*, Vol. 18A, Aug. 1987, pp. 1503-1510.

19. C. U. Hardwicke, "Processing and Properties of Ti-6Al-4V Hollow Sphere Foams From Hydride Powder", Ph.D. Thesis, Georgia Institute of Technology, School of Materials Science and Engineering, August, 1997.

20. CRC Handbook of Chemistry and Physics, 58th Edition, R. C. Weast, ed., CRC Press, West Palm Beach, Fl., p. B-127.

21. L. J. Gibson and M. F. Ashby, Cellular Solids Structures and Properties, Permagon Press, Elsford, N.Y., 1988.

22. Z. Hashin and S. Shtrikman, *J. Mech. Phys. Solids*, 11(1963), pp. 127-140.

23. A. Kraynik, *J. Appl. Mech.*, to be published.

24. Y. Sugimura, J. Meyer, M.Y. He, H. Bart-Smith, J. Grenestedt, and A.G. Evans, "On the Mechanical Performance of Closed Cell Al Alloy Foams", *Acta Materialia*, 45, 1997, pp. 5245-5259.

25. L. B. Torobin, "Method for Making Hollow Porous Microspheres", U.S. Patent 4671909, 9 Jun 87.

26. J. K. Cochran, "Methods for Producing Fiber Reinforced Microspheres Made From Disperse Particle Compositions", U.S. Patent 4867931, 19 Sep 89.

27. M. N. Rahaman, Ceramic Processing and Sintering, Marcel Dekker, Inc., New York, pp. 146-200, 1995.

28. R. J. Calliger, R. J. Turnbull, and C. D. Hendricks, "Hollow Drop Production by Injection of Gas Bubbles Into a Liquid Jet", Rev. Sci. Instrum., Vol. 48, No. 7, July, 1977, pp. 846-851.

29. J. M. Kendall, "Hydrodynamic Performance of an Annular Liquid Jet: Production of Spherical Shells", Proceedings of the Second International Colloquium on Drops and Bubbles, D. H. LeCroissette, ed., NASA-JPL, Pasadena, Ca., 1982, pp. 79-87.

DISTRIBUTION STATEMENT AUTHORIZATION RECORD

Title: The PROCESSING OF TITANIUM HYdRide POWERS INTO UNIFORM HOllOW SPhERES

Authorizing Official: STEVEN FISHMAN

Agency: ONR 332 Ph. No. 703 6960285

☐ Internet Document: URL: ______
(DTIC-OCA Use Only)

Distribution Statement: (Authorized by the source above.)

☒ A: Approved for public release, distribution unlimited.

☐ B: U. S. Government agencies only. (Fill in reason and date applied). Other requests shall be referred to (Insert controlling office).

☐ C: U. S. Government agencies and their contractors. (Fill in reason and date applied). Other requests shall be referred to (Insert controlling office).

☐ D: DoD and DoD contractors only. (Fill in reason and date applied). Other requests shall be referred to (Insert controlling office).

☐ E: DoD components only. (Fill in reason and date applied). Other requests shall be referred to (Insert controlling office).

☐ F: Further dissemination only as directed by (Insert controlling DoD office and date), or higher authority.

☐ X: U. S. Government agencies and private individuals or enterprises eligible to obtain export-controlled technical data in accordance with DoD Directive 5230.25.

NOTES: ______

N. WALTON
DTIC Point of Contact

10/4/99
Date

30. P. R. Chu, “A Model for Coaxial Nozzle Formation of Hollow Spheres from Liquid”, Ph.D. Thesis, Georgia Institute of Technology, School of Materials Science and Engineering, June, 1991.

31. W. B. Rensel, D. A. Steinman, R. L. Crawley, and D. J. Tanner, “Wall Nonuniformity Measurement of Inertial Fusion Targets Using a Rolling Technique, *Rev. Sci. Instrum.*, pp. 1478-1481, 51(11), Nov. 1980.

32. R. A. Johnson, Miller & Freund's Probability & Statistics for Engineers, 5th Ed., Prentice Hall, New Jersey, pp. 506-547, 1994.

33. H. P. Klug and L. E. Alexander, X-ray Diffraction Procedures For Polycrystalline and Amorphous Materials, 2nd ed., John Wiley & Sons, New York, pp. 566-617, 1974.

34. R. Jenkins, Selected Powder Diffraction Data, International Centre for Diffraction Data, Swarthmore, Pa, p. 139, 1988.

35. W. M. Mueller, "Titanium Hydrides", in Metal Hydrides, W. M. Mueller, J. P. Blackledge, and G. G. Libowitz (ed.), Academic Press, pp. 336-382, 1968.

36. S. J. Gregg and K. S. W. Sing, Adsorption, Surface Area and Porosity, 2nd Ed., Academic Press, New York, pp. 41-110, 1982.

37. J. Schaffer, A. Saxena, S. Antolovich, T. Sanders, and S. Warner, The Science and Design of Engineering Materials, Irwin Press, pp. 119-153, 1995.

38. Z. Liu and G. Welsch, "Literature Survey on Diffusivities of Oxygen, Aluminum, and Vanadium in Alpha Titanium, Beta Titanium, and Rutile", *Met. Trans. A*, pp. 1121-1124, Vol. 19A, Apr. 1988.